ABSTRACT

Title of dissertation:	THEORETICAL STUDIES OF THE INTERPLAY BETWEEN SUPERCONDUCTIVITY AND DISORDER
	Anirban Gangopadhyay, Doctor of Philosophy, 2012
Dissertation directed by:	Dr. V. M. Galitski Department of Physics

In this thesis, I explore a variety of disordered condensed matter systems and investigate questions pertinent to transport in such systems. In the first part of the thesis, I seek explanations for the strange feature of a giant magnetoresistance peak seen in the vicinity of superconductor-insulator transitions. To this end, I propose a semiclassical two-component Coulomb glass model for 2D insulators close to such transitions. I show that a local pairing attraction in Coulomb glasses can lead to crucial modification of the low-energy density of states which may affect transport. In another explanation for the peak, I consider an Anderson insulator of localized pairs and develop a theory of their transport. I study the change in localization length of the pairs (treated as bosons) on applying a magnetic field and the consequent change in transport properties. I show that from a statistical consideration alone, one can predict a nonmonotonicity in magnetoresistance. In the process, I also revisit the classic problem of directed polymers in a random media (DPRM) and propose a toy model for magnetoresistance in bosonic insulators based

on DPRM scalings. In the second part of the thesis, I derive a class of exact solutions for two-level systems driven by a time-periodic external field which pertains to loss mechanisms in superconducting charge qubits.

Theoretical studies of the interplay between superconductivity and disorder

by

Anirban Gangopadhyay

Dissertation submitted to the Faculty of the Graduate School of the
University of Maryland, College Park in partial fulfillment
of the requirements for the degree of
Doctor of Philosophy
2012

Advisory Committee:
Dr. V. Galitski, Chair/Advisor
Dr. M. Levin
Dr. C. Lobb
Dr. S. Eno
Dr. A. Dasgupta, Dean's Representative

Acknowledgments

I owe my gratitude to all the people who have made this thesis possible and because of whom my graduate experience has been one that I will cherish forever. First and foremost, I would like to thank my advisor, Victor Galitski, who made me appreciate the importance of creative thinking in research. His guidance was not only invaluable in my research, but also showed me the right direction for my future. Without his able guidance, I would have never appreciated what I am really capable of and where my strengths lie. I am sure that because of this, I have matured into a much more self-aware person during my graduate studies here.

I would then like to thank Dr. Markus Mueller of The International Center for Theoretical Physics, who introduced me to the physics of disordered condensed matter systems. As for my graduate research, I would be especially grateful to him for not giving up on me, even when I had given up on myself. A large part of the work in this thesis came from a very fruitful overseas collaboration involving Dr. Galitski, Dr. Mueller and my fellow graduate student, Joe Mitchell. From Dr. Mueller, I learned one giant lesson which will stay with me forever — the value of tenacity. Chapter 4 in this thesis comes from a year-long research, the large part of which involved mostly fumbling around in the dark with only some meagre clues, which eventually led to some very deep connections. None of which would have been possible without Dr. Mueller's persistence.

I would then like to thank my colleagues and friends, Joe Mitchell, Justin Wilson, Meng Cheng and Juraj Radic. They were with me every step of the way

and lighted up some of the very difficult moments of my journey through graduate school. I would especially thank Joe for patiently introducing me to the nuances of Fortran programming and being always eager to help me out with any question I may have. He never took the easy route of 'I am not familiar with that line of research' and always listened me out, asking some very deep questions at the end. I would also like to thank Dr. Maxim Dzero for my initiation into graduate research and teaching me the importance of sanity checks on mathematical results.

The work of any scientist is a foregone conclusion without the generosity of the organization and agencies that fund scientific research. The large part of the funding for my research came from an NSF-Career award given to Dr. Galitski. I am grateful to both NSF as well as my advisor for fully supporting me during the crucial years of my graduate research.

I would also like to thank my parents and sister who continuously supported me over Skype during some of the hopeless periods of my research. Also, I must make a special mention of my cousin, Anindya Ghosal, whom I could always turn to for directions. Lastly, I would thank all my friends who have made my graduate life a memorable experience– especially, Anirban Ghosh, Kazi Rajibul Islam, Basudev Roy, Subhadeep De, Dibyendu Mandal, Madhura Joglekar, Srimoyee Sen, Ayoti Patra. Alas, I do not have enough space to include the names of many more friends who basically got me through graduate school. Each and every input was equally valuable.

Once again, thanks everyone for your support !!

Table of Contents

List of Figures

Chapter 1

Introduction

1.1 Motivation

Superconductivity is one subfield of condensed matter physics that has never
ceased throwing up new surprises. Since 1911, when Kamerlingh Onnes accidentally
discovered that the resistance of mercury abruptly drops to undetectable values be-
low 4.2 K, there has been a spate of work in this field. Unlike some theoretical fields
(as, topological insulators and physics of ultracold atoms), theory here has mostly
followed experimental results by at times decades. In fact, superconductivity in
its conventional form, received a microscopic theory (the Bardeen-Cooper-Schrieffer
theory or the BCS theory as it is commonly known) only in 1957, more than 40
years after its discovery.

With a large potential for applications, experimentalists have been trying to
come up for the elusive room temperature superconductor since then. This resulted
famously in the discovery of what is known as high-T_c superconductivity ($T_c > 30$
K) in the so-called doped cuprate class of materials in the later 1980-s. It was a
surprising discovery, especially given that the original undoped copper oxides were
highly insulating.

BCS theory failed to explain such a high transition temperature. To this day,
one has not settled on the question of what is the origin of superconductivity in

these materials (recently bolstered by the addition of iron pnictides to the class of high-T_c materials).

Much less publicized and with fewer experimental groups working on it, the story of superconductivity has branched out in another direction, namely that of dirty superconductors. Most of the superconducting materials studied in the laboratory (certainly the oxides formed by annealing of metals) are expected to come with certain degree of disorder (lack of symmetry in the potential under discrete spatial translations). It had been shown in the Nobel-winning work of Philip Anderson [5] that disorder solely by itself can lead to insulating behavior in materials if sufficiently strong.

One then naturally wondered how the presence of disorder would affect superconductivity. With the expectation that the extreme limit of high disorder would lead to an insulator, one of the questions concern the route from superconducting to insulating behavior.

Another reason to study insulators in the context of superconductivity is superconductors in physical contact with insulators. Since superconducting elements have potential applications for quantum computing, the study of power losses during current passage through superconductor-insulator contacts have gained tremendous importance.

In this thesis, I study particular aspects of both questions. First, I study a class of quantum phase transitions referred to as superconductor-insulator transitions, observed in disordered thin films. This class of transitions can be realised either by changing the disorder content or by applying a magnetic field perpendicular or

even parallel to the thin films. Since superconducting and insulating behavior so to speak lie at opposite ends of the spectrum, the passage from one behavior directly into the other has been very intriguing.

The experiments, when carried out further into the insulating regime, show a nonmonotonic variation in resistance, leading to bad metallic behavior at high fields/disorder. This unique signature of superconductor-insulator transitions has been observed across a wide variety of materials such as Indium oxide, TiN, Be (the difference being only in the relative height of the resistance peaks compared to the value at transition). It is, therefore, not implausible that there is a common microscopic origin behind this class of transitions.

The microscopics behind the phenomenon of superconductivity as given by the BCS theory [6] consists of two distinct levels and one can focus on each level independent of the other. The first level pertains to pairing of electrons close to the Fermi level into a bound state. In conventional superconductivity, this pairing attraction is mediated by exchange of phonons (quantum of vibration of the background lattice). However, one can independently start from *assuming* existence of a weak pairing and establish that it can lead to a ground state with nontrivial order signalling long-range coherence between the pairs (Cooper instability).

Breaking down the mechanism of superconductivity thus in two steps allows us to find room for exotic superconductivity. The Cooper instability of conventional superconductivity comes from collaboration of a weak pairing attraction with a large degeneracy at the Fermi surface (see [7] for an exposition). In BCS theory, it turns out that the size of a pair is substantially greater than the average distance between

the pairs. One can estimate that this does not hold for the exotic superconductors, including the high-T_c cuprates [8]. Thus, an alternative theory of superconductivity has evolved over the years, where the pairs are treated as composite bosons and the phenomenon of superconductivity is related to formation of a Bose-Einstein condensate (BEC) of this system of bosons. In fact, it has been shown from field-theoretic approaches that one can incorporate a "BCS-BEC crossover" within a unified microscopic framework (see [9] for a derivation).

Unlike the BCS-theory, the BEC model clearly distinguishes the act of pair formation from their condensation leading to superconductivity. The two events can be set into motion at distinctly different temperatures allowing a window where the pairs are formed but not yet collapsed into a giant macroscopic condensate. It is this window in the phase diagram of these films that has motivated the work in the first part of this thesis. The localized nature of the pairs allows one to borrow a well-developed set of tools from the theory of Anderson insulators and study transport phenomena in the vicinity of a superconductor-insulator transition.

The second context where superconductors and insulators are spoken in the same breath is in relation to a very important area of application of superconductors: namely, in superconducting qubits. Due to the macroscopic ground state of the pairs and suppression of low-energy excitations, superconductors are the ideal choice among solid-state systems for implementation as qubits (two-level quantum systems).

According to the DiVincenzo criteria [10] for a quantum circuit to successfully serve as a qubit, the decoherence time of a qubit has to be much less than the time

required to perform operations on and read out the qubit. Put simply, the quantum circuit has to be able to hold on its information long enough. Hence, a great amount of study has been devoted to understanding the mechanisms for loss of information from the superconducting qubits with a view to increasing their coherence times.

It has been shown recently [11] that a primary mechanism for this loss is through the dielectrics typically employed as spacer elements in the quantum superconducting circuits. This dielectric loss has been previously modelled in terms of two-level systems possessing an electric dipole moment. In the second part of this thesis, I probe the losses in superconducting qubits through an exact solution of a two-level system in an ac electric field. This is, strictly speaking, a study of tunneling states in dielectrics, which, however, gain enormous importance due to their application in superconducting qubits.

Thus, we have two very different contexts falling under the broad ambit of 'superconductors and insulators' and it is imperative that the thesis be divided into two separate parts. The work in both parts has borrowed mathematical techniques from fields completely unrelated to superconductor-insulator transitions (Part I) or dielectric losses in superconducting qubits (Part II). With that in mind, it is not practically feasible to provide an overview of all the theoretical tools already in use in these two vastly developed fields except those that have actually been used in our research. However, whenever possible, I shall guide the interested reader towards past literature in order to provide a more detailed and in-depth survey of the fields.

1.2   Overview of thesis-Part I

In this part of the thesis, I study two-dimensional systems on the insulating side of superconductor-insulator transitions (SIT-s). Seeking a microscopic origin for the nonmonotonic trends in resistance in this regime, I will isolate two very specific causes which may lead to this effect.

1.2.1   Modelling insulators with localized pairing

I begin by reviewing some of the experimental literature on SIT-s, especially focusing on supporting evidence for the BEC model and the localized pair hypothesis. Equipped with ingredients from this survey, I construct a very general model which is expected to simulate the window in the phase diagram where localized pairs can coexist along with single-particle excitations. Although I speculate on the origin of this pairing, this work mostly accepts their existence and studies how they would show up in experimentally measurable quantities. Since the SIT-s can be brought about by a magnetic field $\mathbf{B}$, I clearly mark which ingredients of our model are likely to be affected by $\mathbf{B}$.

1.2.2   Two-component Coulomb glass model

The model/Hamiltonian outlined in the previous section has too many ingredients to be amenable to analysis. I therefore extract reduced Hamiltonians which suppress some of the ingredients and are thus valid in much narrower regions of the phase diagram. For instance, in this chapter, I shall suppress the spread in wave-

function of localized excitations due to quantum tunneling and assume them to be completely confined to their respective sites. The reduced Hamiltonian is therefore classical. Unlike previous approaches towards treating the vicinity of SIT-s which ignore long-range Coulomb interaction, I do retain them leading to a very complex glassy (highly frustrated) system.

As it turns out, such a glassy, classical system without the complication of localized pairing interactions had been treated in the context of doped semiconductors. This is well-known in the literature as the Efros-Shklovskii model. Here, I extend the Efros-Shklovskii model to include localized pairing and notice some remarkable modifications to hitherto universal results of that model, mainly in regard to the low-energy density of states (DOS). Among other things, I also recover the nonmonotonicity in resistance seen experimentally, although I shall only mention it in passing (Transport in these systems with variable-range hopping of two kinds of carriers — single electrons and pairs— require elaborate calculations and deserve another chapter by itself. This part of the research has been mainly driven by my colleague, Joe Mitchell, and therefore this separate chapter with details of the analysis will be later published in his thesis. I simply state the results here for completeness.)

1.2.3   Bosonic Anderson Insulator in a Magnetic Field

Here I step up from a semiclassical model to include quantum tunneling terms. However, one again encounters the problem of "too many ingredients", making it

difficult to pin down the final result to a definite origin. Hence, I make two simplifications. First, long-range Coulomb interactions are ignored. Secondly, I treat tunneling of pairs exlusively. The argument is that, except in a very narrow window, one type of carrier would dominate transport (this argument being supported by transport calculations from the two-component Coulomb glass model). I focus mainly on the pair regime, since the single-regime has already been treated extensively in previous work (although mostly restricted to numerics)— hence the title of the chapter,'bosonic Anderson insulators'.

Despite inclusion of tunneling, the calculations are still restricted to a strongly insulating regime. Thus, I treat the tunneling perturbatively a la Anderson in his Nobel-winning paper.

I focus on studying the magnetoresistance of a two-dimensional bosonic Anderson insulator. This quantity captures the change in spatial decay of localized excitations in response to a magnetic field and is determined by an interference sum over their tunnelling trajectories. Numerically one observes that the excitations become more localized with increasing field (in sharp contrast to generic fermionic excitations which get delocalized) and the change in localization length $\xi(B)$ is given by $\xi^{-1}(B) - \xi^{-1}(0) \sim B^{4/5}$. A theoretical analysis of this result leads to a mapping of the quantum interference problem onto a seemingly unrelated statistical mechanics problem of directed polymers in random media (DPRM). Using this mapping, I probe the complex interference phenomena and recover the observed scalings using a simplified droplet model with the non-trivial DPRM exponents. I end this chapter with a discussion of how one could possibly observe these results in ex-

periments (in addition to them providing a plausible explanation for the observed magnetoresistance nonmonotonicity).

1.3 Overview of Thesis - Part II

Distinctly different from the previous part, I move on to a completely different area of research in condensed matter physics – that of tunneling states in amorphous dielectrics. Theoretically, this also marks a distinct paradigm shift from phenomenological model-building to more rigorous analytical calculations.

1.3.1 Mapping of charge TLS in E-field to spins in B-field

As in the first part, I begin the second part of the thesis with a brief survey of experimental literature on dielectric losses in superconducting qubits. I then review the tunneling-state model of losses in dielectrics introduced independently in 1972 by Anderson et al [12] and W. A. Phillips [3]. I show how the tunneling states in an external electric field can be mapped to spins in an external magnetic field. I derive the Bloch equations for expectation values of spin operators in a magnetic field from the mapping and show how a solution of the Bloch equations can be translated into results pertinent to tunneling states in dielectrics.

1.3.2 Exact solution for quantum dynamics of a periodically-driven two-level system

I then proceed to solve the Schrödinger/Bloch equations in presence of a time-periodic magnetic field. For reasons that will be explained, solving the system exactly for the simplest periodic function, namely a sinusoidal function, is not possible. However, borrowing insights from nonequilibrium superconductivity, I develop a reverse engineering approach to construct solvable models for two-level-systems in a magnetic field. In other words, I explicitly construct periodic functions of the magnetic field which allow calculating exactly the time evolution of magnetization of the system. I then solve this model and find the implications of this solution on the frequency dependence of dielectric loss.

1.4 Conclusion

I end the thesis with future directions for work in both fields. In the study of superconductor-insulator transitions, the future directions mostly involve combining results from the simplified models in a bottom-up approach to obtain a complete picture of the phase diagram of the thin films. I also discuss the implications of this work on the important and still-debated question of what is the route from superconductivity to insulating behavior. In the study of dielectric losses in superconducting qubits, I hope to move forward from an ensemble of isolated two-level systems (where the dissipative effects of the environment are included phenomenologically) to actually involving interactions between the TLS and the environment

in order to more accurately simulate real systems.

PART I. TRANSPORT PHENOMENA NEAR SUPERCONDUCTOR-INSULATOR TRANSITIONS

Chapter 2

Modelling insulators with localized pairing

2.1 Superconductor-Insulator transitions in 2D disordered films

The classic example of correlated many-body effects is superconductivity, which is characterized by phenomena such as zero electrical resistance and Meissner effect (exclusion of magnetic flux from bulk). Superconductivity can be destroyed by an external parameter such as a magnetic field (B) typically leading to a change from the superconducting state to a normal metallic state. In the past three decades, however, it has been observed in certain electron systems [13, 14, 15, 16, 17, 18, 19, 20, 21, 8] that loss of superconductivity is accompanied by transition to an insulating state rather than normal metal. This transition is typically seen in disordered films, and can also be realised by changing the disorder content of the samples.

The common feature of such 'superconductor-insulator transitions' is a decrease in resistance (R) of the films with decreasing temperature below the transition and increase in R above it. The critical magnetic field B_c (or disorder) is marked by the point in the (R, B) phase diagram where the isotherms cross. These are typically low-temperature phase transitions and are quantum in nature, being tuned by a parameter in the Hamiltonian.

On increasing B beyond the phase transition, one observes a dramatic increase in resistance by several orders of magnitude denoting the insulating state. However,

beyond a certain magnetic field B_p, the resistance starts falling and reaches almost its value at the transition point on further increase of B. This nonmonotonicity in magnetoresistance has been a puzzle for quite some time now although several plausible mechanisms have been proposed.

In fact, the route to loss of superconductivity in these films is still under debate [22, 23, 24, 25, 26, 27, 28, 29]. One school of thought endorses path-disorder enhanced Coulomb repulsion destroying pairing before onset of localization ([23], also review [30]).

2.2   Localized pair hypothesis

The other school of thought, which has received heavy experimental support only recently, supports the idea that phase fluctuations destroy global coherence without supression of pairing. The remaining pairs undergo Anderson localization in strong disorder.

It was already understood in Ref. [14] that the presence of this peak, accompanied by Hall measurements, suggested the survival of some local pairing deep in the insulator, which is only gradually destroyed by an increasing magnetic field.

This formation of local pockets of superconducting regions in an insulating matrix has been found in several theoretical studies. A prominent one is a thoretical study of 2D disordered s-wave superconductors by Trivedi et al [25] using mean-field BdG equations. Relaxing the usual condition of a spatially uniform order parameter, they find that the system breaks up into islands of superconducting regions at high

disorder. Despite the uncorrelated disorder strengths between lattice sites, these superconducting islands with nonzero order parameter are spread over several lattice sites. This is reminiscent of granular materials where spatial coherence is retained within each grain (embedded in an insulating sea) although there is no correlation between grains.

It was predicted that the presence of these islands would manifest as a gap in the tunneling density of states (DOS) in scanning tunneling microscopy (STM) without the pile-up of states around the gap indicating global coherence. Very recently, this has been verified in STM experiments [21] which showed the absence of coherence peaks in the tunneling DOS in a high-disorder sample despite cooling below T_c.

In the light of this new evidence for local pairing, I shall revisit the problem of transition from a Bose insulating phase (of localized pairs) to a Fermi insulator (of localized single electrons) and study in detail the strongly insulating regime which incorporates survival of the localized pairs.

2.3   Mechanisms of pairing : conjectures

One of the materials exhibiting the above phenomenology is InO_x, a commercially important and extensively studied semiconductor. Despite the uncertainties about its complex band structure, it is widely believed that the carriers in InO_x originate from oxygen vacancies, likely partially compensated by the triply-negatively-charged indium vacancies. The recent ab initio study of Ref. [31] calculated the

formation energy of oxygen vacancies with different charge and found that a doubly-charged vacancy has the lowest formation energy in a crystalline environment (in zero field). The energetically next best state is an empty site, while a single occupied site corresponds to highly excited state.

It is quite plausible that this tendency for local 'pair' formation underlies the superconductivity in this system, similarly to compounds like PbTe [32], where local negative U interactions have been proposed to lead to a non-standard type of superconductivity of preformed hard core bosons [33]. This mechanism of pairing is unlike the BCS theory, which proposes a phonon-mediated attraction between electrons on the Fermi surface.

2.4   Model

A serious difficulty for the theory of such insulators stems from the need to treat strong disorder and electron pairing effects on equal footing. In addition, recent experiments indicate that long range unscreened Coulomb interactions, often neglected in theoretical approaches, do in fact play an important role in several materials. In particular, the temperature dependence of the resistance in strong disorder [15], or on the high-field side of the mangetoresistance peak in TiN [20] and InO_x [1], is often well described by the Efros-Shklovskii law suggesting variable-range-hopping (VRH) in the presence of a Coulomb gap [34]. Although local pairing attractions, often captured through a negative-U Hubbard model, have been studied quite

---

[1]B. Sacépé, private communication.
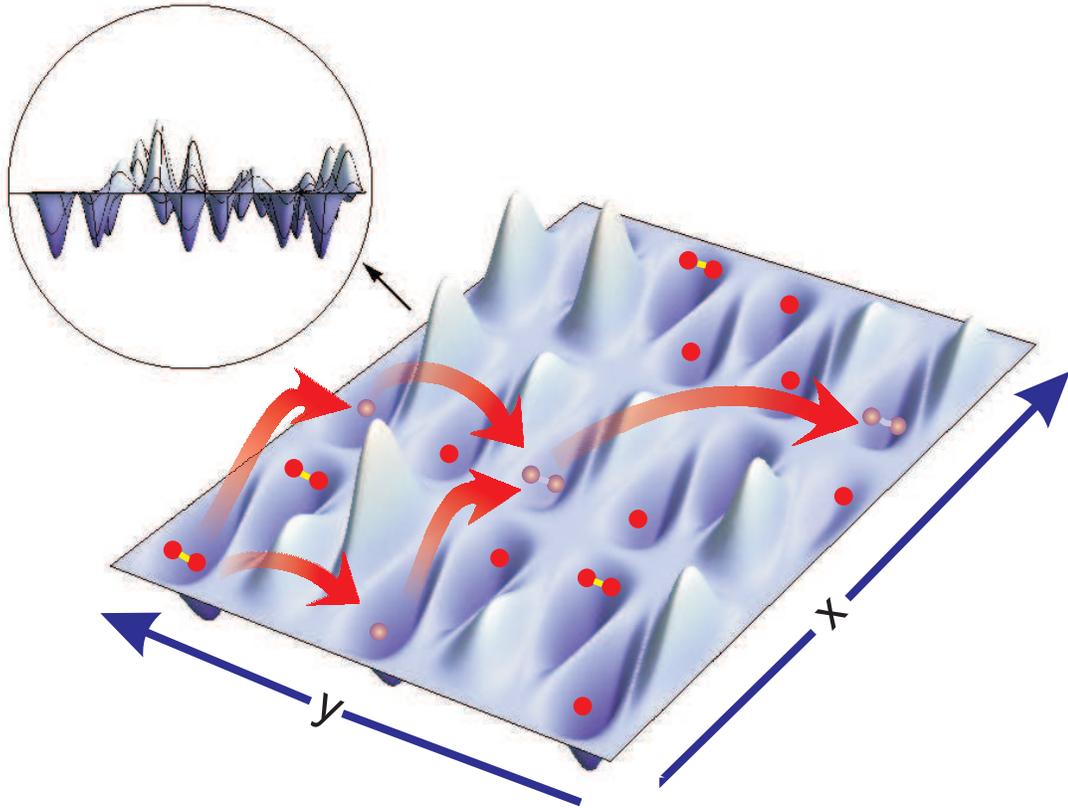
Figure 2.1: Illustration of the two component model: The energy landscape is due to the combination of on-site disorder and Coulomb interactions. The arrows indicate typical hopping processes relevant for the complex low T transport in the two component Coulomb glass.

extensively in previous research focussing on the superconductor-insulator transition [35, 36, 25], such studies have predominantly neglected long range Coulomb interactions. In contrast, in the first approach shown in Chapter 3, we do include the latter and focus on more insulating regimes where Coulomb interactions play a crucial role and compete in a non-trivial way with the local negative U attraction. Our study also has implications on Coulomb glasses in granular materials, where multiple occupation of sites is allowed. These aspects have recently been analyzed in closely

related works [37, 38].

The above experimental motivations lead us to introduce a lattice model that captures the full spectrum of possible ingredients present in the actual materials: strong disorder, local attraction of electrons (favored double occupancy of sites), and long-range Coulomb interactions, together with quantum transport captured by intersite nearest-neighbor hopping. The full Hamiltonian for such a system can be written in a general form, with the experimental tuning parameters (disorder strength W and magnetic field $\boldsymbol{B}$) explicitly written, as follows:

$$\hat{H} = \sum_i \phi_i \hat{n}_i + \frac{1}{2} \sum_{i,j} \frac{e^2}{r_{ij}} (\hat{n}_i - \nu)(\hat{n}_j - \nu) + \sum_i \frac{1}{2} U_i(\boldsymbol{B}) \hat{n}_i(\hat{n}_i - 1) +$$

$$\sum_{\langle ij \rangle} \left(t_{ij}^{(1)} e^{\theta_{ij}(\boldsymbol{B})} \hat{c}_i^\dagger \hat{c}_j + t_{ij}^{(2)} e^{2\theta_{ij}(\boldsymbol{B})} \hat{c}_i^\dagger \hat{c}_i^\dagger \hat{c}_j \hat{c}_j + \text{h.c.} \right) \qquad (2.1)$$

In the above, $\phi_i = O(W)$ represents the random on-site potential due to the disorder, e.g. in the form of randomly positioned dopants. $\frac{e^2}{r_{ij}}$ is the unscreened Coulomb repulsion between the localized carriers and $U_i(\boldsymbol{B})$ is the local pairing interaction renormalized by the Coulomb repulsion between charges localized on the same site (within one lattice spacing). We assume that it is tunable, e.g., by the magnetic field. The last two terms represent quantum hopping of the single electrons as well as of pairs of electrons. While a pair hopping term is obviously generated as a second order process in single electron hopping, the relation between the single electron's tunneling amplitude $t_{ij}^{(1)}$ and that of the transfer of a pair may not be simple in the real materials, since it may involve details of the local electronic structure, which is responsible for the negative U interaction. We therefore allow for

18

a independent pair hopping amplitude $t_{ij}^{(2)}$. When discussing transport, we will take the two hopping amplitudes as independent phenomenological parameters, which translate into two independent localization lengths for localized single electron and pair excitations. The magnetic field enters the hopping terms via the phase factors $\theta_{ij}(\boldsymbol{B})$.

To solve this full quantum Hamiltonian would be an extremely ambitious goal. We shall instead isolate individual aspects of this complex problem. In the next chapter, we make two simplifying assumptions — firstly, we focus on the regime in the phase diagram of these films where the electron pairs are indeed formed locally, but are far from condensation. In technical terms, we treat the hopping terms in the Hamiltonian under the approximation $t_{ij}^{(1,2)} \ll \max(W, \frac{e^2}{a})$ (a being the lattice constant) and thus restrict ourselves to a classical model where transport is primarily through thermally-induced variable-range hopping, among exponentially localized states. This is closely analogous to the standard analysis of doped semiconductors [39]. When discussing variable-range hopping transport the hopping terms are taken into account via the (average) localization lengths, ξ_1 and ξ_2, of the single electrons and pairs, respectively, which are a result of the B-dependent hoppings $t^{(1,2)}$. Obviously, this approach prevents us from capturing superconductivity within the model. Nevertheless, many interesting physical phenomena observed in experiments, such as the giant magnetoresistance peak, often occur rather deep in the insulating phase [8], where such a strongly localized approach is meaningful.

In that chapter, we also assume that the entire effect of magnetic field is to tune the local pairing interaction. It is reasonable to assume a monotonic decrease

of the pairing strength U with increasing magnetic field. We do not include the effects of the B-dependence in the hopping (orbital effects), but focus entirely on the effect of changing the pairing interaction on various physical observables, such as the density of states and longitudinal resistance. In Chapter 4, we study instead the magnetic field dependence introduced by the phases in the hopping terms in Eqn. 2.1 through explicit evaluation of the $\boldsymbol{B}$-dependence of the localization lengths $\xi_{1,2}$. In reality both effects are present simultaneously. We find that they both contribute to a non-monotonic magnetoresistance.

Chapter 3

Two-component Coulomb glass model

3.1 Classical Model

We now focus entirely on this two-component Coulomb glass model[1], which
will be shown to feature a significantly richer variety of phenomena than the canon-
ical Efros-Shklovskii model. The latter considers a lattice of sites, i, with random
on-site energies for electrons, ϕ_i, populated with a filling factor, ν. Each site i can
host only $n_i \in \{0, 1\}$ electrons. The (classical) electrons repel each other with un-
screened Coulomb interaction e^2/r, and the disorder is assumed to be distributed
over a typical range W, e.g., uniformly in $\phi_i \in [-W, W]$. The Efros-Shklovskii
Hamiltonian can be written as

$$H = \sum_i \phi_i n_i + \frac{1}{2} \sum_{i,j} \frac{e^2}{r_{ij}} (n_i - \nu)(n_j - \nu) \tag{3.1}$$

3.2 Coulomb gap

An important hallmark of such systems is the soft Coulomb gap ($\lim_{E \to 0} \rho(E) =$
$0; \rho(E \neq 0) \neq 0$) in the single particle density of states (DOS), $\rho(E)$, close to the
Fermi level. For many materials with compensated doping, including InO_x, the dis-
order is strong, i.e. $W \gg e^2/a$, where a is the typical distance between neighboring

---

[1]The contents of this chapter is based on work done in collaboration with Joe Mitchell, Victor
Galitski and Markus Müller and have been published in Phys. Rev. B, Vol. 85,195141

electrons. In that case, the Coulomb gap is theoretically predicted [40, 41] and empirically found [42] to be essentially universal at low energies: in two dimensions, $\rho(E)$ exhibits linear variation, $\rho(E) = \frac{\alpha}{e^4}|E|$. The co-efficient α is basically independent of the type of lattice, the filling fraction, and the details of the disorder [43, 44]. We find a value $\alpha \approx 0.35 \pm 0.01$ consistent with previous numerical studies [42, 45], but substantially smaller than Efros' analytical estimate $2/\pi$ [39]. The standard Coulomb gap shows up in transport as a stretched exponential resistance of the form

$$R(T) \sim R_0 \exp\left(\frac{T_0}{T}\right)^{\frac{1}{2}}. \tag{3.2}$$

The co-efficient in the exponent,

$$T_0 = C \frac{e^2}{\sqrt{\alpha}\xi_1}, \tag{3.3}$$

involves just one additional parameter: the average localization length, ξ_1, of single particle wavefunctions, apart from a numerical constant, whose value $4 \lesssim C \lesssim 5$ can be extracted from a percolation analysis of random resistor networks [39], as well as from Monte Carlo simulations [46]. Now we extend the Efros-Shklovskii model by allowing double occupancy and electron pairing (cf. Fig. 2.1 for an illustration) with the classical Hamiltonian

$$H = \sum_i \phi_i n_i + \frac{1}{2}\sum_{i,j} \frac{e^2}{r_{ij}}(n_i - \nu)(n_j - \nu) + \sum_i \frac{1}{2}U_i(\boldsymbol{B})n_i(n_i - 1) \tag{3.4}$$

The local attraction energies, U_i, for doubly occupied sites will be our control parameters driving the crossover from the electron-dominated regime (U large and repulsive) to the pair-dominated regime (U large and attractive). In between, we find a mixture of gapless single electron and pair states, which exhibits distinctly unique

22

features that can be captured in experiments. Note that the model (3.4) is also of interest for semiconductors in which doubly occupied sites (the upper Hubbard band) play a significant role [47, 48]. Many of the effects found here generalize in modified form to granular systems as well.

3.3 Single site density of states

3.3.1 Definitions

We start by analyzing the static properties of the two component electron glass. We consider the single site density of states (DOS) within typical metastable states. The latter are defined as classical occupancy configurations which are energetically stable with respect to moves of single electrons, pairs of electrons, as well as with respect to the formation of local pairs by combining two single electrons, or the reverse disintegration process. Let S_n be the set of sites with occupancy $n \in \{0, 1, 2\}$ in such a local minimum configuration. We refer to the total energy to add (remove) a single electron on site i as E_i^{1+} (E_i^{1-}), and as E_i^{2+} (E_i^{2-}) for pair excitations. We define the DOS for electron (pair) excitations, $\rho_{m=1(2)}$, as

$$\rho_m(E) = \frac{1}{N} \sum_{i \in \Sigma_m^+} \delta(E - E_i^{m+}) + \frac{1}{N} \sum_{i \in \Sigma_m^-} \delta(E - E_i^{m-}) \tag{3.5}$$

where N is the number of lattice sites, $\Sigma_1^+ = S_0 \cup S_1$, $\Sigma_1^- = S_1 \cup S_2$, $\Sigma_2^+ = S_0$, and $\Sigma_2^- = S_2$.

In the model without double occupancy ($U \to \infty$), imposing stability with

respect to all possible single-electron moves,

$$E_i^{1+} - E_j^{1-} - e_{ij} \geq 0, \quad e_{ij} \equiv \frac{e^2}{r_{ij}}, \tag{3.6}$$

is sufficient to induce the Coulomb gap in the DOS. Additional multi-particle constraints impose weaker conditions and have been shown to not significantly affect the low-energy profile of the DOS. In contrast, we show below that the presence of double occupancies results in additional constraints, which affect the Coulomb gap very significantly. In the following, we describe the evolution of the DOS as the attraction strength is tuned.

Clearly, for strongly repulsive U, when all double occupancies are forbidden, the system reduces to the standard Efros-Shklovskii model where the canonical Coulomb gap with slope $\alpha \approx 0.35$ is found in the single particle density of states ρ_1.

3.3.2 Spatially Uniform Interaction - Anomalous Coulomb gap

The case of a uniform pair interaction, $U_i = U \, \forall i$, can be understood essentially analytically. Fig. 3.1 illustrates the corresponding evolution of the DOS's with local interaction strength U, which were obtained from numerical simulations which we will describe below. In the attractive case, $U < 0$, all electrons remain paired in local minima, i.e. sites are either empty or doubly occupied. This is so because any singly occupied site would lower the energy by admitting a further electron brought in from far away. The pair-DOS, $\rho_2(E)$, is linear at low E, with the canonical slope $\frac{\alpha}{(2e)^4}$ corresponding to charges $2e$. This results from the pair stability constraint
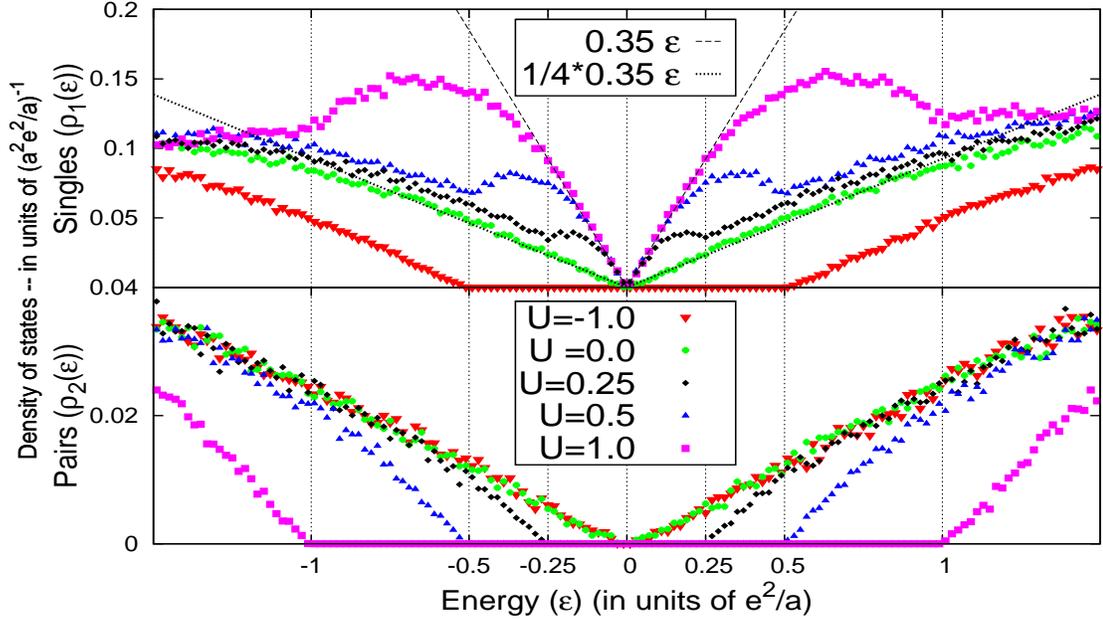
Figure 3.1: DOS for different uniform interaction U. $U = 0$ is a critical point at which both $\rho_{1,2}$ have a linear pseudogap. The slope of the single particle DOS ρ_1 is suppressed to $\alpha/4e^4$. For net repulsion, $U > 0$, ρ_1 has the canonical slope α/e^4 at lowest energy, followed by a hump at the scale $U/2$, crossing over to the critical slope, while pairs are gapped up to $E = U$. For $U < 0$, single electrons have a hard gap $|U|/2$, while pairs are pseudogapped with slope $\alpha/16e^4$. Note: For these plots, the chemical potential was explicitly zeroed when averaging the DOS over the various initial occupancy-distributions

analogous to Eq. (3.6),

$$E_i^{2+} - E_j^{2-} - 4e_{ij} \geq 0. \tag{3.7}$$

This condition automatically ensures stability with respect to single-electron moves and pair formation/disintegration and thus constitutes the dominant condition determining the low-energy pair-DOS. These assertions are easy to check case by case, using that for $U < 0$ single particle excitations are given by

$$E_i^{1\pm} = \frac{E_i^{2\pm} \pm |U|}{2}, \quad (U < 0), \tag{3.8}$$

on empty and occupied sites, respectively, being gapped up to energies $E_g = \frac{|U|}{2}$. As compared to a pair move, a single particle move does not only cost more in terms of onsite energy per particle, but also gives back less in terms of the polaronic interaction term e_{ij}. Likewise, one checks that if (3.7) is satisfied, it is always unfavorable to let a pair disintegrate into two single electrons, partly because one loses the attraction energy U, and partly because one does not gain as much polaronic energy back. The relation (3.8) implies that the single particle DOS is given by

$$\rho_1(E) = 2\rho_2(2E - \text{sgn}(E)|U|), \quad (U < 0). \tag{3.9}$$

From this it follows that the single-DOS at energies beyond the gap and close to it goes as $\rho_1(E) = \frac{\alpha}{4e^4}(|E| - E_g)$.

The point of no net interaction, $U = 0$, constitutes a critical point, where both $\rho_1(E)$ and $\rho_2(E)$ have soft excitations near $E = 0$. However, most remarkably, the slope of ρ_1 is reduced by a factor of 4 from its universal value α/e^4 in the canonical model, as if it were the Coulomb gap of a system with effective charge

$e^* = \sqrt{2}e$. This geometric mean of 2e and 1e arises because the gap imposed by the pair constraints (3.7) is probed by 1e excitations. Indeed, for each pair of sites admitting a pair move, the constraint

$$E_i^{1+} - E_j^{1-} - 2e_{ij} \geq 0 \tag{3.10}$$

must hold, as one obtains by inserting (3.8) for $U = 0$ into (3.7). This is indeed a more stringent constraint than Eq. (3.6).

On the repulsive side, $U > 0$, pairs are gapped up to energy $E_g = U$. Mathematically, this follows simply from the fact that on empty sites, one has

$$E^{2+} = 2E^{1+} + U, \quad U > 0, \tag{3.11}$$

with $E^{1+} > 0$, and an analogous relation for doubly occupied sites. Indeed, to accomodate a pair in a potential well, the well must be at least as deep as $-U$, which ensures that the second electron is just loosely bound. The minimum energy required to remove the pair from such a well is U. Similarly, injecting a pair into an empty site costs at least the repulsion U of the second electron.

On the other hand, for repulsive U, $\rho_1(E)$ remains ungapped. At low energies ($|E| \ll \frac{U}{2}$), the universal single-electron Coulomb gap with slope $\frac{\alpha}{e^4}$ emerges: indeed, the vast majority of stability constraints involving sites at these energies are single-electron constraints. At larger energies, $|E| \gg U$, one can ignore U in the stability constraints, which then reduce again to Eqs. (3.7,3.10) and thus lead to a slope of $\frac{\alpha}{4e^4}$ (for E below the Coulomb gap, $E_{\mathrm{Cb}} \sim \frac{(e^2/a)^2}{W}$). This immediately leads to an interesting prediction: in the repulsive case, at intermediate energies, $U/2 \leq |E| \leq U$, $\rho_1(E)$ is non-monotonic, as is indeed confirmed by the numerical data in Fig. 3.1.

Let us now characterize the single-DOS in this regime in more detail. At small positive $E \ll U$, $\rho_1(E)$ receives essentially equal contributions from empty and singly occupied sites. Likewise, for negative energies, it receives equal contribution from doubly and singly occupied sites . If we denote the respective contributions as $\rho_1^{(0)}(E)$, $\rho_1^{(1)}(E)$ and $\rho_1^{(2)}(E)$ (with superscripts denoting occupancies), we find empirically that

$$
\begin{aligned}
\rho_1^{(1)}(E) &\approx \rho_1^{(0)}(E) \approx \frac{\alpha}{2} \frac{E}{e^4}, \quad 0 < E \ll U, \\
\rho_1^{(1)}(E) &\approx \rho_1^{(2)}(E) \approx \frac{\alpha}{2} \frac{|E|}{e^4}, \quad 0 < -E \ll U,
\end{aligned}
\tag{3.12}
$$

i.e., the ground state occupation is practically uncorrelated with the excitation energy.

From Eq. (3.11) it follows that the pair DOS $\rho_2(E)$ satisfies

$$
\rho_2(E) = \frac{1}{2}\rho_1^{(0)}\left(\frac{E - \mathrm{sgn}(E)U}{2}\right).
\tag{3.13}
$$

Thus, from (3.12), beyond the pair gap it starts off as

$$
\rho_2(E) \approx \frac{\alpha}{8}\frac{|E| - U}{e^4},
\tag{3.14}
$$

as can be seen in Fig. 3.2

Note that the contribution to $\rho_1(E)$ from singly occupied sites is restricted to the energy range $|E| \le U$, since otherwise spontaneous particle rearrangements would occur. Further, $\rho_1^{(1)}(E)$ satisfies the simple relation

$$
\rho_1^{(1)}(E) = \rho_1^{(1)}(E - U), \quad 0 < E < U,
\tag{3.15}
$$

which expresses the relationship $E^{1+} = E^{1-} + U > 0$ between particle addition and
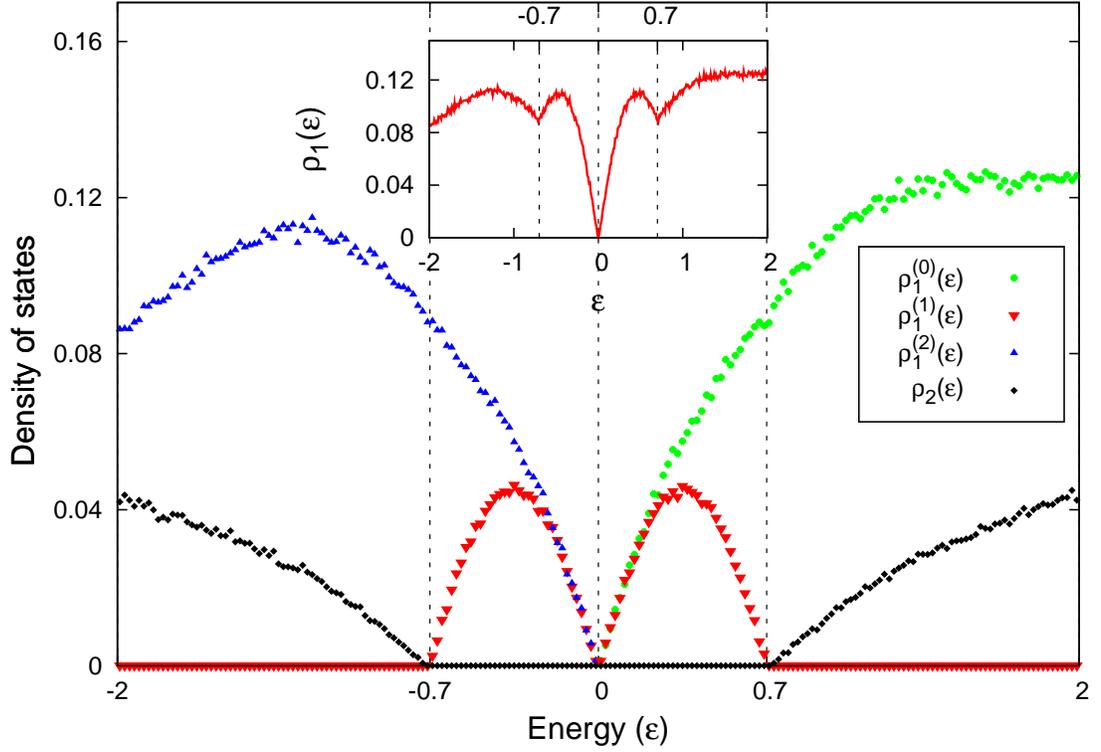
Figure 3.2: Breakup of the single-particle DOS $\rho_1(\epsilon) = \rho_1^{(0)}(\epsilon) + \rho_1^{(1)}(\epsilon) + \rho_1^{(2)}(\epsilon)$ for repulsive $U = 0.7$, split according to the site occupancies, as described by Eqns. 3.12, 3.13 and 3.14. Note that the contribution to $\rho_1(\epsilon)$ from singly-occupied sites ends at $\epsilon = \pm U$, exactly where the pair-DOS $\rho_2(\epsilon)$ begins. Inset: The dip in $\rho_1(\epsilon)$ corresponds to $\rho_1^{(1)}(\epsilon)$ going to zero at $\epsilon = \pm U$, as emphasized by the dashed lines.

removal for singly-occupied sites. Note that this implies in particular that

$$\rho_1^{(1)}(|E| \to U) \approx \frac{\alpha(U - |E|)}{2e^4} \qquad (3.16)$$

tends to zero at $E = \pm U$, and has a maximum around $E = \pm U/2$.

At the same time the contributions $\rho_1^{(0,2)}(E)$ to the single-DOS do not exhibit any sharp features at energies of order U, except that they smoothly roll-over from a slope $\frac{\alpha}{2e^4}$ at $|E| \ll U$ (cf. Eq. (3.12)), to a slope that approaches $\frac{\alpha}{4e^4}$ for $|E| > U$. As a result, the full single particle DOS, which is the sum of these two contributions, exhibits a local maximum around $E = \pm U/2$ and a local minimum around $E = \pm U$, essentially reflecting the properties of $\rho_1^{(1)}(E)$ imposed by the extra constraint (3.15). Very similar physics was found recently in granular systems [37] where the occupancy of sites is nearly unlimited, in which case Eq. (3.15) applies essentially to the whole 1-particle DOS, and imposes mirrored Coulomb gaps.

Despite the absence of quantum fluctuations, the described evolution of the DOS has a lot in common with quantum critical phenomena [49], where U plays the role of the detuning parameter from criticality. The critical behavior is restored at energies $|E| \gg |U|$, with linear DOS-s and anomalous slope of $\rho_1(E)$. At low energies, the non-critical phase appears, where one type of carriers is gapped out, while the other type exhibits a universal Coulomb gap. We also note that the features of the DOS and the underlying mechanisms found here have similarities with those in a recently proposed model of strongly and weakly interacting two-level systems [50].

3.3.3 Numerical simulations

In order to analyze further details of the DOS, as well as the case of random local interaction U_i, we performed numerical studies. To study metastable states, we start from a random configuration of occupancies, n_i ($\in \{0, 1, 2\}$), on a half-filled triangular lattice of size 200×200. We choose a triangular lattice with commensurate filling so as not to introduce extra strain in the system in the limit of weak disorder (note that if the filling is not commensurate there is still some strain from the lattice). However, we focus on strong disorder where the effect of the lattice type is expected to be small.

Following a similar protocol as described in [44], we allow re-distribution of occupancies through single particle moves, pair moves and pair dissociation/formation — the last one within a restricted spatial range — that lower the total energy of the system until the system stabilizes in a local minimum of the energy. In this context, it is important to recall that the appearance of the Coulomb gap in the single particle DOS does not require stability with respect to multi-particle moves, and is not very sensitive to the latter. This is because the single-particle moves impose the strongest stability constraints [44]. By a similar reasoning, the universal features in the DOS for uniform U in the model considered here result from single particle and pair stability constraints. It is thus reasonable to expect that the class of moves considered above imposes the strongest stability conditions, determining the essential features of the single site DOS-s, $\rho_1(E)$ and $\rho_2(E)$, for single electron and pair excitations, respectively. Further multiparticle processes may relax the

system to lower lying metastable states; however, such states are expected to have very similar single site density of states and transport properties. The single site DOS was obtained by calculating the histogram of the energies to add or subtract an electron or pair from each site, cf. Eq. (3.5). These DOS-s were averaged over many different disorder realizations, typically of the order of 100 for the 200×200 sized systems.

We measure all distances in units of the lattice constant a, and in our finite-sized samples, the intersite distance r_{ij}, has been chosen as the minimum distance on a torus defined by periodic boundary conditions. Energies are measured with reference to the chemical potential μ in units of the nearest neighbor Coulomb repulsion $\frac{e^2}{a}$. The chemical potential in this case is determined as the average of the smallest energy to add and remove an extra particle from a given metastable state. Pair energies are measured from the reference energy 2μ.

We choose the on-site disorder ϕ_i to be randomly distributed in the interval $[-W, W]$. It is well-known that a disorder of order unity or more is required for the DOS to tend to an essentially universal Coulomb gap, $\rho_1(E) = \frac{\alpha|E|}{e^4}$ at low energies. In our model, since a site is allowed to have double occupancy, the strong disorder condition is met when W exceeds the typical nearest neighbor interaction of two doubly occupied sites. In order to find DOS features which approach a universal limit, we therefore chose to work with disorder $W = 4$. At substantially weaker disorder the low energy DOS's were indeed found to be non-universal.
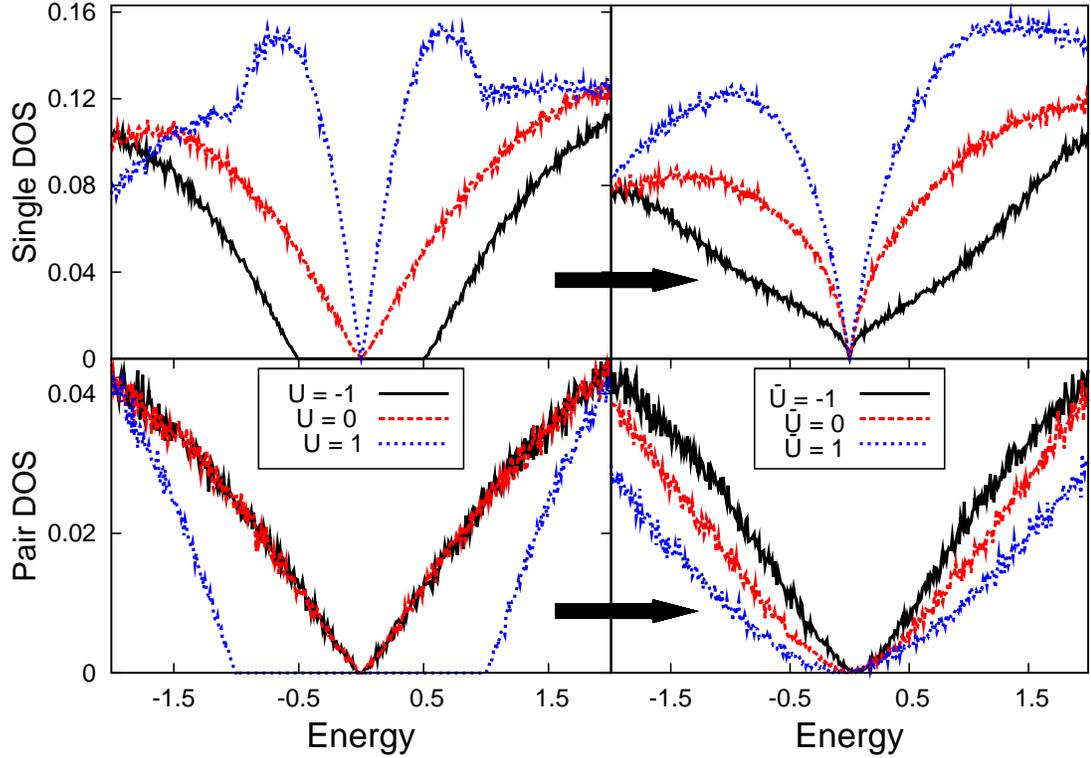
Figure 3.3: Comparison of the DOS's for constant (left) and random (right) U, with strong scatter $\Delta U = 2$ (units of e^2/a). The sharp gaps and humps are smoothed out by disorder, but the overall trend of increase/decrease of the low energy DOS remain intact.

3.3.4 Spatially Disordered Interaction

In a disordered system, it is more realistic that the pairing energies U_i are non-uniform. Fig. 3.3 shows the result for the DOS-s for a model with U_i distributed randomly in an energy range $\left[\overline{U} - \Delta U, \overline{U} + \Delta U\right]$. The sharp features of Fig. 3.1 are smoothened. The gaps in $\rho_1(E)$ and $\rho_2(E)$, for repulsive and attractive $\overline{U}$ respectively, are smeared out. Low energy single particle states leak into the gap of $\rho_1(E)$ as soon as there are positive U_i-s. The density of such states grows with increasing

33

$\overline{U}$, and eventually saturates to the standard linear pseudogap with slope $\frac{\alpha}{e^4}$. Closely analogous considerations apply to $\rho_2(E)$ upon decreasing $\overline{U}$. The detailed behavior in the intermediate regime $|\overline{U}| \leq \Delta U$ is complicated and presumably non-universal.

The non-monotonic humps in ρ_1 discussed in section 3.3.2 survive only if ΔU is sufficiently small as compared to $\overline{U}$. Thus they are probably best sought after in crystalline samples, where the local environment of different impurities are similar, giving rise to a narrow scatter, ΔU.

3.4 Transport and Resistance

3.4.1 Why transport calculations might differ from DOS-predictions

In an insulator, a reduced density of states is usually reflected in an exponentially increased resistance. It is thus interesting to ask what happens in the "mixed regime" of our model, where both pair and single electron excitations are ungapped. If transport was dominated by one type of excitation only, one would expect an increase of resistance upon approaching the mixed regime from either side, since the DOS of the dominant carrier type diminishes. However, transport is more complicated in this two-component Coulomb glass. Electron and pair hops do not take place independently in the sample, but combine to form a network of interconnected pair and single electron moves, as illustrated in Fig. 2.1. Transport is a complex functional of the *combined* density of states. In order to study this insulating regime, we have generalized the construction of an effective network of Miller-Abrahams resistors [51] which include both pair and single particle processes.

In order to elucidate the interplay between pair and single particle transport, we have neglected spin blocking effects in the random resistor network [47] (as may be justified in strong spin orbit coupled materials). Spin dependent effects may be considered elsewhere. The elementary hopping resistances were evaluated in a mean field fashion for selected metastable states [39, 52].

Details of the resistor network, the required steps and approximations, are described elsewhere. The only important point to note is the exponential dependence of the effective resistances of the network on temperature and localization length (for details, see concluding chapter). This restricts the accessed range of energies and typical hopping distances of the electrons participating in the network and using a percolation argument [53], one can determine the functional dependence of the resistance on temperature.

In presence of the Coulomb gap in the density of states, and if one type of carriers dominates the low T transport, the functional dependence is of Efros-Shklovskii type, cf. Eq. (3.2), with

$$T_0^{(i)} = C \frac{Q_i^2 e^2}{\sqrt{\alpha} \xi_i}, \tag{3.17}$$

where $Q_{i=1,2}$ is the charge of the carriers in units of e, ξ_i their average localization length and $C \approx 4-5$. These localization lengths may in principle be evaluated from an analysis of the elementary localized excitations above the ground state, whose spatial extent is governed by the hopping terms in Eq. 2.1. The magnetic field enters this localization length via phases in the hopping and resulting interference effects, as discussed e.g. in Ref. [54, 55]. However, for the purpose of analyzing the

effect of varying pairing strength, we assume the localization lengths to be constant. This may describe very well an experimental situation in which the local interaction U is tuned (by chemical modifications or gating), without affecting the localization lengths. In contrast, in the case where U is tuned by a magnetic field, the effects described below will necessarily be superposed over quantum interference effects, which affect $\xi_{1,2}$ rather sensitively and may well dominate the effects which we address below.

3.4.2 Result in Brief

The main result (which will be discussed in detail elsewhere) is that under certain circumstances we obtain a nonmonotonicity in resistance as a function of U. The latter is most prominent when we have $\frac{\xi_2}{\xi_1} = 4$, in which case the Efros-Shklovskii temperatures $T_0^{(1,2)}$ are the same for both single-electron and pair-transport resulting in an interesting competition when U is tuned across zero. In reality the ratio ξ_2/ξ_1 varies greatly across the phase diagram of disordered films with superconducting correlations. Indeed the localization length of preformed pairs must diverge at the transition to a superconductor, while ξ_1 remains non-critical [56, 57]. On the other hand, far in the insulating regime, ξ_2 is expected to become shorter than ξ_1, because pair tunneling is suppressed. Therefore a regime where $\xi_2 > \xi_1$ should certainly exist, and we consider the particularly interesting case $\xi_2/\xi_1 = 4$. We should keep in mind however, that such a large ratio presumably implies relatively strong quantum fluctuations, due to rather important hopping terms. With this caveat in mind, the

essentially classical description of the two-component Coulomb glass presented here should be taken as a phenomenological approach to capture Coulomb frustration effects on a system with variable range hopping transport of competing carriers.

3.5 Conclusion

The model discussed in this chapter, should be realized in disordered materials with a strong tendency for local attractions (negative Hubbard U). It also predicts interesting effects for cases where local interactions are moderately repulsive, such that multiple occupancy of sites is still possible. The occurrence of negative U interactions is likely to be concomitant with a bosonic type of superconductor-to-insulator transition upon further reduction of the disorder. In such samples, $\overline{U}$ may also be tuned by an external magnetic field which has a depairing effect on the electrons. However, since a magnetic field also sensitively affects localization lengths, it would be desirable to use other, non-magnetic means to influence the local interactions, too (such as pressure, chemical doping etc). If the disorder in the local U-s is large we find a regime around $\overline{U} \approx 0$, where both pairs and single electrons contribute to the activated transport, and a non-monotonic resistance as a function of U results.

For the strongly localized, classical limit of the two-component Coulomb glasses we found several interesting effects on the low energy density of states. In particular, we find that the tendency for local attraction leads to a suppression of the density *beyond* the standard Coulomb gap. At the point where local attraction and

repulsion balance to produce vanishing net interaction $U = 0$ we find that the 2d Coulomb gap is reduced by a factor of 4 from its canonical value. More generally, if multiple charging of the same site with M charges (without paying additional local charging energy) were allowed, one would find a suppression by a factor of M^2.

For the case of moderately repulsive interactions $U > 0$, if the randomness in the interaction energy ΔU is small compared to the average interaction $\overline{U}$, our model predicts the existence of non-monotonic humps in the single particle density of states. If pair transport is suppressed due to strong localization, the non-monotonicity of the single-electron DOS in the repulsive case $U > 0$ should show up as a kink in the resistance $R(T)$ around a temperature $T_* \approx (U/2)^2/(Ce^2/\xi)$, where it crosses over from an Efros-Shklovskii law with a higher value of T_0 to a less steep $R(T)$ and a twice smaller T_0 at lower T. The humps in ρ_1 should also leave traces in AC measurements [58], or more direct measurements of the DOS such as photoemission or tunneling from a broad junction [59]. These DOS features may also be relevant for the more involved experiments of memory effects in deep insulators [60, 61], where doubly occupied sites with repulsive interactions are known to be present [48].

A measurement of the pair-DOS, especially on the attractive side $U < 0$ could be attempted through measurement of the tunnelling conductance from a (wide) superconducting probe, similar to the experiments performed by Dynes et al [62].

In this work we have taken the localization lengths to be independent of the tuning of the local interaction strength. If the latter is tuned by magnetic field, a full description needs to take such quantum effects into account, however. In fact, it will be argued in the next chapter that the field dependence of localization lengths

of pairs and electrons are opposite, which is probably an important ingredient for a strong magnetoresistance peak. Here we show that, on top of that effect, the complex energetics and transport phenomena in the two component Coulomb glass can even enhance such a peak.

Chapter 4

Bosonic Anderson Insulator in a Magnetic Field

4.1   Introduction

Transport in Anderson insulators [5, 63] is crucially determined by the properties of localized wavefunctions. Their structure is very complex, both deep in the insulator, as well as upon approaching the delocalization transition, where they develop a multifractal structure [64]. A particularly important tool in probing the nontrivial structure of localized states in Anderson insulators is magnetoresistance. This is because a magnetic field sensitively affects the quantum interference which in turn influences quantum localization. This effect of the magnetic field has been studied extensively in the past concentrating mostly on non-interacting fermions [1, 2, 65].

Recent experiments on disordered superconducting films provide evidence for *bosonic* insulators with localized electron pairs as carriers [21, 66]. These and other similar systems feature a giant peak in magnetoresistance (MR) [17, 14, 20, 67, 68]. This is often interpreted as a crossover from bosonic to fermionic transport [69, 70], even though the details remain controversial. Bosonic localization problems arise also in disordered granular superconductors in the insulating regime, in cold bosonic atoms in speckle potentials (where artificial gauge fields can mimic a magnetic field) as well as in disordered quantum magnets.

The predominant mode of transport in disordered insulators is variable-range

hopping of carriers between localized excited states [39]. The spatial decay of wave-functions describing these localized excitations determines the inelastic hopping rate and thus the resistance. At low temperature, the (phonon-assisted) hops become significantly longer than the average distance between impurity sites hosting the excitations. In this situation, one needs to know the wave-function amplitudes at distances greater than the Bohr radius of an impurity state. At these distances, the amplitude is reinforced by multiple scatterings from intermediate impurities whereby many alternative paths interfere with each other [1, 65].

A perpendicular magnetic field affects the interference of the scattering paths on all length scales and modifies the localization properties. Interestingly, bosons and fermions behave very differently in this respect: while in the absence of a field fermion paths typically come with amplitudes of arbitrary signs, low energy bosonic amplitudes are positive and thus interfere in a maximally constructive way. The magnetic field suppresses this interference, yielding a strong positive magnetoresistance. It exceeds by far a largely opposite effect seen in fermions, which arises from a subtle suppression of negative interferences [71].

Despite numerous studies of fermionic MR [72, 1, 54, 73], a full understanding of the effect of magnetic field on the large-scale structure of localized wave-functions has not been obtained. In this chapter[1], we study the bosonic cousin of this problem and show that it is amenable to a complete solution. The simplifying circumstance is the absence of additional sign-factors in the latter quantum interference problem,

---

[1]The contents of this chapter is based on work done in collaboration with Victor Galitski and Markus Müller and can be found in arXiv:1210.3726

which allows a mapping to classical statistical mechanics of directed polymers in random media (DPRM). More generally, our analysis of MR is also valid for fermionic problems, provided the interfering paths have essentially only positive amplitudes. This arises, e.g., in the tunneling through the bottom of the conduction band in a solid semiconductor solution [74], or in fermionic impurity bands with Fermi level very close to the band bottom [2].

4.2   The model

Here we study a model of hard-core bosons on a square lattice,

$$H = \sum_i (\varepsilon_i - \mu)c_i^\dagger c_i - t \sum_{\langle ij \rangle} \exp\left[i \int_{\mathbf{r}_i}^{\mathbf{r}_j} d\mathbf{r} \cdot \mathbf{A} \right] c_i^\dagger c_j + \text{h.c.}, \tag{4.1}$$

with uniformly distributed on-site disorder in the range $\varepsilon_i \in [-W, W]$. We take $W = 1$ as the energy unit and consider weak nearest-neighbor tunneling, $t \ll W$. We fix the chemical potential to $\mu = 0$ to study a half-filled impurity band. A perpendicular magnetic field is introduced via the vector potential $\mathbf{A} = Bx\,\mathbf{e_y}$, with B being the flux per plaquette in units of the flux quantum.

We now focus on the spatial structure of an excitation localized around site i. It is characterized by the residue of the pole at $\omega \approx \epsilon_i$ of the retarded Green's function $G_{j,i}^R(\omega) = -i \int_0^\infty dt e^{i\omega t} \langle [c_j(t), c_i^\dagger(0)] \rangle$ [3] Its decay away from the site i defines a localization length. Deep in the insulating regime, $G_{j,i}^R$ can be evaluated using a

---

[2]In the impurity band model considered below, the distance of the Fermi level from the bottom of the band should be $\lesssim 10\%$ of the bandwidth for positive MR to occur in some range of finite B. At smallest B, MR of fermions is almost always negative, however [1, 2].

[3]This follows immediately from the Lehmann representation of the Green's function.

locator expansion [71]. To leading order in small hopping one obtains a sum over all paths Γ of shortest length [1, 2], dist(ij) (cf. Fig. 4.1: only right-going steps are allowed)

$$S_{ji}(B) \equiv \frac{1}{t^{\text{dist}(ij)}} \frac{G^R_{j,i}(\omega)}{G^R_{i,i}(\omega)}\bigg|_{\omega \to \varepsilon_i} = \sum_\Gamma e^{i\Phi_\Gamma(B)} J_\Gamma(\omega = \varepsilon_i), \qquad (4.2)$$

which is closely analogous to the sum over paths for fermionic Anderson insulators [5]. In Eq. (4.2) each path Γ contributes with an amplitude

$$J_\Gamma(\omega) = \prod_{k \in \Gamma \backslash \{i\}} \frac{\text{sgn}(\varepsilon_k)}{\varepsilon_k - \omega}. \qquad (4.3)$$

and an accumulated phase $\Phi_\Gamma(B) = \int_\Gamma d\mathbf{r} \cdot \mathbf{A}$. On average, the larger the excitation energy ε_i, the faster the spatial decay of $|S_{ji}|$ [71]. Henceforth, we focus on low-frequency excitations (relevant for transport at low T) and hence set $\omega = \varepsilon_i = 0$.

Within this "forward-scattering approximation" [1, 2], justified for $t \ll W$, bosons and fermions differ only by the presence and absence (respectively) of the factor $\text{sgn}(\varepsilon_k)$ in the amplitudes (4.3). For bosons, the amplitudes are all positive for $\varepsilon_i = 0$. A magnetic field destroys this complete constructive interference, and thus localizes the wavefunction more [54, 71, 75]. In contrast, typical fermionic problems [1, 2] feature amplitudes which vary in sign, depending on the number of sites on the path with $\varepsilon_i < \mu$ which are occupied in the ground state. In this case the dominant effect of a magnetic field lies in destroying negative interferences of competing paths, which tends to delocalize the wave function slightly. Both cases are readily amenable to efficient numerical studies via transfer matrices [1, 2, 72], which we use below. The results shown in Fig. 4.2 illustrate the opposite trends.

43
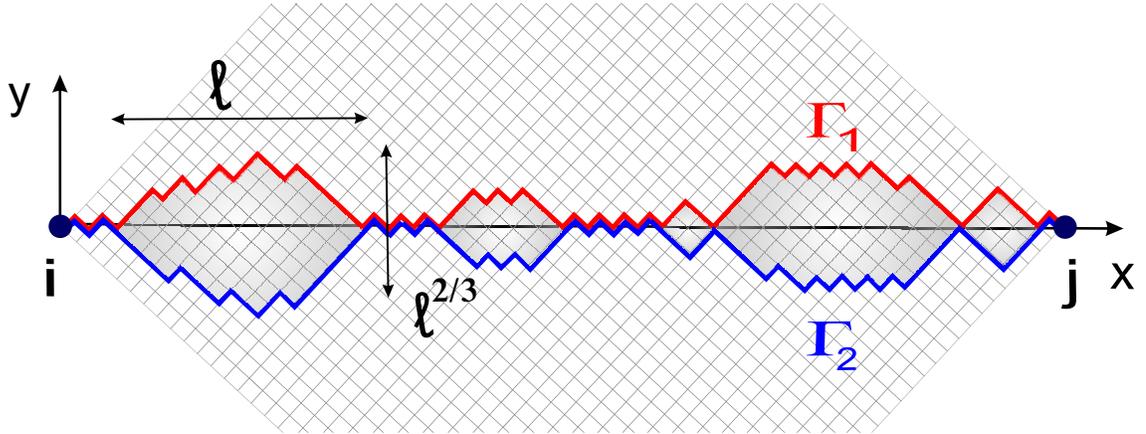
Figure 4.1: The approximation of directed propagation [1, 2] maps the wavefunction to a directed polymer. The droplet picture suggests that traces of localized wavefunctions, or low energy polymer configurations, form a string of loops of competing/interfering paths. Relevant loops of size ℓ have transverse roughness $\sim \ell^{\zeta=2/3}$). They are rare, being separated by a typical distance $\ell^{1+\theta} = \ell^{2\zeta} \gg \ell$. Two competing paths $\Gamma_{1,2}$ are shown, and the loops/droplets they form.

The relevant quantity for transport is the *typical* spatial decay of localized excitations. Therefore one focuses on the (typical) magnetoconductance, defined as [1, 2]

$$\Delta\sigma_N(B) = \exp\left(\overline{\ln[|S_{ji}(B)/S_{ji}(0)|]}\right), \quad N \equiv \mathrm{dist}(ij), \tag{4.4}$$

where the overbar denotes the disorder average. We take (i, j) on opposite corners of a square [4] (cf. Fig. 4.1). The linear variation with distance in Fig. 4.2 implies that at large scales B changes the typical decay rate, i.e., the inverse localization length $1/\xi$, of the excitations.

4.3 Numerical evaluation

One numerically evaluates $S_{ji}(B) \equiv S_{x_j,y_j}(B)$ (with i as origin) by recursion

$$S_{x+1,y}(B) = V_{x+1,y}\left[e^{i\phi_-}S_{x,y-1}(B) + e^{i\phi_+}S_{x,y+1}(B)\right] \tag{4.5}$$

with $\phi_\pm = \int_{\Gamma_\pm}\mathbf{A}\cdot d\mathbf{r}$, where $\Gamma_\pm : (x, y\pm 1)\to(x+1,y)$ are straight paths along the lattice links and $V_{x,y} = 1/|\varepsilon_{x,y}|$. $\Delta\sigma_N(B)$ evaluated from this varies as B^2N^3 for small (B, N) and shows a sharp crossover to $NB^{4/5}$ at larger fields/distances (cf. Fig. 4.3). The data for different N is found to collapse onto a scaling function

$$|\ln\Delta\sigma_N(B)| = N^{-1/3}\Phi\left(NB^{3/5}\right), \tag{4.6}$$

$$\Phi(x \ll 1) = b_1 x^{10/3} \quad ; \quad \Phi(x \gg 1) = b_2 x^{4/3}.$$

---

[4]This comes closest to the situation of more realistic disordered lattices where the disorder average is isotropic. [1, 2] Note that the Hamming distance N corresponds to the Euclidean distance measured in units of one half of the plaquette diagonal.
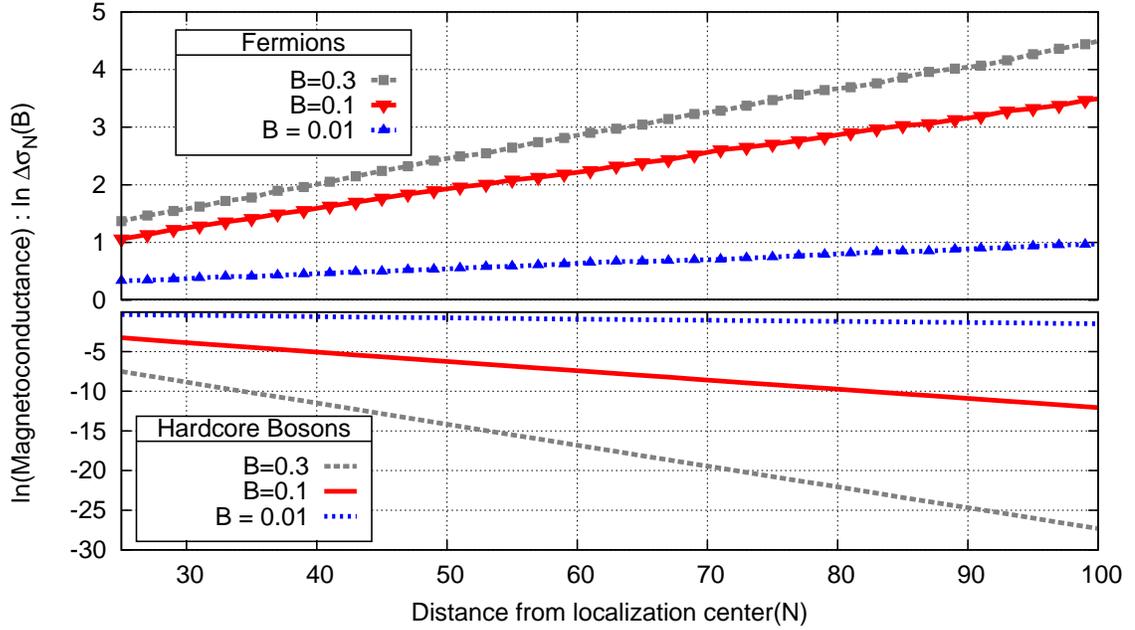
Figure 4.2: Magnetoconductance of fermions and bosons as a function of distance N in a half filled impurity band ($\mu = 0$). The linear dependence implies that the magnetic flux B changes the localization length ξ. While it increases slightly for fermions, it shrinks rather substantially in bosons.

with $b_1 \approx 0.31, b_2 \approx 0.56$. This scaling is expected theoretically from the physics of directed polymers (DPRM), as we explain below.

4.4 Mapping to directed polymers -

By virtue of the positive path amplitudes $S_{ji}(B = 0)$ can be interpreted as the partition sum of a DPRM in 1+1 dimensions [76, 77] with random onsite energies $\ln |\varepsilon_i|$ (at temperature $T = 1$) and ends fixed at sites i and j. Each polymer

configuration corresponds to a directed path Γ of the expansion (4.2).

In low dimensions, DPRM exhibit a pinned phase at large scales, as the random potential is relevant under renormalization [78, 79]. Beyond a characteristic pinning scale L_c (of the order of the lattice scale here), the random potential competes strongly with the polymer's entropic elasticity and induces roughness exceeding that of random walks: On longitudinal scales ℓ, typical transverse excursions of configurations grow as ℓ^ζ with $\zeta > 1/2$. A low energy excitation that differs from dominant configurations on scale ℓ, has typical excitation energy $E(\ell) \sim \ell^\theta$, with energy exponent $\theta = 2\zeta - 1$ [80]. In 1+1 dimensions (MR in 2d), the value $\zeta = 2/3$ is known exactly [81], while $\zeta_{3d} \approx 0.62$ is known numerically [82].

When $B \neq 0$, the polymer configurations acquire complex weights. Studies of ζ and θ exponents of complex DPRM [83] suggest that the scalings of the pinned phase do not change with complex weights. In fact, for fermions at $B = 0$, where negative path weights are abundant, there is numerical evidence that the wavefunctions are still governed by DPRM exponents [84, 85, 86]. One can thus assume that the DPRM exponents hold for finite fields as well.

It is interesting to note that for weak fields, Eq. (4.5) admits a continuum limit, where S obeys the equation

$$D_x S = D_y^2 S + V(x, y)S \tag{4.7}$$

with a δ-correlated random potential term $V(x, y)$ and $D_{\alpha=(x,y)} \equiv \partial_\alpha - iA_\alpha(x, y)$ being the gauge-covariant derivative (in Landau gauge $A_y = 0$). This generalizes the Kardar-Parisi-Zhang (KPZ) equation [87] to the presence of complex potentials
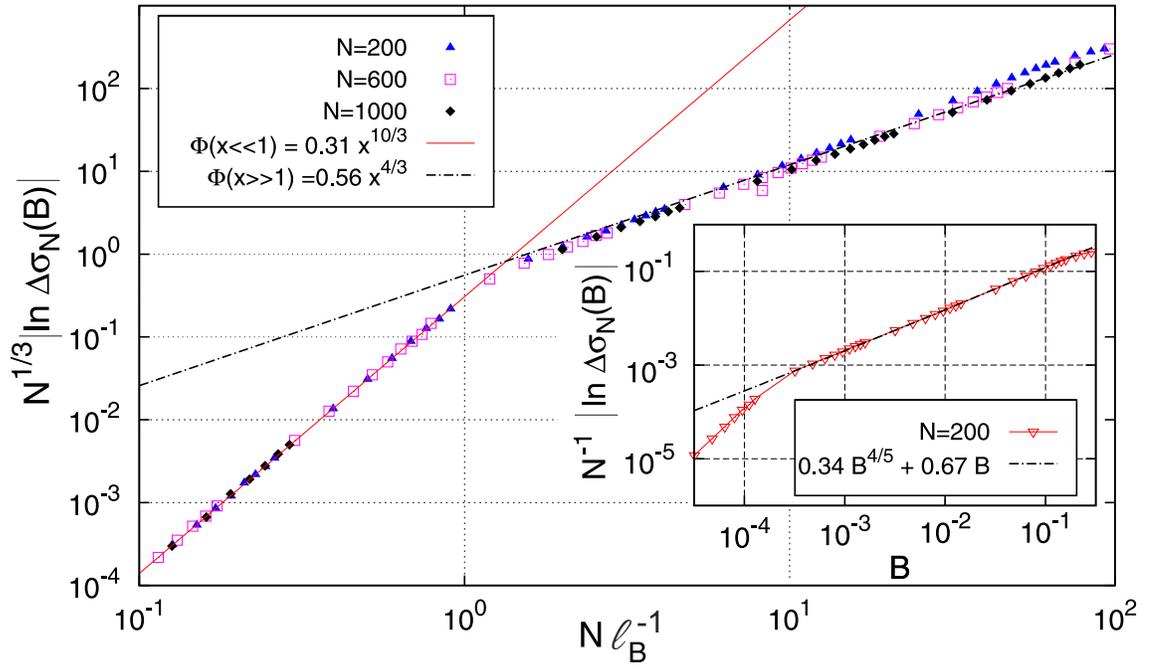
Figure 4.3: Scaling of the magnetoconductance, $\Delta\sigma$, with distance N and flux per plaquette, B. The crossover from the perturbative regime $|\ln\Delta\sigma_N(B)| \sim B^2 N^3$ to the non-perturbative regime $|\ln\Delta\sigma_N(B)| \sim NB^{4/5}$ occurs at $N \sim \ell_B$, where many successive interfering loops start contributing. Inset: change of inverse localization length for $N = 200$, and best fit to the leading virial terms (4.11), $\xi^{-1}(B) - \xi^{-1}(0) = c_1 B^{4/5} + c_2 B$.

$V \to V + iA_x$, and may render bosonic MR amenable to a field theoretic analysis similar to Refs. [88, 89]. However, a rigorous study of this modified KPZ equation is not attempted here.

In DPRM language, the magnetoconductance can be cast as a thermodynamic average of the phase factors $e^{i\Phi_\Gamma(B)}$ over polymer configurations, and the ratio of amplitudes S_{ji} takes the manifestly gauge-invariant form:

$$\left| \frac{S_{ji}(B)}{S_{ji}(0)} \right|^2 = \left[\frac{\sum\limits_{\Gamma,\Gamma'} e^{-E_\Gamma - E_{\Gamma'}} \cos\left(BA_{\Gamma\Gamma'}\right)}{\sum\limits_{\Gamma,\Gamma'} e^{-E_\Gamma - E_{\Gamma'}}} \right]. \tag{4.8}$$

Here $E_\Gamma = \sum_{k \in \Gamma \setminus i} \ln |\varepsilon_k|$ is the energy of configuration Γ, and $A_{\Gamma\Gamma'}$ is the oriented area enclosed by Γ and Γ'.

4.5   MR in weak fields

For weak fields or short distances one can evaluate $\Delta\sigma_N(B)$ perturbatively in B. Typical loops of linear extent ℓ enclose a flux $\sim B\ell^{1+\zeta}$. Of the N/ℓ possible independent loops only a fraction $\sim \ell^{-\theta}$ interfere significantly, cf. Fig 4.1, and are thus sensibly affected by B. As long as $N \ll \ell_B \equiv B^{-\frac{1}{\zeta+1}}$ the dominant contribution to Eqn. 4.8 comes from the largest loops of length $\ell \sim N$, which still enclose only a fraction of a flux quantum. This results in the magnetoconductance (4.4) $\Delta\sigma_N \propto -N^{-\theta}(BN^{1+\zeta})^2 = -B^2 N^3$. Note that the roughness exponent drops out of this perturbative result. We therefore recover the same scaling as previous authors predicted for interfering paths with positive weights [1, 2], even though they assumed random walk scaling, $\zeta = 1/2$. However, this coincidence hides the fact that typical wavefunctions are less strongly affected by B than might be suggested by $\Delta\sigma_N$, the

disorder average being dominated by rare events.

4.6 MR in strong fields

For $N > \ell_B$, DPRM scalings show more clearly in the magnetoresponse. The dominant contribution to $\Delta\sigma_N$ comes from reduced interference in loops of length ℓ_B, each of which decreases $\Delta\sigma_N$ by $O(1)$. Larger loops contribute similarly, but their probability to interfere significantly decreases as $\ell^{-\theta}$. On the other hand, smaller loops, albeit more abundant and likely to interfere, enclose a small fraction of a flux quantum, and thus have a negligible effect. The contribution from loops of size ℓ_B gives rise to an extensive $\ln(\Delta\sigma_N)$ proportional to the density of significantly interfering loops,

$$\frac{\ln\Delta\sigma_N}{N} \equiv -\Delta\left(\frac{1}{\xi}\right) \sim -\ell_B^{-1}\ell_B^{-\theta} = -B^{\frac{1+\theta}{1+\zeta}} = -B^{\frac{2\zeta}{1+\zeta}}. \tag{4.9}$$

This is equivalent to a reduction of the inverse localization length by $-B^{4/5}$ in 2d. In $3d$ the same arguments apply, with an exponent $2\zeta/(1+\zeta) \approx 0.765$. Both exceed the value $2/3$ obtained upon neglecting pinning and assuming random walk scaling with $\zeta = 1/2$ [1, 2, 90, 54].

So far we have discussed the leading scaling with magnetic field. However, the numerical data show small subleading corrections (cf. inset of Fig. 4.3). Those are indeed to be expected from spatially overlapping loops. To understand their effect, we introduce a hierarchical model which incorporates the essential ideas of droplet theory for directed polymers [79, 80]. At a given length scale L, the polymer has typically a preferred set of configurations, which compete with alternative,

subdominant sets of paths. The leading subdominant family of paths has a higher free energy by $O(L^\theta)$ and wanders off the dominant configuration by L^ζ, enclosing a typical loop area $O(L^{1+\zeta})$. This pattern repeats at all length scales. We simplify this phenomenology by considering a model where loops and alternative paths are restricted to lengths $L_k = N2^{-k}$ where $N \gg 1$ is the fixed distance between endpoints. Each parent loop of size L_k is composed of a dominant and a subdominant set of paths, each being made up of two successive loops of size L_{k+1}, cf. Fig. 4.4. We define the propagation amplitude over the distance N recursively. For a parent loop $\mathcal{L}$ at level k we encapsulate DP scaling by defining the amplitude

$$S_{\mathcal{L}}^k = S_{\mathcal{L}_1'}^{k+1} S_{\mathcal{L}_2'}^{k+1} + e^{-f_{\mathcal{L}} L_k^\theta} e^{i a_{\mathcal{L}} B L_k^{1+\zeta}} S_{\mathcal{L}_1''}^{k+1} S_{\mathcal{L}_2''}^{k+1}, \tag{4.10}$$

where $\mathcal{L}_{1,2}'$ and $\mathcal{L}_{1,2}''$ are the child loops along the dominant and the subdominant path, resp. $f_{\mathcal{L}} > 0$ and $a_{\mathcal{L}}$ are random variables of order $O(1)$, with a probability density $\rho(f_{\mathcal{L}}, a_{\mathcal{L}})$, assumed to be i.i.d. for all loops Ł. The recursion is closed by setting all $S_{\mathcal{L}}^k = 1$ for k with $L_k \lesssim \ell_B$ [5]. The magnetoresistance is defined as $\Delta\sigma_N = \overline{\ln(|S_{0N}(B)/S_{0N}(0)|)}$.

This model has elements in common with the hierarchical lattices analyzed in Ref. [91]. However, here we *explicitly* include the known scaling of excitation energies and areas of loops. The latter is necessary to discuss physically meaningful magnetoresponse. Note that significant interference between the paths $\mathcal{L}'$ and $\mathcal{L}''$ (as given in Eqn. 4.10) occurs only for rare 'active loops' $\mathcal{L}$ for which $f_L L^\theta \lesssim 1$.

[5]See the Appendix A, Sec. IA, for a discussion of the short scale cut-off, and an alternative definition of the hierarchical model with no restriction on the loop lengths.
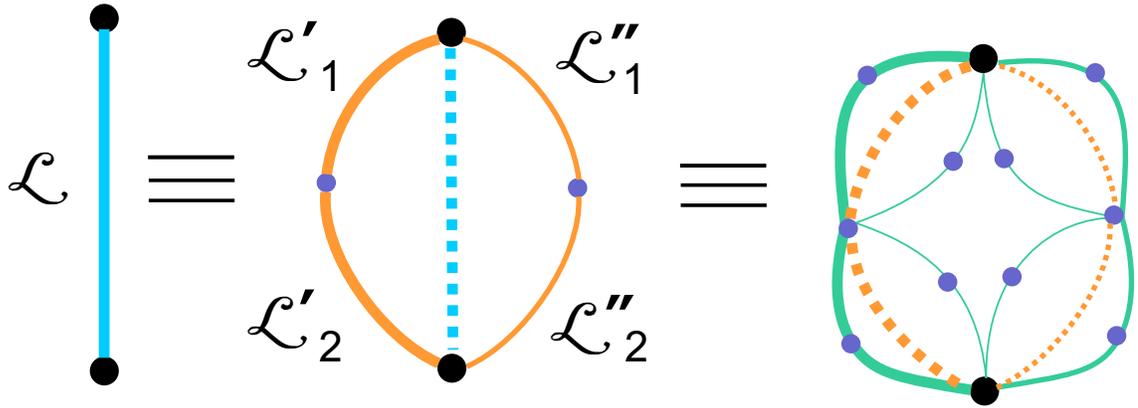
Figure 4.4: Hierarchical droplet model for computing $\Delta\sigma_N$, showing the hierarchical construction. At each level, contribution from a parent loop $\mathcal{L}$ (composed of a dominant and subdominant branch) is split into four loops, two along the dominant branch ($\mathcal{L}'$) and two along the subdominant one ($\mathcal{L}''$)(indicated by relative thickness), cf. Eqn. 4.10. The parent levels are denoted by dashed lines while the splitting of a branch into two successive loops at the next level are indicated by dots.

The perturbative scaling $\Delta\sigma_N \sim B^2 N^3$ is easy to obtain in this model [6]. In the non-perturbative regime ($N \gg \ell_B \gg 1$), using that active loops are sparse, one can expand $\ln \Delta\sigma_N(B)$ in powers of the density of active loops of linear size ℓ_B, [7]

$$\frac{\ln \Delta\sigma_N(B)}{N} = -B^{\frac{2\zeta}{1+\zeta}}[c_1 + c_2 B^{\frac{\theta}{1+\zeta}} + c_3 B^{\frac{2\theta}{1+\zeta}} + \cdots], \qquad (4.11)$$

where the constants c_i depend only on the distribution $\rho(f, a)$. Similar to the Mayer cluster expansion for a system of interacting particles, one obtains a term of $O\left(B^{(1+n\theta)/(1+\zeta)}\right)$ by collecting contributions with exactly n active loops. The leading coefficient c_1 is positive definite, and we found $c_2 > 0$, independently of our choice of the distribution $\rho(f, a)$. Subleading terms due to interfering loops thus enhance the negative MR of bosons. This may explain a similar effect seen in the numerical data on the original lattice (inset of Fig. 4.3), where a fit yields $c_1 \approx 0.34, c_2 \approx 0.67$, and hence, $\ln \Delta\sigma$ appears to follow a power with slightly larger exponent than $4/5$ at finite B.

4.7   Experimental consequences -

In variable-range-hopping transport at fixed T, the resistance depends on the localization length as $R(\xi) = \rho \exp\left(A/\xi^\alpha\right)$, with $\alpha = 1/2$ with Coulomb gap and $2/3$ without (Mott's law in $d = 2$) [39]. According to (4.9) a perpendicular magnetic field reduces the bosons' localization length ξ as

$$1/\xi(B) \approx 1/\xi + \Delta[1/\xi](B), \quad B_{\min} \lesssim B. \qquad (4.12)$$

---

[6]See Sec. II, Appendix A, for details.

[7]See Sec. IB, Appendix A, for details.

where $B_{\min} = [\xi \ln(R(0)/\rho)]^{-5/3}$ is the field required for ℓ_B to be shorter than the typical hopping distance. To lowest order this effect increases the resistance by the factor

$$R(B)/R(0) = [R(0)/\rho]^{\alpha\,\xi\Delta[1/\xi]}, \quad B_{\min} \lesssim B. \tag{4.13}$$

For $B \ll 1$, the exponent is $\alpha c_1 \xi B^{4/5}$. For $B \to 1$, it receives subleading enhancements, reaching values as big as $0.3\alpha\xi$ [8] , cf. Fig. 4.3. As resistances up to $R(0)/\rho \sim 10^6$ are measurable, and localization lengths $\xi \lesssim 2$ are expected to be within the regime of applicability of forward scattering (as loops are sufficiently suppressed) our theory predicts positive bosonic MR by factors of up to two orders of magnitude, within both theoretical and experimental limitations. The effects are even stronger when resonances are suppressed, and we also expect an extra enhancement in the critical regime where loops must be included. In rather stark contrast, the analogous fermionic problem exhibits negative MR, however, with a much smaller maximal amplitude of the effect (cf. Fig. 4.2). The size and importance of the bosonic MR makes it likely to be a key ingredient in the positive magnetoresistance side of the MR peak observed in superconducting films with pre-formed pairs [17].

---

[8]Upon excluding resonances by constraining $\epsilon_i \in [-1, -1/2]\cup[1/2, 1]$, one can reach even higher values of MR. The exponent in Eqn. 4.13 increases to $0.6\alpha\xi$ leading to an enhancement of almost four orders of magnitude.

PART II. DEFECTS IN SUPERCON-DUCTING QUBITS AS TWO-LEVEL SYS-TEMS

Chapter 5

Mapping of charge TLS in E-field to spins in B-field

As mentioned in the introduction, this section of the thesis concentrates on a completely unrelated problem : that of dielectric losses in superconducting qubits. First, we make a brief note of the experimental literature. Qubits are quantum analogs of the classical units of storage which can assume a value one or zero at any given time. Physical representations of classical bits therefore occupy one of two possible states at any given time. A quantum bit on the other hand can be in a quantum superposition of the two states. Not only that, a physical representation of a quantum bit has to be able to store the superposed state sufficiently long enough for a readout.

Of solid-state realisations of qubits, superconducting circuits are the preferred choice due to the macroscopically coherent ground state of superconductors. Because of the superconducting gap, low-energy excitations are eliminated which counters the effect of a large number of degrees of freedom in a typical solid-state representation. This makes it possible to preserve the quantum state of the superconducting qubit, an essential requirement for any qubit implementation. However, interactions with the environment cannot be completely avoided because of the necessity to perform and read out results of operations on the qubits. It is in these necessary interactions with the environment that the bulk of the losses in SC qubits are introduced (an

inherent contradiction in any qubit operation).

Superconducting qubits are essentially nonlinear resonators comprising of the Josephson inductance of a superconductor-insulator-superconductor tunnel junction and the capacitance of the junction (see Fig. 5 for a schematic representation). Loss of coherence in these qubits occur due to noise in these electrical elements.

Traditionally, the loss of energy in the capacitors has been ignored under the assumption that at low temperatures, this is not a major source of decoherence. In fact, it has been found [99] that crystalline materials like Si and Al_2O_3 exhibit negligible loss in that way. However, wiring in more sophisticated superconducting devices typically require amorphous SiO_2 which is much more lossy at low drive amplitudes [11].

It was seen in the same paper that the qubit shows avoided level crossings as the qubit bias voltage is changed. It was conjectured that this is due to resonant coupling with two-level systems inside the amorphous tunnel barrier. Plotting the density of avoided level crossings versus the size of the crossing, the authors found a dependence which could be justified if the dielectric losses originated from an ensemble of identical two-level systems (TLS-s). This confirmed that the primary loss mechanism in the qubits are two-level systems in the dielectrics forming the tunnel barrier. Thus it is essential to study TLS dynamics in order to probe losses in SC qubits. We shall describe this in more detail in the next chapter. Here, we give a brief overview of the general theoretical approach in this field.

The dielectric losses are typically modelled through tunneling states absorbing radiation from an electromagnetic field. The tunneling states are essentially asym-
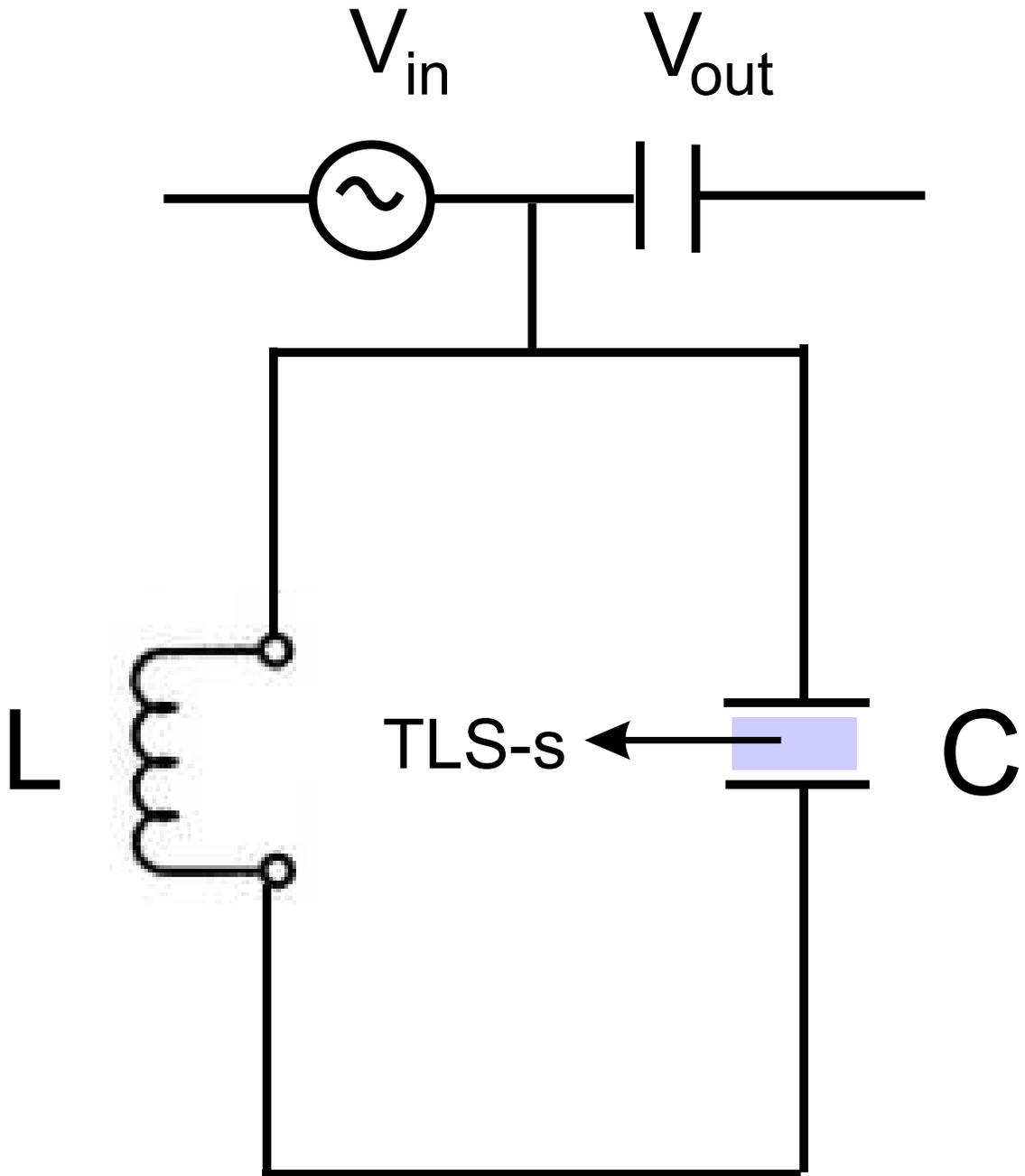
Figure 5.1: Schematic representation of a superconducting qubit. The primary source of loss/decoherence comes from the dielectrics in the capacitive elements. These losses can be modelled through an ensemble of identical two-level systems (TLs-s) interacting with an external electromagnetic field.

metric double wells with a wide distribution of asymmetry and barrier heights. In this section, we describe how to map these tunneling states to spins in a magnetic field and how a solution for the latter problem can lead to a frequency dependence of the dielectric constant.

5.1   Tunneling states to two-level systems to spins

The idea of tunneling states was first considered in the context of polyatomic molecules. It was noted by Hund [92] that despite the symmetry of the molecules with respect to certain changes in orientation, a particular orientation of the molecule was more prevalent in nature than the other. A classic example is the sugar molecule which exists in the form of two optical isomers, which are exact mirror images of each other. However, in nature, glucose is found to be strongly dextrorotatory.

To explain this anomaly, Hund introduced the concept of tunneling states. He proposed that a symmetric harmonic-oscillator double-well captures the two chiralities of the sugar molecule in the above example. Solving the Schrödinger equation for a particle in this double-well [93], one obtains that the normal single-harmonic oscillator states (with frequency ω) are split in pairs. Typically, one concentrates on the lowest-energy pair comprising of a symmetric and an antisymmetric eigenstate. If the particle is in one of these eigenstates, by definition, it stays in that state forever. However, if instead of an eigenstate, the particle was initially localized in one of the wells, it oscillates between the two wells at the frequency [93]

$$\omega_t = 2\omega(2V_0\pi\omega)^{1/2}\exp(-2V_0\omega) \tag{5.1}$$

where V_0 is the height of the barrier between the two potential wells. This exponential factor makes the oscillation frequency critically dependent on the barrier height and for large enough barriers, this frequency can be almost negligible giving the impression of the particle being localized in one of the wells.

The concept of tunneling states in solid state systems was first introduced by Pauling [94]. He was investigating an unrelated question of how the rotational states of a polyatomic molecule were changed when the molecule crystalized into a lattice. If ϕ is the rotation angle, he modelled the crystal field through the potential

$$V(\phi) = V_0 \left[1 - \cos(2\phi)\right] \tag{5.2}$$

This again had two minima, only this time as a function of an angular co-ordinate ϕ instead of a linear co-ordinate. The eigenstates again came in pairs $\{\psi_i^1, \psi_i^2\}$ with energies $\{E_i^1, E_i^2\}$ respectively. If $E_i = \left(E_i^1 + E_i^2\right)/2$ was the average energy of a pair i, then the condition that one can focus exclusively on the lowest energy pair at low enough temperature is given by

$$\left| E_i^2 - E_i^1 \right| \ll E_{i+1} - E_i \tag{5.3}$$

The use of an asymmetric double-well model to describe losses in dielectrics was first done by W. A. Phillips [95]. Although the two potential minima in a crystal field (with respect to orientation angle ϕ) are symmetric, in presence of an electric field, the dipole moment $\mathbf{p}$ of one orientation of the molecule gets energetically more favored by the $\mathbf{p}.\mathbf{E}$-coupling as compared to the other. In presence of a weak dc-electric field, it is thus more natural to use the asymmetric double well-potential instead of the symmetric one. If the asymmetry is small compared to barrier height,

condition 5.3 still holds and one can continue to focus on the lowest-energy pair at low temperatures. It is this pair that will be mapped onto two-level systems (TLS) which contribute to energy loss in dielectrics.

One can project the Hamiltonian of the system to a basis of the two lowest-energy states $\{\Phi_1^0, \Phi_2^0\}$ localized in one or the other of the potential minima. In this localized-state basis, the Hamiltonian can be written as

$$H = \begin{pmatrix} -\epsilon & \Delta \\ \Delta & \epsilon \end{pmatrix} \tag{5.4}$$

where ϵ is the difference in energy between the two energy minima and Δ is the coupling energy between the two wells. Diagonalizing this matrix, one easily obtains the eigenenergies of the lowest-lying pair

$$E_0^1 = -\sqrt{\epsilon^2 + \Delta^2}, \quad E_0^2 = \sqrt{\epsilon^2 + \Delta^2} \tag{5.5}$$

The wave-functions of the two lowest-lying eigenstates are given by

$$\psi_1^0 = \Phi_1^0 \cos\delta + \Phi_2^0 \sin\delta,$$

$$\psi_2^0 = \Phi_1^0 \sin\delta - \Phi_2^0 \cos\delta. \tag{5.6}$$

where

$$\tan 2\delta = \frac{\Delta}{\epsilon} \tag{5.7}$$

Any two-dimensional traceless, Hermitian matrix can be expressed in terms of the Pauli sigma matrices

$$\sigma_x = \begin{pmatrix} 0 & 1 \\ 1 & 0 \end{pmatrix}, \quad \sigma_y = \begin{pmatrix} 0 & -i \\ i & 0 \end{pmatrix}, \quad \sigma_z = \begin{pmatrix} 1 & 0 \\ 0 & -1 \end{pmatrix} \tag{5.8}$$

In the localized-state-basis $\{\Phi_1^0, \Phi_2^0\}$, the Hamiltonian can be written as

$$H = \epsilon\sigma_z + \Delta\sigma_x \qquad (5.9)$$

while in the eigenstate-basis $\{\psi_1^0, \psi_2^0\}$,

$$H = \sqrt{\epsilon^2 + \Delta^2}\sigma_z \qquad (5.10)$$

With the formal mapping of the Pauli sigma matrices to spins, $\mathbf{S} = \frac{\sigma}{2}$, one obtains the Hamiltonian of a single spin in a magnetic field

$$H = -\mathbf{B}.\mathbf{S} \qquad (5.11)$$

where $\mathbf{B} = \{\Delta, 0, \epsilon\}$ in the localized-state basis and $\{0, 0, \sqrt{\epsilon^2 + \Delta^2}\}$ in the diagonal basis.

One can now introduce the additional complication of a time-varying electric field $\mathbf{E}$ (or strain field) on top of the dc-field contributing to the asymmetry. It is generally assumed in TLS theory [96, 97] that the effect of this electric/strain field is confined to a change in the asymmetry energy ϵ – change in the coupling Δ can be ignored. The validity of this approximation stems from the fact that the wavelength of the em-field photons or the strain-field acoustic phonons is much greater than the spatial extent of a two-level system. Thus the electric field can be considered approximately uniform in that spatial extent leading to almost negligible change in the barrier height; however the asymmetry arising from the difference in coupling of the two dipole moments with the electric field is changed significantly.

Thus, the interaction Hamiltonian H_{int} is diagonal in the localized-state basis. Transforming to the eigenstate basis, one obtains the following form for H_{int} [98] :

62

$$H_{\text{int}} = \begin{pmatrix} \cos 2\delta & \sin 2\delta \\ \sin 2\delta & -\cos 2\delta \end{pmatrix} (\mathbf{d} \cdot \mathbf{E}) = \left[\frac{\epsilon}{\sqrt{\Delta^2 + \epsilon^2}} \sigma_z + \frac{\Delta}{\sqrt{\Delta^2 + \epsilon^2}} \sigma_x \right] (\mathbf{d} \cdot \mathbf{E}) \quad (5.12)$$

where $\mathbf{d}$ is the dipole moment when the particle is localized in one of the two minima (in other words, for a particular orientation of the polyatomic molecule). Thus, in the diagonal basis, the 'magnetic field' to which the equivalent spins are subjected assumes a form $\mathbf{B} = (B_x = \mathbf{d} \cdot \mathbf{E} \cos 2\delta, 0, B_z = \mathbf{d} \cdot \mathbf{E} \sin 2\delta)$. It must be noted that for a time-varying electric field, in the localized-state basis, only B_z is time-varying while in the eigenstate basis, both B_x and B_z are time-varying. We shall consider the former basis in the calculations of the following chapter.

5.2   Dielectric power loss in terms of tunneling states

The interaction of two-level systems with electromagnetic fields is a subject extensively treated in the context of atomic physics. The treatment of TLS in dielectrics follows along those lines. In this section, we describe the frequency dependence of power loss in dielectrics in terms of tunneling states with a broad distribution of barrier height and asymmetry.

In the eigenstate-basis $\{\psi_1, \psi_2\}$ (superscript '0' from earlier, denoting ground state-pair of the asymmetric double-well suppressed), a general state of the two-level system can be written as

$$\Psi(t) = c_1(t)e^{iEt}\psi_1 + c_2(t)e^{-iEt}\psi_2 \quad (5.13)$$

with $E = \sqrt{\Delta^2 + \epsilon^2}$. Normalisation imposes the condition $c_1^* c_1 + c_2^* c_2 = 1$. The form

of the co-efficients in Eqn. 5.13 for a general time-varying state represents what is known as the interaction picture of time-dependent quantum mechanics.

Time-variation of the co-efficients $c_1(t)$ and $c_2(t)$ in presence of an ac-electric field $\mathbf{E}(t)$ are obtained from solving the time-dependent Schrödinger equation for $\Psi(t)$

$$H\Psi(t) = i\frac{\partial \Psi(t)}{\partial t} \tag{5.14}$$

with the full Hamiltonian

$$H = [E + \mathbf{d} \cdot \mathbf{E}(t)\cos 2\delta]\,\sigma_z + [\mathbf{d} \cdot \mathbf{E}(t)\sin 2\delta]\,\sigma_x = H_0 + H_{\mathbf{int}}(t) \tag{5.15}$$

with $H_0 = E\sigma_z$ being the zero-field Hamiltonian and $H_{\mathrm{int}} = (\mathbf{d} \cdot \mathbf{E}(t))(\sigma_z \cos 2\delta + \sigma_x \sin 2\delta)$ the interaction with the external field. Note that in all instances where it has been mentioned, $\mathbf{d} = q\mathbf{x}$ where $\mathbf{x}$ is the expectation value of the position operator when the particle is localized in one of the two potential minima.

Substituting Eqn. 5.13 and Eqn. 5.15 in Eqn. 5.14, we obtain the following equations for the time-variation of the co-efficients

$$i\frac{dc_1}{dt} = \left[\langle \psi_1 | H_{\mathrm{int}} | \psi_1 \rangle\, c_1 + \langle \psi_1 | H_{\mathrm{int}} | \psi_2 \rangle\, e^{-2iEt} c_2 \right] \tag{5.16}$$

$$i\frac{dc_2}{dt} = \left[\langle \psi_1 | H_{\mathrm{int}} | \psi_2 \rangle\, e^{2iEt} c_1 + \langle \psi_2 | H_{\mathrm{int}} | \psi_2 \rangle\, c_2 \right] \tag{5.17}$$

where we have transferred to a bra-ket notation. Since $c_1(t)$ and $c_2(t)$ are complex variables related by the normalization condition, they can be represented by three real variables. By convention, this information is obtained through time evolution

of the following variables

$$u = c_1^* c_2 e^{2iEt} + c_1 c_2^* e^{-2iEt} \tag{5.18}$$

$$v = i \left[-c_1^* c_2 e^{2iEt} + c_1 c_2^* e^{-2iEt} \right] \tag{5.19}$$

$$w = c_1^* c_1 - c_2^* c_2 \tag{5.20}$$

This choice of variables is particularly convenient due to a closure property : the differential equations for the time evolution of any variable in the set $\{u, v, w\}$ involves only terms linear in the other two variables. The reason behind this is particularly illuminating if we recast the variables in the spin-language introduced in the previous section. One notes that

$$u \to \langle S_x \rangle, \quad v \to \langle S_y \rangle, \quad w \to \langle S_z \rangle \tag{5.21}$$

where the notation $\langle \cdots \rangle$ denotes expectation value in the state $\Psi(t)$, i.e. $\langle S_i \rangle = \langle \Psi(t) | S_i | \Psi(t) \rangle$. Thus, in the spin language, one can embody the evolution of a generic state under the influence of a magnetic field through the evolution of the expectation values $\langle S_i \rangle$.

One can calculate these expectation values by considering the time-dependant spin-operator in the interaction picture $S_i(t) = e^{iH_0 t} S_i e^{-iH_0 t}$. These operators obey the Heisenberg equations of motion

$$\frac{dS_i}{dt} = i \left[H_{\text{int}}, S_i \right] = (\mathbf{S} \times \mathbf{B})_i, \quad i \in \{x, y, z\} \tag{5.22}$$

where the field $\mathbf{B}$ follows from the mapping of the TLS to a spin problem. The second equality follows from the spin commutation relations. One can take the

expectation value of both sides of Eqn. 5.22 with respect to the state $e^{iH_0 t}\,|\Psi(0)\rangle$ which leads to an equation of the same form as 5.22 with S_i replaced by $\langle S_i \rangle$.

So far, we have included only interaction with a driving field. One can phenomenologically introduce an interaction with a bath of thermal phonons into the above set of equations. The claim is that the population difference between the ground state and excited state $(c_1^* c_1 - c_2^* c_2 \equiv \langle S_z \rangle$)tends to relax to its equilibrium value

$$\langle S_z \rangle_{\text{eq}} = \tanh\left(\frac{E}{k_B T}\right) \tag{5.23}$$

with a relaxation time T_1. At the same time, any coherence between the states ψ_1 and ψ_2 relaxes to zero with a second relaxation time parameter T_2. Including these in Eqn. 5.22, one obtains the well-known Bloch equations first discovered in the context of nuclear magnetic resonance

$$\frac{d\langle S_x \rangle}{dt} = \langle S_y \rangle B_z - \langle S_z \rangle B_y - \frac{\langle S_x \rangle}{T_2} \tag{5.24}$$

$$\frac{d\langle S_y \rangle}{dt} = \langle S_z \rangle B_x - \langle S_x \rangle B_z - \frac{\langle S_y \rangle}{T_2} \tag{5.25}$$

$$\frac{d\langle S_z \rangle}{dt} = \langle S_y \rangle B_z - \langle S_z \rangle B_y - \frac{\langle S_z \rangle - \langle S_z \rangle_{\text{eq}}}{T_1} \tag{5.26}$$

$$\tag{5.27}$$

One can solve the Bloch equations for a time-harmonic magnetic field $\mathbf{B}(t) = \mathbf{B}^0 \cos(\omega t)$ under the assumption that B_z^0 can be treated perturbatively. The standard procedure is to linearize the equilibrium expectation value $\langle S_z \rangle_{\text{eq}}$ as

$$\langle S_z \rangle_{\text{eq}}(B_z(t)) = \tanh\left(\frac{E}{k_B T}\right) + \frac{B_z'(t)}{k_B T} \operatorname{sech}^2\left(\frac{E}{k_B T}\right) \tag{5.28}$$

We intend to explore beyond this linearization procedure in the next chapter and find a particular class of nonlinear solutions to the Bloch equation.

However, to complete the narrative, the next step involves looking for a time-harmonic solution for the spin expectation values

$$\mathbf{S}(t) = \sum_n \mathbf{S}^n e^{in\omega t} \tag{5.29}$$

From this solution, one can find the linear magnetic susceptibility defined as

$$S_x^1 = \chi_x(\omega) B_x^0 \tag{5.30}$$

$$S_z^1 = \chi_z(\omega) B_z^0 \tag{5.31}$$

We simply state the result below

$$\chi_x(\omega) = \frac{S_z^0}{2} \left[\frac{1}{E + \omega - iT_2^{-1}} + \frac{1}{E - \omega + iT_2^{-1}} \right] \tag{5.32}$$

$$\chi_z(\omega) = \frac{1}{k_B T} \operatorname{sech}^2 \left(\frac{E}{k_B T} \right) \frac{1 - i\omega T_1}{1 + \omega^2 T_1^2} \tag{5.33}$$

with

$$S_z^0 = \frac{1 + (E - \omega)^2 T_2^2}{1 + (B_x^0)^2 T_1 T_2 + (E - \omega)^2 T_2^2} \tanh \left(\frac{E}{k_B T} \right) \tag{5.34}$$

Note the different forms of the susceptibilities : while $\chi_x(\omega)$ has the form of a resonant response, $\chi_z(\omega)$ describes a relaxation process at work. At this point, one can map back to the original two-level system problem to obtain a frequency dependent electric susceptibility with the resonant response given by $\chi_x(\omega)$ and the relaxation response given by $\chi_z(\omega)$. It is this frequency dependence of the electric susceptibility that determines the power loss in dielectrics.

With this brief introduction, in the next chapter, we derive a class of nonlinear solutions of the Bloch equation by reverse-engineering the magnetic field in the spin Hamiltonian to obtain a solvable model.

Chapter 6

Exact solution for quantum dynamics of a periodically-driven

two-level system

6.1 Introduction

The problem of a periodically-driven two-level system (TLS) appears in many physical contexts including magnetism, superconductivity, structural glasses and quantum information theory. [100, 101, 12, 102, 103, 104, 105] The interest in this old problem has been revived recently due to advances in the field of quantum computing (see, *e.g.*, Refs.[106, 107, 108, 109, 110] and references therein). First of all, a qubit itself is a two-level system and the question of its evolution under an external time-dependent perturbation is obviously of interest. Also, the physical mechanism that currently limits coherence particularly in superconducting qubits is believed to be due to other types of unwanted TLSs within the qubit, whose charge dynamics under a periodic-in-time electric field gives rise to dielectric losses directly probed in experiment. [11, 111] In what follows, we mostly apply our solution to the latter charge TLS model, but the general methods and some particular results of this work evidently can be applied to a much broader range of problems (see, *e.g.*, Ref.[112] and references therein).

One of the key metrics of a superconducting qubit is the quality factor, which

is defined as a ratio of the real and imaginary parts of the dielectric response function, $\varepsilon(\omega)$, evaluated at the resonant frequency of the corresponding LC-circuit, $Q = \mathrm{Re}\,\varepsilon(\omega_\mathrm{r})/\mathrm{Im}\,\varepsilon(\omega_\mathrm{r})$. Very high values of the quality factor are required for the qubit to be operational. However, existing experiments consistently show significant dielectric losses that occur in an amorphous dielectric (*e.g.*, in $\mathrm{Al_2\,O_3}$) used as a barrier in the Josephson junctions. It is believed that the losses are primarily due to the presence of charge two-level system defects in the barrier and/or the contact interfaces, which respond to an AC electric field in the LC-resonator. It is still unclear what the physical origin of these defects is, but an early work of Phillips [3] as well as very recent comprehensive density functional theory studies of Musgrave [4] point to the OH-rotor defects as a very likely source of the dielectric loss. To determine the physical origin and the properties of the TLSs responsible for the dielectric loss is one of the central questions in the field of superconducting quantum computing and it has been largerly the main physical motivation for our work.

The usual theoretical approach to calculating the quality factor and more generally the full dielectric response function, $\varepsilon(\omega)$, involves a formal mapping of charge dynamics in a double-well potential onto the problem of "spin" dynamics in an AC field, described by the "spin" Hamiltonian $\hat{\mathcal{H}}(t) = \mathbf{b}(t) \cdot \hat{\boldsymbol{\sigma}}/2$, where $\hat{\boldsymbol{\sigma}}$ denotes the Pauli matrices and $\mathbf{b}(t) = 2\left(\Delta_t, 0, \varepsilon + \vec{d}_\mathrm{TLS} \cdot \vec{E}(t)\right)$ is an effective "magnetic field" that drives TLSs, with ε, Δ_t, and $\vec{d}_\mathrm{TLS}$ being the TLS energy splitting, the tunneling amplitude between its two states, and the TLS dielectric moment correspondingly and $\vec{E}(t)$ is the AC electric field. A linear analysis within the canonical TLS model predicts that the dielectric function due to identical TLSs is peaked at the frequency,
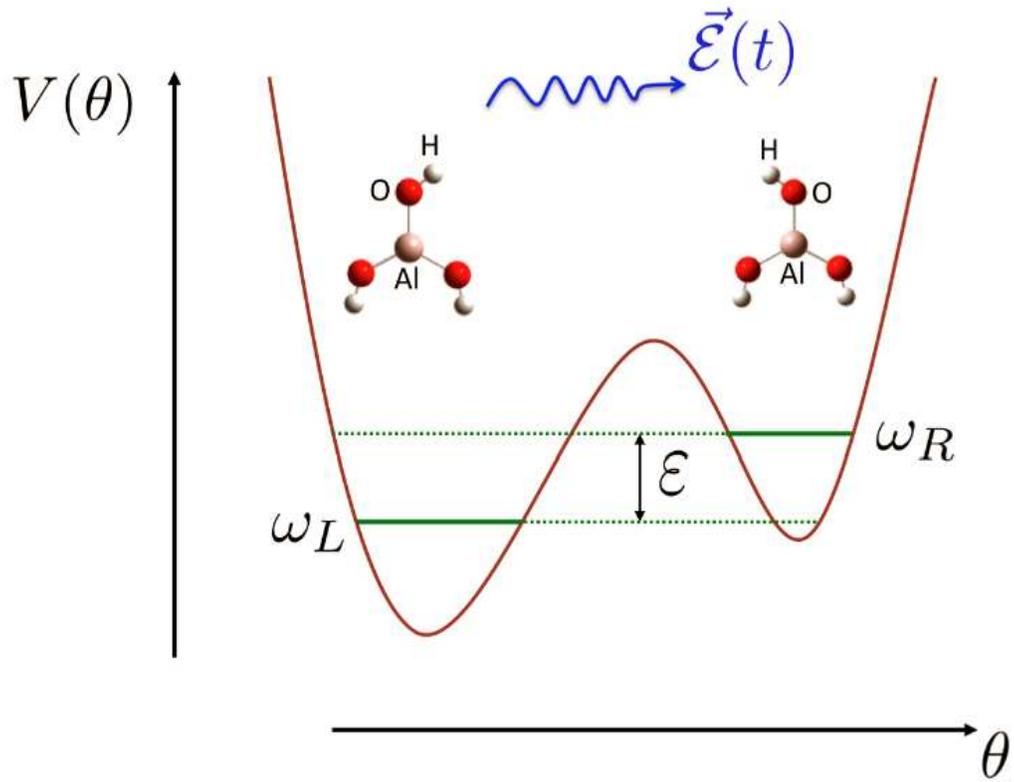
Figure 6.1: Schematic representation of an OH-rotor two-level system in an Al_2O_3 oxide. [3, 4] Here, the role of the generalized variable is assigned to the angle θ defined as an angle between the OH-bond and an axis perpendicular to the vertical AlO bond. At low enough temperatures, the phase space an isolated rotor is reduced to the two-states corresponding to the minima of the double-well potential $V(\theta)$. Application of external ac-field parametrically coupled to the rotor's dipole moment induces oscillations between the two minima.

$\nu = \sqrt{\Delta_{\mathrm{t}}^2 + \varepsilon^2}$. Ad-hoc inclusion of T_1 and T_2 relaxation processes and the assumption about random distribution of TLS energy-splittings and tunnelings (typically assumed to be uniform and log-uniform correspondingly) lead to the quality factor $Q \propto \sqrt{1 + (E_0/E_{\mathrm{c}})^x}$, with $x \sim 2$, E_0 being the amplitude of an applied AC electric field and E_c is a critical value of the amplitude which also encodes the information on the strength of the relaxation processes (see, *e.g.*, Ref.[103]). Both formulas are used widely in interpreting experimental data and probing energetics of the relevant TLS defects [103, 11]. While this linear analysis is a fine approximation to describe a majority of regimes currently studied experimentally, the existing experiments are certainly capable and some do [113] access non-linear regimes as well, where the energy of the applied electric field is comparable or larger than the relevant TLS energies. Hence, this non-perturbative regime is of clear experimental and theoretical interest. More importantly studies of non-linear dynamics may provide another effective means to probe the properties of TLSs.

The mathematical formulation of the non-linear TLS dynamics problem studied in this chapter [1] is deceptively simple: We wish to solve the Schrödinger equation for a spinor wave-function, $\Psi = \begin{pmatrix} \psi_+ \\ \psi_- \end{pmatrix}$, $i\partial_t \Psi = \frac{1}{2}\mathbf{b}(t) \cdot \hat{\boldsymbol{\sigma}}\, \Psi$ that describes a half-integer spin subject to a periodic-in-time magnetic field of the form, $\mathbf{b}(t) = 2\left(\Delta_{\mathrm{t}}, 0, f(t)\right)$, where Δ_{t} is a constant describing the coupling between the two states and the function $f(t) = f(t + T)$ describes the time dependent perturbation. Despite the simplicity of the formulation, the problem is generally unsolvable in analytic form

for most cases of practical interest. The origin of this surprising fact can be understood if we introduce a new function $R(t) = \psi_+(t)/\psi_-(t)$, which reduces the matrix Schrödinger equation to the Riccatti equation $\partial_{(-it)} R = 2fR + \Delta_t \left[1 - R^2\right]$. It is a non-linear differential equation that has known analytic solution in a very limited number of cases (note that the case of a monochromatic perturbation is not one of them). Therefore, to solve for TLS dynamics driven by a specific non-equilibrium field is equivalent to generating a particular solution to the Riccatti equation corresponding to this perturbation. Clearly this is a challenging mathematical task and this observation partially explains the current deficit of exact mathematical results. The difficulties in obtaining exact solutions have led to the emergence of several perturbative approaches, used in particular to characterize relaxation and dephasing rates in qubits as a function of driving amplitude (see, *e.g.*, Ref. [112] and references therein). These analyses provide very useful physical insights and correctly describe the physics if the time-dependent perturbation is weak, but it is also clear that there exist non-linear effects beyond perturbation theory and it is desirable to have exact results to access this qualitatively different physics.

The mathematical approach that we use in this chapter to obtain exact results is to "reverse engineer" exactly solvable Hamiltonians of specific form relevant to the problem of interest. A key observation in our analysis is that finding a Hamiltonian corresponding to a given solution is much easier than solving the Schrödinger equation with a given Hamiltonian. In some generalized sense, the two procedures are related to one another much like differentiation relates to integration. To see this, it is useful to consider the evolution operator, or the $\hat{S}$-matrix, which relates

73

the initial state at $t = 0$ to a final state at $t > 0$ as follows, $\Psi(t) = \hat{S}(t)\Psi(0)$. In the absence of relaxation process the time-evolution is unitary and it satisfies the Schrödinger equation, $i\partial_t \hat{S}(t) = \hat{\mathcal{H}}(t)\hat{S}(t)$. If we choose an arbitrary S-matrix, $\hat{S} = \exp\left[-\frac{i}{2}\boldsymbol{\Phi}(t) \cdot \hat{\boldsymbol{\sigma}}\right] \in SU(2)_2$, we can immediately reconstruct the corresponding Hamiltonian that gives rise to such evolution as follows $\hat{\mathcal{H}}(t) = i\partial_t \hat{S}(t)\hat{S}^\dagger(t)$. Using this method, one can generate an infinite number of exact non-equilibrium solutions and explicit models. These solutions may be of importance to physics of NMR, to the question of physical implementation of gate operations on a qubit as well as of some mathematical interest. Nevertheless without additional constraints such analyses would generally produce Hamiltonians of little importance to the problem of dynamics of TLS charge defects.

A very useful insight that allows us to constructively narrow down the range of relevant dynamical systems comes from the mathematically related problem of far-from-equilibrium superconductivity [114, 115, 116, 117, 118, 119]. It is well-known that the reduced BCS Hamiltonian is algebraically equivalent to an interacting XY-spin model in an effective "inhomogeneous" magnetic field in the z-direction, whose profile is dictated by the bare single particle-energy dispersion. Far from equilibrium, dynamics of a given Anderson pseudospin [5] is determined by an effective time-dependent self-consistent field of other pseudo-spins that it interacts with. [120] In many cases (determined by specific initial conditions), this BCS self-consistency constraint dynamically selects a specific order-parameter, such that the dynamics of essentially infinite number of spins is equivalent to the dynamics of few spins only. [119] For special sets of initial conditions, these spins move in

unison and therefore the self-consistent "magnetic field" (or superconducting order parameter in the language of BCS theory) is periodic in time. The reduced BCS model is integrable and there exists a very elegant prescription for constructing exact non-equilibrium solutions to it, developed primarily by Yuzbashyan and collaborators. [115, 119, 121] These solutions contain, in particular, exact spin dynamics in a periodic time-dependent field that can be expressed in terms of elliptic functions. In this chapter, we generalize such anomalous soliton solutions of Yuzbashyan [122] to encompass a wider range of time dependencies relevant to the problem of TLS dynamics, which is of our primary interest.

This chapter is organized as follows: Sec. II summarizes a general mathematical structure behind the "reverse engineering" approach to constructing exact solutions for non-linear TLS dynamics. The specific Ansatz and technical details of our particular family of solutions for periodically-driven TLS dynamics are given in Sec. III. In Sec. IV, we use some representative solutions to illustrate the emergence of the coherent destruction of tunneling phenomenon. We also derive the spectrum of exact dielectric response function due to an ensemble of identical charge TLS in the presence of dissipation, which is introduced phenomenologically. In Sec. V we provide a summary of our results. In Appendix B, we list some technical details of our calculations as well as useful relations aimed to shed more light on the subtle features of our theory.

6.2 General Framework for Constructing Exact Solutions

In this chapter, we derive a family of exact solutions for the non-dissipative TLS dynamics subject to an external ac-field. The main ingredient of our approach is a special Ansatz for the TLS's dynamics that corresponds to periodic-in-time but non-monochromatic external fields. Before proceeding to the specific Ansatz, let us first introduce a general algebraic framework for "reverse engineering" of exact solutions.

We are interested in solving the non-equilibirum Schrödinger equation for the spinor $\Psi(t)$

$$i\partial_t \Psi(t) = \hat{\mathcal{H}}(t)\Psi(t), \quad \Psi(t) = \begin{pmatrix} \psi_+ \\ \psi_- \end{pmatrix}. \tag{6.1}$$

where the Hamiltonian is $\hat{\mathcal{H}}(t) = \frac{1}{2}\mathbf{b}(t)\cdot\hat{\boldsymbol{\sigma}}$. As mentioned in the introduction, instead of solving Eq. (6.1) for the wave-function, we can consider the Schrödinger equation for the evolution operator that relates the initial and final states, $\Psi(t) = \hat{S}(t)\Psi(0)$. This equation for the S-matrix has the form identical to Eq. (6.1):

$$i\partial_t \hat{S}(t) = \hat{\mathcal{H}}(t)\hat{S}(t), \text{ and } \hat{S}(0) = \hat{1} \tag{6.2}$$

but now it is an equation for the matrix function $\hat{S}(t)$, which belongs to the two-dimensional representation of the $SU(2)$ group, while the Hamiltonian expressed in terms of $SU(2)_2$ generators belongs to the two-dimensional representation of the $\mathfrak{su}(2)$ algebra. Note that the form of Eq. (6.2) is such that it may be generalized to an arbitrary spin or equivalently to an arbitrary-dimensional representation of $SU(2)$ or it can be viewed as an equation of motion in the abstract group such that

$\hat{\mathcal{H}}_{\text{abs}}(t) = \mathbf{b}(t) \cdot \hat{\boldsymbol{J}}_{\text{abs}} \in \mathfrak{su}(2)$ and $\hat{S}_{\text{abs}}(t) = \exp\left[-i\boldsymbol{\Phi}(t) \cdot \hat{\mathbf{J}}_{\text{abs}}\right] \in SU(2)$, where $\hat{\mathbf{J}}_{\text{abs}}$ are the corresponding generators. Therefore, a solution of the problem in a particular representation, *i.e.*, an explicit form of $\boldsymbol{\Phi}(t)$, immediately gives the corresponding solutions in all other representations (*e.g.*, a two-level-system dynamics uniquely determines a "d-level system" dynamics in the same field). This TLS problem that we are interested in corresponds to the two-dimensional generators $\hat{J}_\alpha^{(2)} = \frac{1}{2}\hat{\sigma}_\alpha$ with $\hat{\sigma}_\alpha$ ($\alpha = x, y, z$) being the familiar Pauli matrices.

The problem of determining the solution, $\boldsymbol{\Phi}(t)$, from the magnetic field time-dependence $\mathbf{b}(t)$ is a complicated one, but the inverse problem is almost trivial. Indeed, if we select a specific S-matrix (defined uniquely by the choice of a specific function, $\boldsymbol{\Phi}(t)$), the Hamiltonian will read

$$\hat{\mathcal{H}}(t) = i\partial_t \hat{S}(t)\hat{S}^\dagger(t), \tag{6.3}$$

where

$$\hat{S}(t) = \exp\left[-\frac{i}{2}\boldsymbol{\Phi}(t) \cdot \hat{\boldsymbol{\sigma}}\right]. \tag{6.4}$$

Using the algebraic identities for the Pauli matrices, we obtain the corresponding magnetic field

$$\mathbf{b}(t) = \dot{\Phi}\,\mathbf{n} + \sin\Phi\,\dot{\mathbf{n}} + (1 - \cos\Phi)\left[\mathbf{n} \times \dot{\mathbf{n}}\right], \tag{6.5}$$

where $\boldsymbol{\Phi}(t) = \Phi(t)\mathbf{n}(t)$, with $|\mathbf{n}(t)| \equiv 1$. Note that one can generate exactly-solvable models by simply picking an arbitrary $\boldsymbol{\Phi}(t)$ dependence and using Eq. (6.3) to find the corresponding Hamiltonian. However, without guidance or luck, such an analysis would generally produce complicated non-equilibrium fields that have little to do with an underlying physical problem. Let us however mention here that

this procedure may be of interest to quantum computing in general, because the time-evolution governed by an S-matrix can be viewed as a "gate operation" on the spin (if the TLS/spin corresponds to a qubit rather than to a defect within a qubit). By picking "trajectories," $\boldsymbol{\Phi}(t)$, on the algebra that start in the origin, $i.e.$ $\boldsymbol{\Phi}(0) = \mathbf{0}$, but end at a specific point at a time T, one can immediately determine the non-equilibrium magnetic pulse, $\mathbf{b}(t)$, or a class of such pulses, that will give rise to a desired gate operator $\hat{G} \equiv \hat{S}(T) = \exp\left[-\frac{i}{2}\boldsymbol{\Phi}(T) \cdot \hat{\boldsymbol{\sigma}}\right]$.

Let us note here that the function, $\boldsymbol{\Phi}(t)$, contains complete information about the solution to the original problem, Eq. (6.1), including the overall quantum phase accumulated by the wave-function during the time evolution (as we shall see below, this phase is of particular interest to the problem of dielectric response of TLSs in superconducting qubits). An interesting question is whether and how this purely quantum phase can be restored from a solution of the corresponding classical Bloch equations that are usually considered in this context. Let us recall that a classical mapping can be achieved by introducing the average magnetic moment,

$$\mathbf{m}(t) = \Psi^\dagger(t)\frac{\hat{\boldsymbol{\sigma}}}{2}\Psi(t). \tag{6.6}$$

Therefore, $\mathbf{m}^2(t) \equiv 1/4$ and the classical equations of motion for the spin moment follow from $\partial_t\mathbf{m}(t) = \frac{1}{2}\Psi^\dagger(t)\left[\hat{\mathcal{H}}(t), \hat{\boldsymbol{\sigma}}\right]\Psi(t)$ and yield the familiar Bloch equations as derived in the previous chapter

$$\partial_t\mathbf{m}(t) = \mathbf{b}(t) \times \mathbf{m}(t). \tag{6.7}$$

Let us recall that these Bloch equations are a saddle point of quantum spin dynamics, much in the same way that Newton's equations of motion governed by the force,

$[-\boldsymbol{\nabla} V(\mathbf{r})]$, represent a saddle point of the action describing a quantum particle in the potential, $V(\mathbf{r})$, and therefore do not contain direct information about quantum interference and tunneling effects. Similarly, Eqs. (6.7) do not directly contain the quantum phase and to determine it one has to go back to the Schrödinger equation. Another more abstract way to see this is by noticing that Eqs. (6.7) describe the motion on a two-dimensional (Bloch) sphere, $\mathbf{m}(t) \in S^2$, while the original quantum problem Eq. (6.2) describes motion on a three-dimensional sphere since $\hat{S}_{\mathrm{abs}}(t) \in SU(2) \sim S^3$. Now let us recall that there exists the Hopf fibration such that $SU(2)/U(1) = S^2$, which summarizes the fact that classical equations, namely Eqs. (6.7), represent quantum motion modulo the $U(1)$ phase dynamics. Fortunately, this phase dynamics can generally be restored from exact dependence of the $\mathbf{m}(t)$ solution, albeit in a non-local way. To see this, we can write the magnetization in terms of the S-matrix as follows $\mathbf{m}(t) = \frac{1}{2}\Psi^\dagger(0)\left[\hat{S}^\dagger(t)\boldsymbol{\sigma}\hat{S}^\dagger(t)\right]\Psi(0)$, where $\Psi(0)$ and the corresponding $\mathbf{m}(0) = \Psi^\dagger(0)\frac{\hat{\boldsymbol{\sigma}}}{2}\Psi(0)$ are initial conditions for the wave-function and Bloch magnetization, correspondingly. Using again the well-known identities for the Pauli matrices, we find the evolution matrix for the Bloch equations, $m_\alpha(t) = R_{\alpha\beta}(t)m_\beta(0)$, as follows

$$R_{\alpha\beta}(t) = \delta_{\alpha\beta}\cos\Phi + n_\alpha n_\beta\left(1 - \cos\phi\right) - \varepsilon_{\alpha\beta\gamma}n_\gamma\sin\Phi. \tag{6.8}$$

This three-dimensional matrix describes a rotation, $\hat{R}(t) \in SO(3)$, and can be rep-

resented equivalently as

$$\hat{R}(t) = \exp\left[-\boldsymbol{\Phi}(t)\cdot\hat{\mathbf{L}}\right], \text{ where } \hat{\mathbf{L}} = \begin{pmatrix} 0 & -\mathbf{e}_z & \mathbf{e}_y \\ \mathbf{e}_z & 0 & -\mathbf{e}_x \\ -\mathbf{e}_y & \mathbf{e}_x & 0 \end{pmatrix}, \qquad (6.9)$$

where $\hat{\mathbf{L}} \in \mathfrak{so}(3) \sim \mathfrak{su}(2)$ belong to the three-dimensional vector representation of the $\mathfrak{su}(2)$ algebra. They are related to the "usual" spin-1 representation (where $\hat{J}_z^{(3)}$ is diagonal) via a simple linear transform.

Therefore, we see that if we know an arbitrary solution to the Bloch equations, $\mathbf{m}(t)$ we can at least in principle restore the function, $\boldsymbol{\Phi}(t)$, [see, Eqs. (6.9) and (6.4)], which uniquely determines the entire quantum solution. It also suggests that if we choose an arbitrary dynamic function on a sphere we may be able to restore the quantum Hamiltonian that would give rise to it, via mappings $\mathbf{m}(t) \rightarrow \hat{R}(t) \rightarrow \boldsymbol{\Phi}(t) \rightarrow \hat{S}(t) \rightarrow \hat{\mathcal{H}}$. However, the second step in this chain of transforms involves effectively calculating a logarithm of the rotation matrix, which due to a complicated "analytic" structure of this matrix-logarithm function requires a careful calculation non-local in time.

The subsequent Sections are devoted to constructing exactly solvable periodic-in-time Hamiltonians based on a specific Ansatz for the classical Bloch "magneti-zation," $\mathbf{m}(t)$. It further involves a restoration of the corresponding quantum $U(1)$ phase via a straightforward integration. More specifically, we "reverse engineer" the following Hamiltonian

$$\hat{\mathcal{H}} = \Delta_t \hat{\sigma}_x + f(t)\hat{\sigma}_z. \qquad (6.10)$$

where $f(t) = f(t + T_f)$ is a periodic function, with an arbitrary period, T_f. Our

solution below also allows tuning of the average splitting, $\varepsilon = \langle f(t) \rangle_{T_f}$, and the AC field amplitude, $\mathcal{A}_f \sim \sqrt{\langle [f(t) - \varepsilon]^2 \rangle_T}$. As mentioned in the introduction, this problem is of great importance to the physical problem of externally-driven TLS dynamics in superconducting qubits (with Δ_t corresponding to tunneling between the wells, ε to a splitting of energy levels in a double-well potential, and T_f and A_f being the period and the amplitude of the AC-electric field correspondingly).

Our "guess" for the relevant Ansatz for the Bloch "magnetization," $\mathbf{m}(t)$, is based on a set of formal solutions discovered in the related problem of quenched dynamics of fermionic superfluids. [114, 115, 119, 121, 122] Formally, the quenched dynamics of each individual Cooper pair is described by the Bogoliubov-de Gennes Hamiltonian, which is essentially a spin Hamiltonian that reduces to (6.10) after the unitary transformation $\hat{\sigma}_x \to \hat{\sigma}_z$ and $\hat{\sigma}_z \to -\hat{\sigma}_x$, with Δ_t corresponding to a single particle energy level and $f(t)$ to the superfluid order parameter. A realization of each particular form of the superfluid order parameter dynamics in a steady state can be unambiguously determined by the initial conditions [119] using the exact integrability of BCS model. [115] Note that a self-consistency condition for the order parameter provides a limitation on the set of functions for which the corresponding problem is integrable and for some initial conditions periodic-in-time self-consistent dynamics, $f(t)$, can be realized. While in our TLS problem, there is no natural self-consistency constraint, such insights and constraints from the BCS problem help us narrow down the range of possible Ansatze to restore reasonable physical Hamiltonians, which are also exactly solvable by construction.

In what follows, we generalize the soliton analysis of Yuzbashyan [122] and

find a general soliton configuration, characterized by three independent parameters, which we denote as $\Delta_\pm$ and Δ_a. For the physical problem of interest, this conveniently implies that some, generally speaking, non-trivial combination of these parameters will determine the arbitrary frequency, amplitude, and the dc-component of the field. Due to the periodicity, we can generally represent the AC-perturbation as a Fourier series

$$f(t) = \varepsilon + \mathcal{A}_f \sum_{n=1}^{\infty} \tilde{f}_n \cos(n\omega_f t). \tag{6.11}$$

Note that for certain specific choices of the parameters $\Delta_{\pm,a}$, the leading coefficient $\tilde{f}_1 \gg \tilde{f}_n$ ($n = 2, 3, ...$) and one recovers the limit of a monochromatic AC-field, albeit in the regime of weak driving ($\mathcal{A}_f \tilde{f}_1 \ll \max\{\Delta_t, \varepsilon\}$). Therefore, our nonlinear analysis contains the standard linear response results as a simple special case.

6.3 Non-dissipative dynamics of the ac-driven TLS

In this Section we provide the details on the derivation of the exact solution for the TLS dynamics. We devote the special attention to the analysis of the U(1) phase of the wave function. We also elucidate the relations between the parameters of our solution and the amplitude, phase and the dc-component of the external field, which may be useful for experimental applications of our theory.

6.3.1 Ansatz

We now focus on the Schrödinger equation for the half-integer spin in the magnetic field, $\mathbf{b}(t) = 2(\Delta_t, 0, f(t))$. When written in terms of spinor components,

it has the form

$$\begin{cases} i\dot{\psi}_+ = \Delta_t \psi_- + f(t)\psi_+ \\ \\ i\dot{\psi}_- = \Delta_t \psi_+ - f(t)\psi_- \end{cases}.$$

(6.12)

The corresponding Bloch equation is

$$\dot{\mathbf{m}}(t) = 2(\Delta_t, 0, f(t)) \times \mathbf{m}(t).$$

(6.13)

Let us now make the following Ansatz for its exact solution: [122]

$$m_x = D - Cf^2, \quad m_y = B\dot{f}, \quad m_z = Af(t) + F.$$

(6.14)

From two of the Eqs. (6.13) we find $A = 2\Delta_t B$ and $B = C$. Thus among five parameters in (6.14) only three are independent: F, B and D. The equation for the external field, $f(t)$, can be obtained from (6.14) using the condition $\mathbf{m}^2 = 1/4$. This resulting equation for the function $f(t)$ acquires the form

$$\dot{f}^2 = -f^4 - 4c_2 f^2 + 8c_1 f - 4c_3,$$

(6.15)

where coefficients c_j are given by some combinations of parameters B, D and F [see Eqs. (6.30) below]. Equation (6.15) can be cast to a more symmetric form, using another set of parameters Δ_a and $\Delta_\pm$, which are chosen to be positive and are related to coefficients c_j as follows:

$$c_1 = -\frac{\Delta_a}{4}(\Delta_+^2 - \Delta_-^2),$$

$$c_2 = -\frac{1}{4}(\Delta_+^2 + \Delta_-^2 + 2\Delta_a^2),$$

(6.16)

$$c_3 = -\frac{1}{4}(\Delta_+^2 - \Delta_a^2)(\Delta_a^2 - \Delta_-^2).$$

Without loss of generality and to be more specific we also assume $\Delta_+ \geq \Delta_-$ for the remainder of this chapter, while Δ_a can be assigned an arbitrary value. By virtue

of expressions (6.16) equation (6.15) now reads

$$\dot{f}^2 = [(f - \Delta_a)^2 - \Delta_-^2][\Delta_+^2 - (f + \Delta_a)^2]. \tag{6.17}$$

Below we will make several transformations that allow us to reduce (6.17) to an equation for the Weierstrass elliptic function. [123] Firstly, let us introduce a function, $y(t)$,

$$f(t) = \Delta_+ \left[\frac{2}{y(t)} - 1 \right] - \Delta_a \tag{6.18}$$

which satisfies the following equation

$$\left(\frac{dy}{dx} \right)^2 = 4(y - a_+)(y - a_-)(y - 1), \quad x = \frac{\Delta_+ t}{\sqrt{a_+ a_-}}, \tag{6.19}$$

where $a_\pm = 2\Delta_+/(\Delta_+ + 2\Delta_a \pm \Delta_-)$. Now, Eq. (6.19) can be easily reduced to a well-known equation for the Weierstrass elliptic function by rescaling the parameters via the transformation

$$y(x) = Z(x) + \frac{a_+ + a_- + 1}{3}, \tag{6.20}$$

so that

$$\left(\frac{dZ}{dx} \right)^2 = 4(Z - e_1)(Z - e_2)(Z - e_3), \tag{6.21}$$

where parameters e_j satisfy the following conditions $e_1 > e_2 > e_3$ and $e_1 + e_2 + e_3 = 0$. Coefficients e_j are determined by the parameters Δ_a and $\Delta_\pm$. The specific expressions for the coefficients e_j, however, depend on the relative values of the initially introduced set of parameters and are given in Appendix A. Solution of the equation (6.21) is

$$Z(x) = \mathcal{P}(x + \omega'), \quad \omega' = \frac{\mathbf{K}(\kappa')}{\sqrt{e_1 - e_3}}, \tag{6.22}$$

84

where $\mathcal{P}(x)$ is a Weierstrass elliptic function, $\mathbf{K}$ is a complete elliptic integral of the first kind [123] and $\kappa' = \sqrt{(e_1 - e_2)/(e_1 - e_3)}$. Function $Z(x)$ is a doubly-periodic function with the period along the physical time axis determined by, $l = 2\omega$, where $\omega = \mathbf{K}(\kappa)/\sqrt{e_1 - e_3}$ and $\kappa = \sqrt{1 - \kappa'^2}$ is a modulus of elliptic functions. Combining (6.22) with Eqs. (6.20) and (6.18) allows us to express $f(t)$ in terms of elliptic functions. Expression for $f(t)$ can be compactly written in terms of Jacobi elliptic functions. Just as it is the case for the parameters e_j, the particular form of the resulting expression depends on the relation between Δ_a and $\Delta_\pm$ (see Appendix A).

All cases considered here are summarized by the following compact expression for the function, $f(t)$, written in terms of Jacobi elliptic function sn as follows:

$$f(t) = \Delta_+ \frac{\eta_+ \mathrm{sn}^2(z, \kappa) - 1}{\eta_- \mathrm{sn}^2(z, \kappa) + 1} - \Delta_a, \tag{6.23}$$

where variable z is

$$z = \frac{(t - t_0)}{2} \sqrt{[(\Delta_+ + 2\Delta_a)^2 - \Delta_-^2](e_1 - e_3)} \tag{6.24}$$

and $t_0 = -\omega'\sqrt{a_+ a_-}/\Delta_+$. If we consider $\Delta_\pm$ fixed, then the parameters $\eta_\pm$ are given by one of the following expressions depending on the value of Δ_a:

$$\eta_\pm = \begin{cases} \frac{1}{e_1 - e_3} \pm 1, & \Delta_a > \frac{\Delta_+ + \Delta_-}{2} \\ \frac{1}{e_1 - e_3} \pm \kappa^2, & \frac{\Delta_+ - \Delta_-}{2} \leq \Delta_a \leq \frac{\Delta_+ + \Delta_-}{2} \\ \frac{1}{e_1 - e_3}, & \Delta_a < \frac{\Delta_+ - \Delta_-}{2} \end{cases} \tag{6.25}$$

Fig. 2 displays some representative dependencies of the driving field from the class of solutions described by Eqs. (6.23), (6.24), and (6.25). Note that the curve in Fig. 2a is visually indistinguishable from a harmonic periodic signal, Fig. 1b and
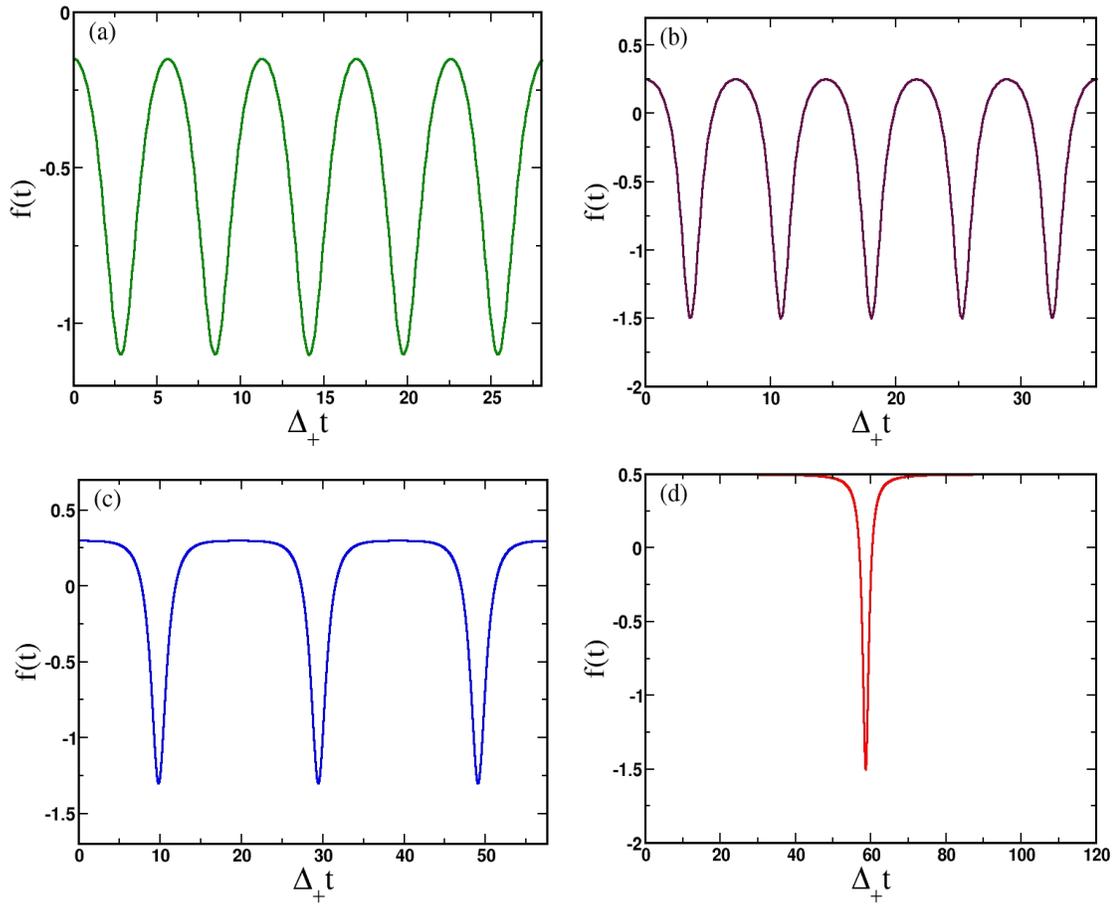
Figure 6.2: Plots of the function $f(t)$ (6.23) in units of Δ_+ for different values Δ_a:

(a) $\Delta_a = 0.1\Delta_+$, $\Delta_- = 0.3\Delta_+$; (b) $\Delta_a = 0.5\Delta_+$, $\Delta_- = 0.3\Delta_+$; (c) $\Delta_a = 0.3\Delta_+$, $\Delta_- = 0.1\Delta_+$; (d) $\Delta_a = 0.5\Delta_+$, $\Delta_- = 0.001\Delta_+$. We note that for the choice of the parameters (d) the period of $f(t)$ diverges. The curves above are plotted for the value of $\Delta_t = 0.5\Delta_+$.

Fig. 1c contain apparent non-monochromatic contributions to the periodic signal, and finally Fig. 2d provides an example of a degenerate case, or a single soliton, where the period of the elliptic function is taken to be infinite. Fig. 3 shows dynamic trajectories of the "magnetization" on the Bloch sphere given by exact Eq. (6.14) that correspond to these particular $f(t)$-dependencies.

From the expression for the external field (6.23) it is, however, not immediately clear what set of parameters correspond to the regimes of weak and strong ac-driving. To clarify this issue, let us re-write (6.23) in the form more useful for practical applications. Let us first explicitly derive the amplitude, frequency and the dc-component of function $f(t)$. The period and the amplitude of oscillations of $f(t)$ can be immediately deduced from (6.23,6.24):

$$
\begin{aligned}
T_f &= \frac{4\mathbf{K}(\kappa)}{\sqrt{[(\Delta_+ + 2\Delta_a)^2 - \Delta_-^2](e_1 - e_3)}}, \\
\mathcal{A}_f &= \frac{\Delta_+}{2}\left(\frac{\eta_+ + \eta_-}{\eta_- + 1}\right).
\end{aligned}
\tag{6.26}
$$

Lastly, the average value of the function $f(t)$ over its period is

$$
\langle f(t)\rangle = \frac{\Delta_+ \eta_+}{\eta_-}\left[1 - \frac{(\eta_+ + \eta_-)}{\eta_+ \mathbf{K}(\kappa)}\Pi(-\eta_-, \kappa)\right] - \Delta_a \equiv \varepsilon,
\tag{6.27}
$$

with $\mathbf{K}(\kappa)$ and $\Pi(n, \kappa)$ being an complete elliptic integral of the first and third kind correspondingly. As we have already mentioned, quantity (6.27) describes the dc-component of the external field. One can view Eqs. (6.26, 6.27) as the definition of yet another set of parameters $\mathcal{A}_f$, $\omega_f = 2\pi/T_f$ and $\varepsilon = \langle f(t)\rangle$, which allows us to cast external field $f(t)$ into the form given by (6.11). We plot the dependence of these parameters on the ratio Δ_-/Δ_+ in Fig. 6.4 for different values of Δ_a while keeping the value of Δ_t fixed. As we can see from 6.4 the limits of strong and weak
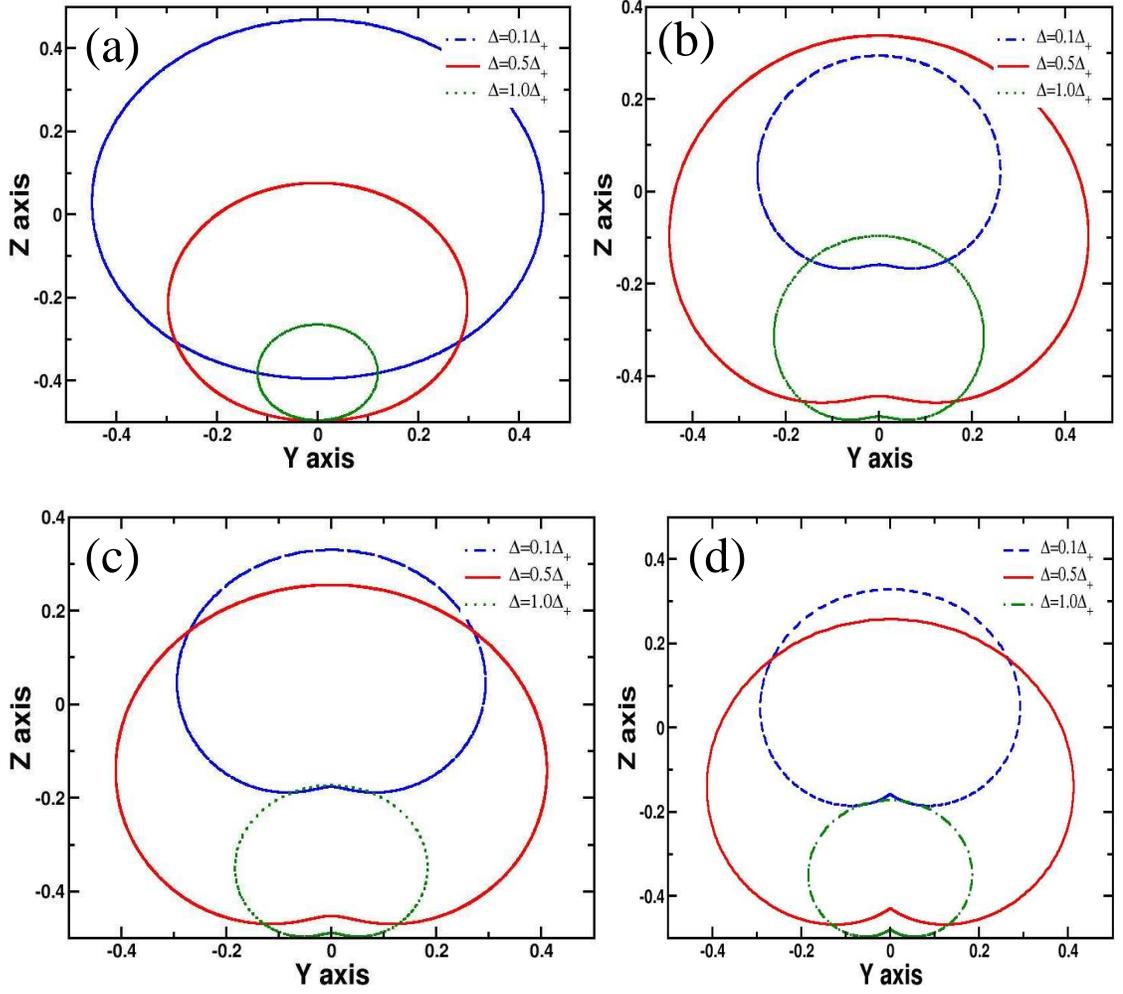
Figure 6.3: TLS dynamics on the Bloch sphere (6.13,6.14). Trajectories of TLS for the solutions described by Eq. (6.23) and depicted in Fig. 2 for the various set of parameters Δ_a and $\Delta_{\pm}$. The latter take the same values used on Fig. 2.

ac-driving are easily attainable with the frame of our solution. In particular, we see that the regime of the strong ac-driving should be achieved for moderate values of Δ_a and $\Delta_-/\Delta_+ \sim 0.2$.

Expressions (6.23,6.24,6.25) constitute one of the main technical results of this chapter. To get a further insight into the properties of our solution we refer the reader to Appendix B where we consider few limiting cases for the function (6.23). Quite generally, our solution represents the superposition of monochromatic waves with frequencies integer multiples of $\omega_f = 2\pi/T_f$. As discussed in the Appendix B, solution (6.23) can be reduced to the monochromatic wave with frequency $2\Delta_+$ when $\Delta_a = 0$ and $\Delta_- \simeq \Delta_+$.

6.3.2 Wave function

Having determined the form of the periodic field $f(t)$ we employ the relations (6.6) to compute the amplitudes $\psi_+(t)$ and $\psi_-(t)$. First let us represent these functions as follows [121]

$$\psi_\pm(t) = |\psi_\pm(t)|e^{\mp i\phi(t)}e^{i\alpha(t)}. \tag{6.28}$$

From these expressions, it follows that absolute values of the components ψ_+ and ψ_- as well as their relative phase $\phi(t)$ are determined by the instantaneous value of magnetization (6.14). From Eqs. (6.6,6.14), we find

$$|\psi_\pm(t)| = \sqrt{\frac{1}{2} \pm 2\Delta_t B f(t) \pm F},$$
$$\tan[2\phi(t)] = \frac{\dot{f}}{(D/B) - f^2(t)}, \tag{6.29}$$

89
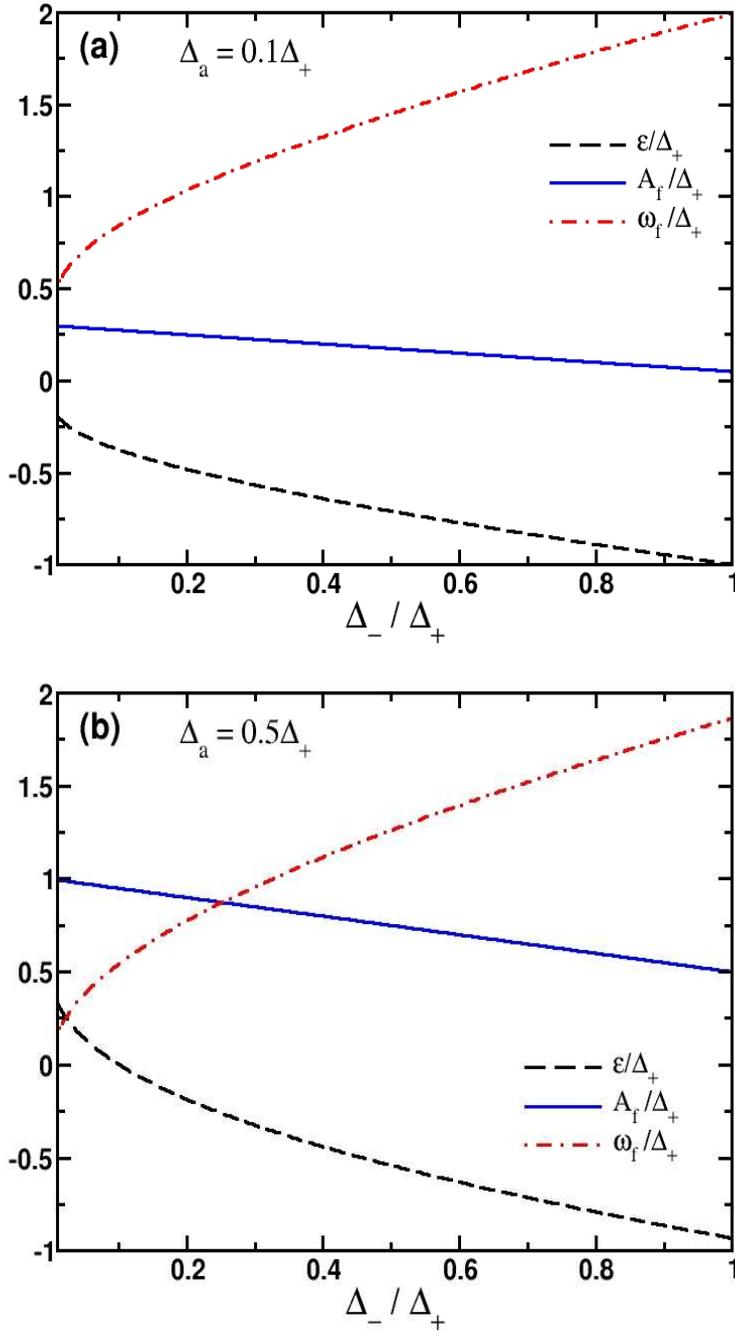
Figure 6.4: Plots of the amplitude $\mathcal{A}_f$, frequency ω_f and dc-component ε of the external field $f(t)$, Eq. (6.11): (a) $\Delta_a = 0.1\Delta_+$, $\Delta_t = 0.3\Delta_+$; (b) $\Delta_a = 0.5\Delta_+$, $\Delta_t = 0.3\Delta_+$.

where parameters B and D are determined from

$$\frac{D}{B} = 2(\Delta_t^2 - c_2), \ B = \frac{1}{4\sqrt{(\Delta_t^2 - c_2)^2 + \frac{c_1^2}{\Delta_t^2} - c_3}}, \tag{6.30}$$

$$F = -2c_1 B/\Delta_t.$$

and parameters c_j's are given by (6.16). Note that apparent ambiguity in signs for the parameters B and D as well as for parameter F is resolved by fulfilling the condition $m^2 = 1/4$.

6.3.3 Restoring the U(1) phase

It has been mentioned above that the common phase $\alpha(t)$ has to be determined from the solution of the equations (6.12). At first sight the resulting equation for $\alpha(t)$ appears to be very complicated, but it can be significantly simplified using Eqs. (6.29), so that

$$\dot{\alpha} = -\frac{1}{2} \frac{f(t) m_z(t)}{[1/4 - m_x^2(t)]}. \tag{6.31}$$

After some algebraic manipulations, we find

$$\alpha(t) = \int_0^t \left\{ \Delta_t \left[\frac{d_+^2}{f^2(t') - d_+^2} - \frac{d_-^2}{f^2(t') - d_-^2} \right] + \frac{F}{2B^2} \frac{f(t')}{[f^2(t') - d_+^2][f^2(t') - d_-^2]} \right\} dt' + \alpha_0, \tag{6.32}$$

where α_0 is determined by the initial conditions, $d_\pm^2 = (1/2B) \pm D/B$. One can evaluate the integral in (6.32) exactly and express in terms of elliptic σ and ζ functions (see Apendix C for details of this calculation). We note that on the grounds of Floquet theory we can represent an expression for the phase $\alpha(t)$ as a

sum of two terms:

$$\alpha(t) - \alpha_0 = -\nu t + \gamma(t), \tag{6.33}$$

where $\gamma(t) = \gamma(t + T_f)$ is a periodic function and ν is a constant. Analytic expression for both of these quantities can be extracted from the analytic expression for $\alpha(t)$ listed in Appendix C. For example, from (6.33) it follows $\nu = [\alpha(t) - \alpha(t + T_f)]/T_f$. In the limit when $\Delta_a = 0$ and $\Delta_+ = \Delta_-$ we find $\nu = (\Delta_t^2 + \Delta_+^2)^{1/2}$, while in the limit when $\Delta_a = 0$ and $\Delta_- = 0$ we obtain $\nu = \Delta_t$. For a general set of values Δ_a and $\Delta_\pm$ the resulting expression for ν is not as simple as those listed above. For practical purposes, however, one can construct an approximate expression for ν. By analyzing the behavior of $\alpha(t)$ numerically we find that for $\Delta_a = 0$, frequency ν can be approximated (see Fig. 6.5a) by:

$$\nu(\Delta_a = 0) \approx \frac{1}{T_f} \int\limits_0^{T_f} \sqrt{\Delta_t^2 + f^2(t)} dt. \tag{6.34}$$

We find qualitatively different behavior of ν as a function of $\delta = \Delta_-/\Delta_+$ for nonzero Δ_a. In that case, there appears to be a discontinuity in ν at some critical value of Δ_-/Δ_+. The source of this discontinuity at least for small Δ_a lies in the fact that $\dot{\alpha}(t) \propto m_z(t)$ changes sign during its time evolution. For non-zero Δ_a there are always exists δ_c such that $m_z(t = 0) = 0$, while for $\delta > \delta_c$ one observes $m_z(0 < t_{1,2} < T_f) = 0$. The sign change in $m_z(t)$ implies that the derivative of the quantum phase will change sign also (6.31), so that the subsequent integration yields the value of ν smaller than the one found for $\delta < \delta_c$, Fig. 6.5b.

In order to get further insight into the physical meaning of the quantity ν, we can employ the analogy between the TLS and spin-1/2 and define the magnetization

92
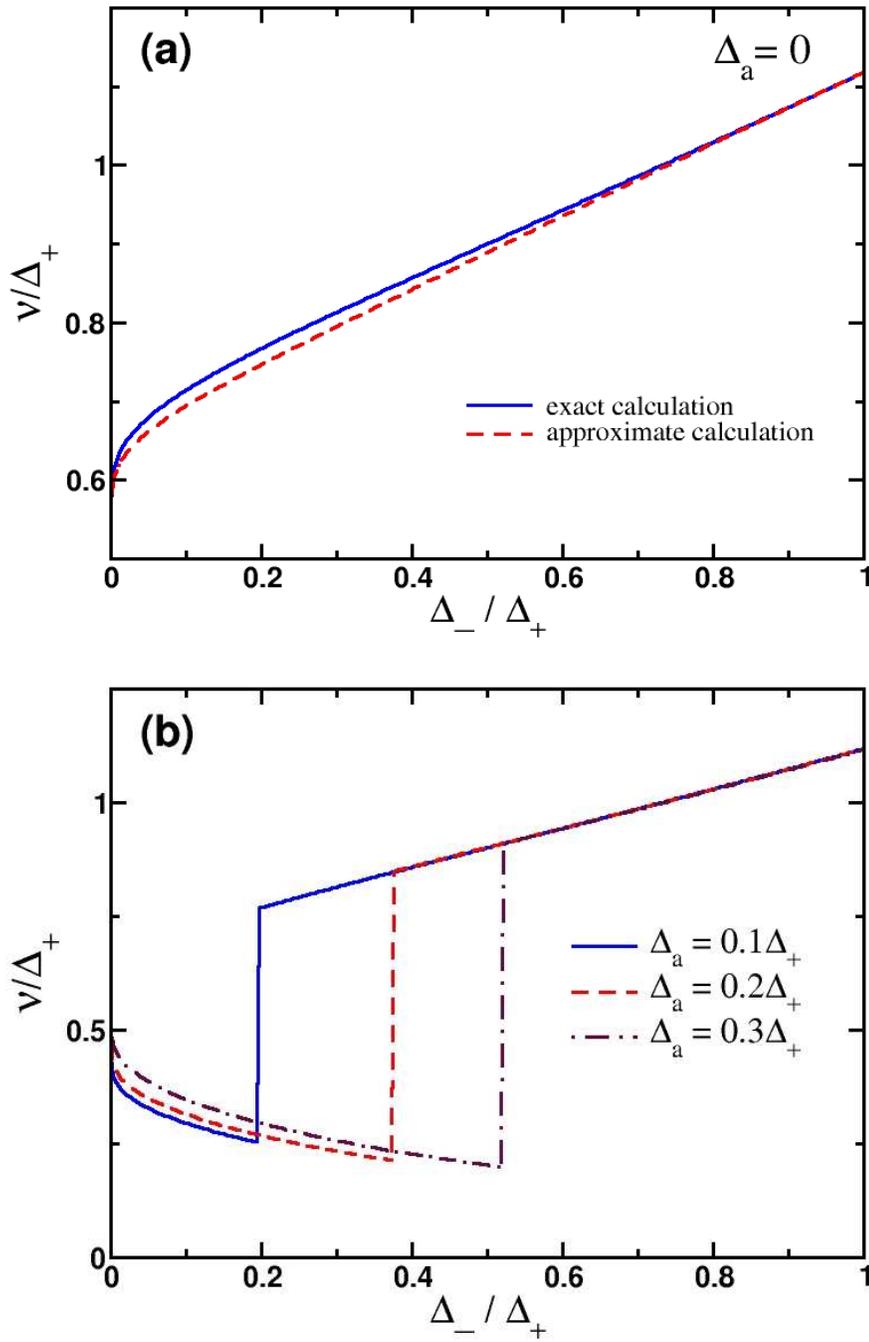
Figure 6.5: Dependence of exponent ν as a function of the ratio Δ_-/Δ_+ for various values of Δ_a. On panel (a) we compare the result of numerical computation of ν from (6.32) and compare them with approximate expression (6.34) when $\Delta_a = 0$. Panel (b) shows the dependence of ν for $\Delta_a \neq 0$.

$M_\alpha(t) = \langle \Psi_g(t)|\hat{\sigma}_\alpha|\Psi_g(t)\rangle/2$, where $\Psi_g(t)$ is a general solution of the Schrödinger equation and can be expressed as a linear combination of the particular solution $\Psi(t)$ (see below). Then one can show [121] that the dynamics of the vector $\vec{M}$ can be represented as a linear superposition of vector $\vec{m}(t)$ precessing with the frequency of the field $f(t)$ and a vector $\vec{h}(t)$ such that $\vec{h} \cdot \vec{m} = 0$. Each component of the latter oscillates with frequency ν. Our results from Fig. 3b suggest that the rate of precession of vector $\vec{h}$ will be significantly reduced as one tunes the parameter Δ_-/Δ_+.

The solution of the Schrödinger equation we described above is only a particular solution from which the general solution can be constructed straightforwardly by taking advantage of the underlying symmetries of Eqs. (6.12). A general solution for the wave function, $\Psi^\dagger = (\psi_+^*, \psi_-^*)$, can be presented as

$$\Psi_g(t) = C_1 \begin{pmatrix} \psi_+(t) \\ \psi_-(t) \end{pmatrix} + C_2 \begin{pmatrix} \psi_-^*(t) \\ -\psi_+^*(t) \end{pmatrix}, \tag{6.35}$$

where $C_{1,2}$ are integration constants, which satisfy $|C_1|^2 + |C_2|^2 = 1$ and are to be determined from the initial conditions. For example, for the specific choice of an initial condition when the TLS at $t = 0$ resides in one of its two states,

$$\Psi_g(0) = \begin{pmatrix} 1 \\ 0 \end{pmatrix}, \tag{6.36}$$

the coefficients $C_{1,2}$ are

$$C_1 = \psi_+^*(0), \quad C_2 = \psi_-(0). \tag{6.37}$$

Expressions listed in this subsection amount to full description of the ac-driven dynamics of an isolated TLS. In the next Section, we will briefly outline several

applications of our theory. For simplicity, we will mostly focus on the properties of the non-dissipative dynamics.

6.4   Experimental manifestations

In this Section we discuss the physical behavior of several quantities which can be probed experimentally for various physical realizations of the TLS. Before we proceed with the discussion on the application of our results and computation of physical observables, we derive the expression for the evolution operator and the density matrix which will allow us to compute probabilities which characterize the dynamics of the TLS.

Evolution operator $\hat{S}(t)$ is defined by

$$\Psi_g(t) = \hat{S}(t)\Psi_g(0). \tag{6.38}$$

From expressions (6.35) one can always write down a general expression for the evolution operator, which is valid for arbitrary initial conditions:

$$\hat{S}(t) = \begin{pmatrix} \psi_+(t) & \psi_-^*(t) \\ \psi_-(t) & -\psi_+^*(t) \end{pmatrix} \begin{pmatrix} \psi_+^*(0) & \psi_-^*(0) \\ \psi_-(0) & -\psi_+(0) \end{pmatrix} \tag{6.39}$$

Note that it is now straightforward to derive the density matrix from (6.39) using the following expression: [124]

$$\hat{\rho}(t) = \hat{S}(t)\hat{\rho}_0\hat{S}^\dagger(t), \tag{6.40}$$

where $\hat{\rho}_0$ is the density matrix of an initial state of the TLS. The expressions (6.39,6.40) can be used as a basis to analyzed the effects of the environment dissipa-

tion on the dynamics of the TLS. In particular, one can determine the probability of the TLS to remain in the initially prepared state $P_{\uparrow \to \uparrow}(t)$.

6.4.1 Coherent destruction of tunneling

The phenomenon of the coherent destruction of tunneling (CDT) has been predicted theoretically [125, 126, 127] for various physical realizations. Qualitatively, this phenomenon can be interpreted as the dynamical trapping of the TLS in one its states. For example, CDT occurs when the survival probability of the initial state dynamically approaches unity. This phenomenon has its counterpart known in literature as driving induced tunneling oscillations. This effect has been first analyzed theoretically in a series of papers [128, 129, 130] and observed experimentally for the first time by Nakamura *et al.* [131] To compute the survival probability $P_{\uparrow \to \uparrow}(t)$ we can use the density matrix (6.40). It is, however, easier to use an expression for the wave function (6.35) with the initial conditions (6.36,6.37). In particular, let us choose the initial amplitudes such that both C_1 and C_2 are real and introduce an angle ϑ, so that $C_1 = \cos(\vartheta/2)$.

After some algebra, we obtain the following expression for the return probability

$$
\begin{aligned}
P_{\uparrow \to \uparrow}(t) = &\frac{1}{2} + \cos \vartheta \cdot m_z(t) + \\
&+ \sin \vartheta \cos[2\alpha(t)] \cdot \sqrt{\frac{1}{4} - m_z^2(t)}.
\end{aligned}
\tag{6.41}
$$

The CDT occurs when $P_{\uparrow \to \uparrow}(t) \approx 1$ and we assume the initial conditions (6.36). From (6.41) it follows that if we perform an averaging over time frame longer than T_f and $T_h = 2\pi/\nu$, the third term in (6.41) averages out to zero, so that employing
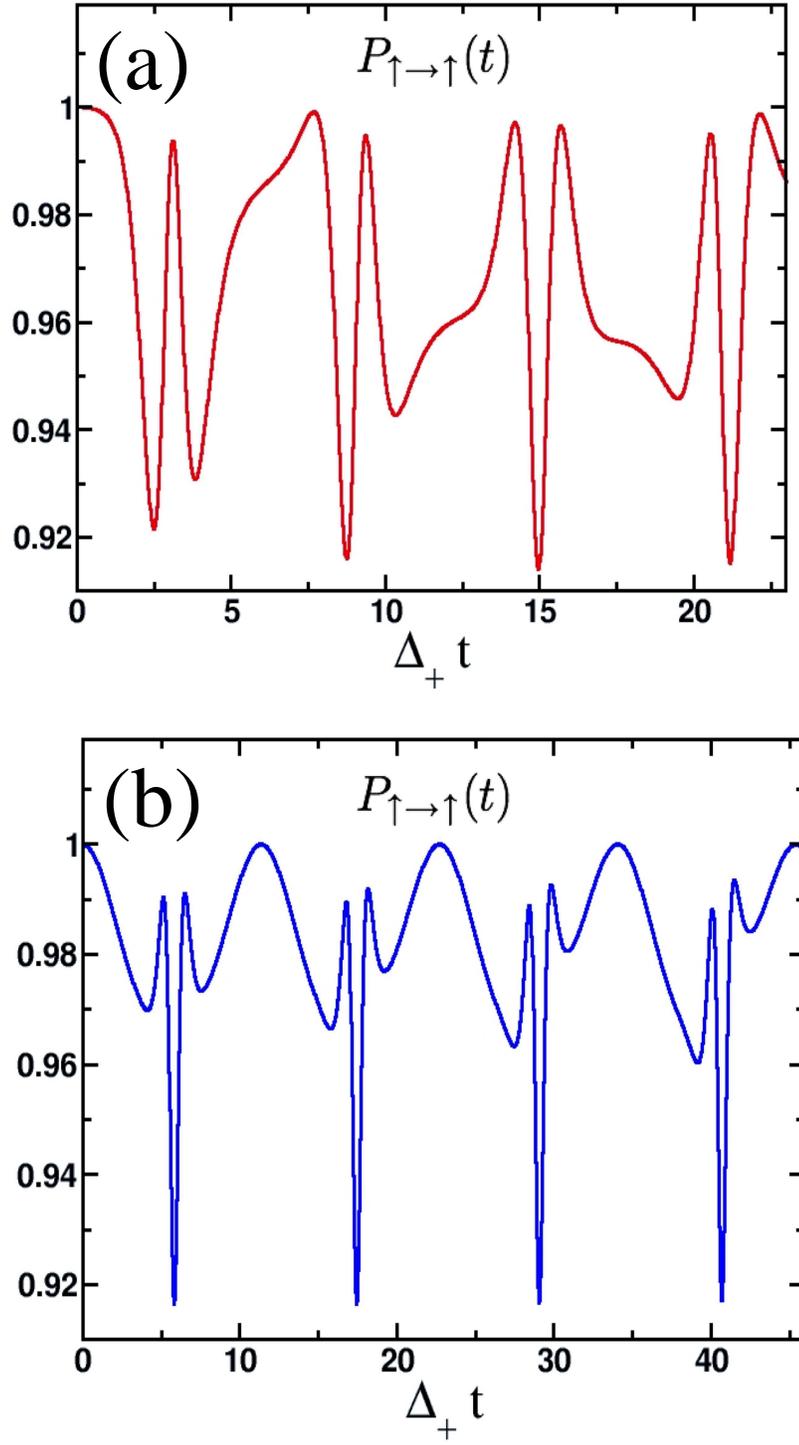
Figure 6.6: Plots of the return probability $P_{\uparrow \to \uparrow}(t)$, Eq (6.41), in the limit of the strong ac-driving: (a) $\varepsilon = 8.5\Delta_{\mathrm{t}}$, $\mathcal{A}_f = 13.5\Delta_{\mathrm{t}}$, $\omega_f = 21\Delta_{\mathrm{t}}$; (b) $\varepsilon = 0.1\Delta_{\mathrm{t}}$, $\mathcal{A}_f = 13.5\Delta_{\mathrm{t}}$, $\omega_f = 8\Delta_{\mathrm{t}}$.

(6.14) we find

$$\langle P_{\uparrow\to\uparrow}(t)\rangle \simeq \frac{1}{2} + 2\cos\vartheta\Delta_{\mathrm{t}}B\left(\varepsilon - \frac{c_1}{\Delta_{\mathrm{t}}^2}\right). \tag{6.42}$$

This equation approximately determines the parameter range for which CDT occurs. Fig. 5 displays representative results for the return probability and illustrates the CDT phenomenon: As we can see, in the limit of strong driving, i.e. when $\mathcal{A}_f \gg \Delta_{\mathrm{t}}$ and $\omega_f \gg \Delta_{\mathrm{t}}$, the return probability remains of order unity, which implies that the tunneling processes become strongly suppressed. We also have found that CDT remains robust and is present as long as the parameters Δ_a and $\Delta_\pm$ are such that the dynamics of the TLSs remains in the strong driving regime. This qualitative behaviour of tunneling was found to be essentially independent of the ratio $\varepsilon/\Delta_{\mathrm{t}}$. These our findings agree qualitatively with the results reported previously in Ref.[112] for the monochromatic AC-field. Finally, we note that if a system of charged TLSs, e.g. OH-rotors present in Al_2O_3 dielectrics, is driven into such non-linear CDT regime by an external AC electric field, then the TLS tunneling and the corresponding dipole polarization dynamics will be strongly reduced. This suggest that a strong non-linear drive may actually correspond to lower losses.

6.4.2 Dielectric response

Fig. 1 provides a pictorial example of a TLS charged defect, – an OH-rotor, which is one of the most likely candidates of physical two-level-systems responsible for dielectric losses in superconducting qubits. This rotor has a non-zero dipole moment $\vec{p}$ and, therefore, responds to an applied external electric field $\vec{\mathcal{E}}(t)$. In

the absence of other interactions which may affect TLS dynamics, the Hamiltonian describing the dynamics is (6.10) with $f(t) = \varepsilon + \vec{p} \cdot \vec{\mathcal{E}}(t)$. By construction, the average dipole moment of an isolated TLS is determined by the following average within the spin mapping [103]

$$\vec{d}(t) = m_z(t)\vec{p}. \tag{6.43}$$

The linear dielectric response function can be computed from (6.43) by differentiating the corresponding components of the average dipole moment with respect to the amplitude of an external field $\vec{\mathcal{E}}$. To define a non-linear dielectric response function corresponding to a solution $m_z(t)$, which generally is a complicated function of the amplitude, we consider the spin-spin correlation function. Up to a pre-factor, given by the angle between the initial direction of the dipole moment relative to the external electric field, the dielectric response of an isolated TLS is defined by the Fourier component of the following correlator [103]

$$\epsilon(\omega) = \frac{i}{4} \int\limits_{0}^{\infty} e^{i\omega t} e^{-t/\tau} \langle [\hat{\sigma}_z(t), \hat{\sigma}_z(0)] \rangle dt \tag{6.44}$$

where square brackets denote a commutator between the corresponding spin operators. The exponential prefactor describes the dissipative effects of the environment and averaging is taken over the initial state of the TLS. We are introducing the dissipative effects on a phenomenological level only and ignore the difference between the relaxation and dephasing processes. This is sufficient to get insight into the general properties of the exact spectrum of the dielectric response due to an ensemble of identical TLS. Operators $\hat{\sigma}_\alpha(t)$ in Eq. (6.44) correspond to the Heisenberg

representation:

$$\hat{\sigma}_z(t) = \hat{S}^\dagger(t)\hat{\sigma}_z\hat{S}(t). \tag{6.45}$$

We remind the reader that formally the evolution operator $\hat{S}(t)$ is given by

$$\hat{S}(t) = \hat{T}\exp\left[-i\int_0^t H(t')dt'\right], \tag{6.46}$$

with $\hat{T}$ being a time-ordering operator. Using (6.39) and assuming the initial conditions $\Psi^\dagger(0) = (a^*, b^*)$, for the correlator $\mathcal{K}(t) = \frac{i}{4}\langle[\hat{\sigma}_z(t), \hat{\sigma}_z(0)]\rangle$ under the integral in (6.44) we find:

$$\mathcal{K}(t) = 4(|a|^2 - |b|^2)m_\perp(t)\sin[2\alpha(t)] + 8i\mathrm{Im}[a^*b]\times$$
$$\times \{m_z(0)m_x(t) - m_x(0)m_\perp(t)\cos[2\alpha(t)]\}. \tag{6.47}$$

Here $m_\perp(t) = \sqrt{1/4 - m_x^2(t)}$ and we have fixed the initial value of the field so that $\dot{f}(0) = 0$. The subsequent time integration yields an expression for the dielectric response function. Analytic analysis of the response function $\epsilon(\omega)$ is hindered by the fact that the correlation function $\mathcal{K}(t)$ is only a quasi-periodic function of time, since it is expressed as a combination of two periodic functions with different periods T_f and T_h (6.33), so that we have to resort to numerical calculation. In Fig. 6, we present representative plots of the real and imaginary part of $\varepsilon(\omega)$ (6.44) for the initial conditions (6.36). To interpret our results, we recall that the common phase, $\alpha(t)$, can be written as a sum of a linear-in-t term plus a periodic function (6.33). Since $m_\perp(t)$ is a periodic function with the period T_f, we can express the corresponding terms in (6.47) in a Fourier series. Subsequent time integration yields
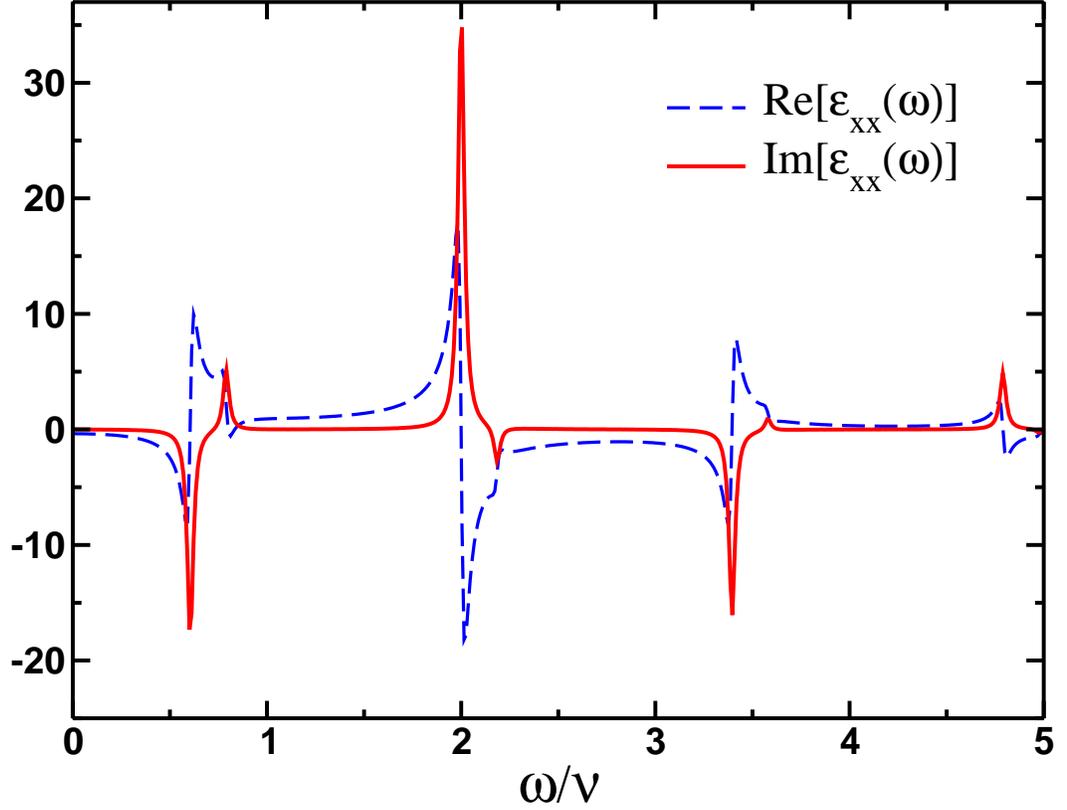
Figure 6.7: Plot of real and imaginary part of the response function $\epsilon(\omega)$. Note that discontinuities in real part and the peaks in imaginary part of the response function appear at frequencies $\omega_{dis} = 2(n\omega \pm \nu)$, $(n = 0, \pm 1, \pm 2...)$ in agreement with expression (6.48). These plots has been obtained for the following values of the parameters: $\Delta_a = 0.15\Delta_+$, $\Delta_- = 0.3\Delta_+$ and $\Delta_t = 0.5\Delta_+$.

a response function of the following type:

$$\epsilon(\omega) = \sum_{n=-\infty}^{\infty} \frac{\chi_n}{\omega - 2n\omega_f \pm 2\nu + \frac{i}{\tau}}, \tag{6.48}$$

where ε_n are the corresponding Fourier coefficients. From this expression, we see that the peaks in the imaginary part of the response function describing the energy losses due to TLSs appear at frequencies, $\omega_{dis} = 2(n\omega \pm \nu)$, commensurate with the driving frequency but with an overall shift determined by the quantum mechanical phase collected by a TLS over one cycle, ν. Note that within the linear response theory, one typically keeps only the lowest Fourier harmonic in the spectrum ($n = 0$) and neglects all others. For the case of a monochromatic field the Fourier component with $n = 0$ is kept so that

$$\epsilon_{lin}(\omega) = \varepsilon_0 \sum_{a=\pm} \frac{1}{\omega + 2a\nu + \frac{i}{\tau}}, \tag{6.49}$$

and we recover the textbook result for the dielectric response function. [103] For a fixed set of parameters, however, one would only keep the largest contribution to the imaginary part of $\epsilon(\omega)$. For example, the imaginary part of $\epsilon(\omega)$ is the largest for $\omega^* \simeq 2\nu$. Note also that apart from a difference in the value of the resonant frequency (which in the regime of weak driving is given by the energy that governs a stationary time evolution of a TLS eigenstate in the absence of any perturbations, $\nu = \sqrt{\Delta_t^2 + \varepsilon^2}$, the response functions for the case of monochromatic field and the field given by (6.23) are qualitatively the same.

In the array of non-interacting TLS, the response function must be averaged over a distribution of the barrier heights, direction of the electric field etc. We leave

the detailed analysis directly applicable to the array of non-interacting and pairwise interacting TLS for a future publication.

6.5   Conclusions

In this chapter we presented an exact solution for the problem of AC-driven dynamics of a generic two-level system. Our approach was based on constructing a non-linear differential equation for the driving field, which has admitted an exact solution. The key feature of our solution for the external field is that it is fully described by three independent parameters. We have shown that one can interpret different nonlinear combinations of these parameters as an amplitude, frequency and a DC-component of the field. Being very general in nature, we believe that our results and methods can be applied to a wide variety of experiments ranging from NMR to the analysis of dielectric losses in amorphous materials.

Chapter 7

Conclusion and future work

Other than the common theme of 'superconductors and insulators/dielectrics' linking the two parts of this thesis, there is another methodological connection between them. Both works are based on conjectures made from experimental data and construct analytically solvable models based on these conjectures.

In part I, the conjecture is related to the BEC model of superconductivity and the consequent localized pairing hypothesis. The microscopic origin of this localized pairing is a matter of debate and we carefully sidestep this debate in this thesis. We limit ourselves to introducing the additional complication of localized pairing to two well-known models of insulators : the Efros-Shklovskii model (classical disordered insulators with unscreened Coulomb interactions) and the Anderson model (disorder with tunneling treated perturbatively). Using techniques tailored for these models, we find the changes introduced into the original results solely from the pairing. Put in a different way, we designed ways to extend models of insulators to make them applicable to a much broader domain, namely in the vicinity of transition to superconductivity.

In part II, the conjecture is that power loss in dielectrics comes from resonant absorption of radiation by two-level systems. We again carefully sidestep the question of microscopic origin of the tunneling states. Faced with the obstacle that

even the simplest time-varying electric field does not lend itself to a solvable model, we look into the question of whether one can reverse-engineer solvable models from known time-evolutions.

7.1   Part I: Superconductor-insulator transitions

The main experimental motivation behind this part was the resistance non-monotonicity on the insulating side of a superconductor-insulator transition. In chapters 3 and 4, we suggested two possible scenarios to explain this nonmonotonicity. The Hamiltonians of both models can be extracted from the general Hamiltonian in Eqn. 2.1 in the appropriate limit. While the two-component Coulomb glass model is obtained at zeroth order in the quantum hopping and incorporates localized single electrons and pairs in one framework, the Anderson models allow hopping, ignore Coulomb interactions and focus on one kind of carrier only. The idea behind this two-prong approach is to isolate the individual factors that, by themselves, could lead to nonmonotonicity in magnetoresistance of the kind observed in experiments.

The role of the magnetic field is also different in the two cases. In the two-component Coulomb glass model, it tunes the local pairing strength and thus effectively the ratio of pairs versus singles in a critical percolation network. In Chapter 3, we discussed the effect of this change on the single and pair density of states, leading to crucial modification of the universal Coulomb gap. We discussed the potential implications of this on transport measurements. The remarkable feature to note there is that unlike the canonical variable-range-hopping (VRH) transport

which is otherwise insensitive to a change in carrier density at fixed temperature, tuning carrier density in the single-channel by pair formation and locking away the pairs from transport does modify transport properties. Here, the newly formed pairs merely dictate the single-DOS profile through Coulomb stability constraints. In this way, pair-formation acts as a potential knob for reducing carrier density in these disordered insulators that also influences low-temperature transport. Hence, it is legitimate to consider it as representative of all the tuning parameters (magnetic field, disorder strength, gate voltage) that lead to a variation in resistance of these insulators.

Applying a magnetic field affects more than one of the ingredients involved in VRH transport. In fact, it is beneficial at this point to revisit the philosophy of variable-range-hopping transport. As described earlier, such a transport involves thermally induced transfer of localized carriers between impurity states. The variable-range nature of the hopping arises from a competition between the energy cost (in transfer of the localization center to a nearby site) and the distance traversed. This is expressed through the following relation for the transition probability Γ^0_{ij} of a single electron between two sites i and j [39, 132]

$$\Gamma^0_{ij} \sim \exp\left(-\frac{r_{ij}}{\xi}\right) N\left(\Delta\epsilon_{ij}\right) f_i \left(1 - f_j\right) \qquad (7.1)$$

where r_{ij} = distance between the sites,

ξ = localization length of the carrier wave-functions,

$\Delta\epsilon_{ij}$ = energy cost in transfer from site i to site j,

$N\left(\Delta\epsilon_{ij}\right) = \left|\frac{1}{\exp\left(\frac{\Delta\epsilon_{ij}}{T}\right)-1}\right|$ = number of phonons involved in the transfer (for

energy conservation),

$$f_i = \frac{1}{1+1/2\exp(\epsilon_i-\mu)/T} = \text{probability of site } i \text{ being occupied, with } \epsilon_i \text{ being the}$$

energy associated with site i.

This is equivalent to a resistor joining the two sites $R_{ij} = \frac{1}{\beta e^2 \Gamma^0_{ij}}$. At low enough temperatures, one can reduce this expression to the simplified form $R_{ij} = \exp\left(\frac{\Delta\epsilon_{ij}}{T} + \frac{r_{ij}}{\xi}\right)$. One can estimate a typical resistance for a network of such resistors using simple Mott-like arguments or using a percolation method. Since the typical distance between localized states at energy ϵ can be estimated at $r(\epsilon) = (\rho_1(\epsilon))^{-1/2}$ (ρ_1 being the one-particle DOS), the two summands in $\ln R_{ij}$ compete with each other, settling on a compromise of the two at the critical resistance value.

Thus, it is premature to conclude about the magnetoresistance from the one-particle density of states alone. One also needs to take into account the effect of magnetic field on the localization length ξ of the carrier wave-functions. It is clear from the equivalent hopping resistance R_{ij} that a delocalized carrier favors hopping transport. Chapter 4 discusses the effect of magnetic field on the localization length using the Anderson insulator models. The spatial decay of wave functions is studied to leading order in hopping over disorder strength, thus still representing a strongly localized regime.

This effect is treated entirely separately for fermionic and bosonic insulators without any mixing between the two. It is shown that from purely statistical effects, one finds opposite B-dependences of localization length for fermionic and bosonic carriers. While the magnetic field localizes the bosonic carriers and thus hinders transports, it favors fermionic hopping transport by spreading the wave functions

further. This opposing behavior is predicted to be a major player behind the giant magnetoresistance peak.

Moreover, the exact B-dependence of localization length for bosonic Anderson insulators is established through a mapping to the well-studied problem of directed polymers in a random media. The mapping to DPRM is cleaner in the bosonic case due to the positive definite character of contribution to wave function delocalization from individual tunneling paths and has been studied completely. Since most experiments on superconductor-insulator transitions focus on transport phenomena, the observed B-dependence could form an easily testable consequence of the localized pair hypothesis. Additionally, one can also establish variable-range-hopping of localized pairs as the dominant mode of transport in these insulating films.

The merit of our approach as opposed to previous studies lies in starting from a general microscopic Hamiltonian and systematically studying it with controlled approximations. The next obvious direction of research lies in relaxing the various approximations involved and checking whether the conclusions are radically modified. One natural exercise involves using the disorder distribution as a handle to tune between uniform density of states and a Coulomb gap at the Fermi level. In this semiclassical approach, one begins from the Anderson models of disorder except that the disorder distribution has the linear Coulomb gap artificially built in it. In this way, one can possibly check whether the directed polymer mapping of the forward path sum for bosonic insulators survives unscreened Coulomb interactions.

Another direction of research can involve finding the decay amplitude from the bosonic Anderson model relaxing the forward scattering approximation. This

essentially involves adding an increasing number of backward detours on the fwd-scattering paths at each higher order in the tunnel hopping parameter t. Physically, this represents an approach to the critical point of the superconductor-insulator transition from the insulating side.

7.2 Part II:Dielectric losses in superconducting qubits

As described in Chapter 5, dielectric power losses in amorphous materials can be represented by a broad distribution of two-level systems interacting with a thermal bath and driven by a time-dependent electric field. These systems in turn can be mapped to spin systems in a time-dependent magnetic field.

Spin systems interacting with a generic time-dependent magnetic field do not lend themselves to an analytical solution. With an approach developed in the context of nonequilibrium superconductivity, in Chapter 6, we engineered time-dependences of the magnetic field which allow us to easily write down the solutions of the corresponding Schrödinger equation. This is made possible by the fact that we started from the latter solutions themselves and reverse engineered the Hamiltonian. (More precisely, we actually started from solutions of the corresponding Bloch equation — which are the evolution equations for the expectation values of the spin operators. We reverted to the original Schrödinger equations only to obtain the phase of the wave function.)

To obtain the dielectric loss from this magnetic-field-driven spin-evolution, we followed the standard TLS recipe of relating the frequency-dependent dielectric

constant to the Fourier-transform of the spin-spin correlator. We introduced any interaction with a thermal bath through an exponential time-decay with a phenomenological decay-rate. A more rigorous approach would involve including terms corresponding to the thermal bath as well as their interaction with the TLS in the Hamiltonian of the system, somewhat akin to the Jaynes-Cummings model [133].

More importantly, the technique developed in this chapter is applicable to a much wider variety of systems and can potentially allow one to mathematically proceed further with several hard problems. We have been so far able to exploit this only for two-level systems due to their convenient $SU(2)$ group structure. In a related work [134], a similar approach has also been shown for the Bose-Hubbard model where the Heisenberg group structure has been used for the time-evolution.

To continue with the common thread linking the two parts of this thesis, future directions of research can involve probing the microscopic origins of the premises behind the models constructed. For the first part of the thesis, this would mean locating the origin of localized pairing in the 2D films undergoing superconductor-insulator transition. For the second part, this would involve understanding what exactly are the two-level systems in amorphous solids which couple to an external electric field. Only with a reasonable understanding of these premises can one hope to provide a complete picture of these materials.

Appendix A

Analysis of hierarchical model for directed polymers

A.1 Hierarchical loop model

Here we analyze in more detail the hierarchical loop model defined in the main text. This model implements the ideas of the droplet picture in an analytically tractable and mathematically precise way.

Our focus will be on the analytical calculation of magnetoconductance in the perturbative and the non-perturbative regimes. However, we have also studied the crossover between the two regimes numerically. We found the crossover, the asymptotic power laws and subleading corrections to be very similar to those observed in the full lattice model of forward-directed paths. This suggests that the hierarchical droplet model captures indeed most of the relevant physical ingredients of magnetoconductance.

A.1.1 Models

Imposing the scaling of individual droplet degrees of freedom actually does not fully specify a hierarchical droplet description, but leaves some freedom in the definition of the model. The resulting models differ in the way they treat correlations between energies of spatially overlapping droplets. As we will see this translates primarily into differences in the numerical coefficients of subleading terms.

A.1.1.1 Normalized recursion

We first discuss the hierarchical construction as defined in the main text, cf. Eq. (10). It is defined by iterating the following recursive construction from the largest scale N down to the lattice scale, the loops or branch segments having lengths $L_k = 2^{-k}N$ for $0 \leq k \leq K \equiv \lfloor \log_2(N) \rfloor$,

$$
\begin{aligned}
S_{\mathcal{L}} &= 1, \quad \text{if} \quad L_{\mathcal{L}} = 2^{-K}N, \\
S_{\mathcal{L}} &= \frac{S_{\mathcal{L}_1'}S_{\mathcal{L}_2'} + W_{\mathcal{L}}(B)S_{\mathcal{L}_1''}S_{\mathcal{L}_2''}}{1 + W_{\mathcal{L}}(0)}, \tag{A.1} \\
W_{\mathcal{L}}(B) &= \exp\left[-fL_{\mathcal{L}}^{\theta} + iBa_{\mathcal{L}}L_{\mathcal{L}}^{1+\zeta}\right] \tag{A.2} \\
&= \exp\left[-fL_{\mathcal{L}}^{\theta} + ia_{\mathcal{L}}\left(\frac{L_{\mathcal{L}}}{\ell_B}\right)^{1+\zeta}\right].
\end{aligned}
$$

We have defined $\ell_B \equiv B^{-1/(1+\zeta)}$ and have dropped the explicit dependence of $S_{\mathcal{L}}$ on B. Note that the normalization factor in the denominator in Eq. (A.1) ensures that $S_{\mathcal{L}}(B = 0) = 1$. Therefore $fL_{\mathcal{L}}^{\theta}$ is precisely the free energy difference between the leading and subleading branches of paths, which this model treats as independent from loop energies at smaller scales. In weak fields the magnetic field response will be insensitive to the precise value of the small scale cutoff, $L_{\min} = N2^{-K}$, as long as it is much smaller than the relevant magnetic length, $L_{\min} \ll \ell_B$. Indeed, up to small corrections, $S_{\mathcal{L}}(B) \approx 1$ for all loops with $L_{\mathcal{L}} \ll \ell_B$.

A.1.1.2 Non-normalized recursion

The above model assumes that free energy differences between a dominant and subdominant branch are independent of the energies (and thus interferences) on smaller scales along those branches. A more realistic model should take into

account that if positive interferences occurred along a branch, the resulting free energy of the branch is statistically bigger than if the interferences were negligible. Such effects can be built into a hierarchical construction by modifying the recursion to

$$S_{\mathcal{L}} = 1, \quad \text{if} \quad L_{\mathcal{L}} = 2^{-K}N,$$

$$S_{\mathcal{L}} = S_{\mathcal{L}'_1}S_{\mathcal{L}'_2} + W_{\mathcal{L}}(B)S_{\mathcal{L}''_1}S_{\mathcal{L}''_2}, \tag{A.3}$$

with the same weight factor $W_{\mathcal{L}}(B)$ (A.2), but dropping the normalization. In this case $S_{\mathcal{L}}(0)$ is not normalized to the same value 1 at all length scales. This ensures that the explicit contribution to free energy difference between two branches, $fL_{\mathcal{L}}^{\theta}$, is supplemented by an extra contribution which incorporates the sum over paths at smaller scales.

This non-normalized recursion follows a similar hierarchical construction by Derrida and Griffith [91]. They assigned to each loop random energies that however didn't scale with the level of the hierarchy. This generated randomly fluctuating free energies, with a free-energy exponent which is only slightly smaller than the value $\theta = 1/3$. In this version of the recursion, we retain the spirit of the Derrida-Griffiths approach with the only difference being that we introduce the DP-scaling by hand through the free-energy $fL_{\mathcal{L}}^{\theta}$.

A.1.2 Magnetoconductance

We now study the magnetoconductance of the above models,

$$\ln \Delta \sigma_N(B) \equiv \overline{\ln \left| S_{\mathcal{L}=\{0N\}}(B) \right|} - \overline{\ln \left| S_{\mathcal{L}=\{0N\}}(0) \right|}, \tag{A.4}$$

113

where $\overline{[\cdots]}$ denotes the average over the set of reduced free energy and area variables, $\{h \equiv (f, a)\}$. We assume the two variables associated with each loop to be independent and identically distributed,

$$P(\{h\}) = \prod_{\mathcal{L}} \rho(f_{\mathcal{L}}, a_{\mathcal{L}}) df_{\mathcal{L}} da_{\mathcal{L}}. \tag{A.5}$$

The product runs over all loops $\mathcal{L}$, the support of ρ being $\{f, a\} \in [0, \infty) \times (-\infty, \infty)$. However, as we will see, only the values of $\rho(f = 0, a) \equiv \rho_a(a)$ will enter the analytical results. For quantitative calculations, we will assume a simple Gaussian form,

$$\rho(f = 0, a) \equiv \rho_a(a) = \rho_0 \frac{\exp[-a^2/2a_0^2]}{\sqrt{2\pi} \, a_0}. \tag{A.6}$$

The (non-normalized) density $\rho_a(a)$ is a free input parameter of the hierarchical models. More realistic densities could be determined by studying the distributions of loop areas in the full lattice model.

Let us now analyze the magnetoconductance,

$$F(\{h\}) \equiv [\ln|S_{0N}(B)| - \ln|S_{0N}(0)|] (\{h\}) \tag{A.7}$$

as a functional of the disorder realization $(\{h\})$. F can be viewed as the free energy difference between a directed polymer with B-induced complex weights and one in zero field, where all weights are positive.

In typical disorder realizations most loops do not play a significant role in modifying the interference of alternative tunneling paths. A loop $\mathcal{L}$ is involved significantly only if $f_{\mathcal{L}} \lesssim L_{\mathcal{L}}^{-\theta}$, in which case we refer to it as 'active'. Large active loops are dilute, while small ones are more abundant, but contribute very little to

magnetoconductance. One can thus expand F in the spirit of a droplet or virial expansion into a sum of terms $\mathcal{V}_k$, which involve an increasing number k of spatially overlapping loops,

$$
\begin{aligned}
F\left(\{h\}\right) &= \mathcal{V}_1 + \mathcal{V}_2 + \mathcal{V}_3 + \dots \\
&= \sum_{k \geq 1} \sum_{\{\mathcal{L}_1 \neq \dots \neq \mathcal{L}_k\}} F^c\left(h_{\mathcal{L}_1}, \dots, h_{\mathcal{L}_k}\right).
\end{aligned}
\tag{A.8}
$$

The sums are over all (non-ordered) sets of distinct loops. The decomposition in Eq. (A.8) is exact, given that the connected functions F^c are defined recursively as

$$
F^c(h_{\mathcal{L}_1}) = F\left(\{h_{\mathcal{L}} \,|\, f_{\mathcal{L} \neq \mathcal{L}_1} \to \infty\}\right),
\tag{A.9}
$$

$$
F^c(h_{\mathcal{L}_1}, h_{\mathcal{L}_2}) = F\left(\{h_{\mathcal{L}} \,|\, f_{\mathcal{L} \neq \mathcal{L}_1, \mathcal{L}_2} \to \infty\}\right) - F^c(h_{\mathcal{L}_1}) - F^c(h_{\mathcal{L}_2}),
\tag{A.10}
$$

$$
\vdots
$$

$$
F^c(h_{\mathcal{L}_1}, \dots, h_{\mathcal{L}_k}) = F\left(\{h_{\mathcal{L}} \,|\, f_{\mathcal{L}} \to \infty \, \forall \mathcal{L} \notin \{\mathcal{L}_1, \dots, \mathcal{L}_k\}\}\right) - \sum_{m=1}^{k-1} \sum_{\{\mathcal{L}'_1 \neq \dots \neq \mathcal{L}'_m\} \subset \{\mathcal{L}_1, \dots, \mathcal{L}_k\}} F^c(h_{\mathcal{L}'_1}, \dots, h_{\mathcal{L}'_m}).
$$

$$
\tag{A.11}
$$

The subtraction of the disconnected terms in Eqs. (A.10,A.11) ensures that F^c tends to 0 as one of its free energy arguments becomes large, $f_i \to \infty$, which turns the corresponding loop inactive. It is also easy to verify that F^c vanishes, unless the loops associated with its arguments belong to a single spatially entangled cluster. This follows immediately form the fact that disconnected sets of loops contribute additively to $\ln |S_{0N}(B)|$. This clustering property ensures an extensive result in the large distance limit, $N \gg \ell_B$ (for every order of the expansion $\overline{\mathcal{V}_k} \sim N$), i.e., we

must have

$$\ln |S_{0N}(B)| - \ln |S_{0N}(0)| = -\Delta(\xi^{-1})N + o(N), \qquad (A.12)$$

where the coefficient $\Delta(\xi^{-1})$ is expected to be self-averaging. As the notation suggests, this coefficient represents a correction to the inverse localization length ξ^{-1}.

The disorder average is carried out term by term. Thereby, the disorder variables, especially $f_{\mathcal{L}}$, take the role of relative positions of particles played in the cluster expansion of gases. The role of a low gas density is played by the small likelihood of large loops to be active. The term $\mathcal{V}_k$ in the expansion (A.8) captures the interference contribution from *exactly* k active loops, similar to droplet expansions at low T in related disordered systems. [135, 136, 137] This is akin to the virial expansion, which corrects the ideal gas behavior by summing n-particle contributions at order n^k in an expansion in the density n.

The various contributions to $\mathcal{V}_k$ can easily be represented graphically by enumerating all spatially connected sets of k loops, and summing over their sizes, see Figs. A.1 and A.2 .

A.1.3   Evaluation of leading terms

A.1.3.1 1st order term

The first term in Eq. (A.8) can be rewritten as

$$\mathcal{V}_1 \;=\; \sum_{\mathcal{L}} \ln \left| \frac{1 + W_{\mathcal{L}}(B)}{1 + W_{\mathcal{L}}(0)} \right| \tag{A.13}$$

$$= \; \frac{1}{2} \sum_{\mathcal{L}} \ln \left[1 - \frac{4 e^{-f_{\mathcal{L}} L_{\mathcal{L}}^{\theta}} \sin^2 \left(\frac{a_{\mathcal{L}}}{2} B L_{\mathcal{L}}^{1+\zeta} \right)}{\left(1 + e^{-f_{\mathcal{L}} L_{\mathcal{L}}^{\theta}} \right)^2} \right] ,$$

for both the normalized and the non-normalized recursive definitions of the model.

Reorganizing this as a sum over looplengths $\ell_k = N 2^{-k}$, and performing the disorder average, we find

$$\overline{\mathcal{V}_1} \;=\; \frac{1}{2} \sum_{k=0}^{K} \frac{N}{\ell_k} \overline{\ln \left[1 - \frac{\sin^2 \left(\frac{a}{2} B \ell_k^{1+\zeta} \right)}{\cosh^2 \left(\frac{f}{2} \ell_k^{\theta} \right)} \right]}^{a,f} . \tag{A.14}$$

A.1.3.2 2nd order term

The second term in the droplet expansion, $\mathcal{V}_2$, picks up contributions from disorder realizations where two active loops spatially overlap. This can occur in two distinct ways, c.f., Fig. A.1: either (I) the smaller loop is part of the dominant; or (II) part of the subdominant branch of the larger loop. Let us refer to the bigger and smaller loop as $\mathcal{L}_1$ and $\mathcal{L}_2$, respectively, with lengths $L_{1,2}$.

The following expressions apply to the normalized model. The discussion of differences for the non-normalized version will be discussed further below when we evaluate the terms. Denoting $W_i(B) \equiv W_{\mathcal{L}_i}(B)$, $\mathcal{V}_2$ can be written as

$$\mathcal{V}_2 = \sum_{\substack{\mathcal{L}_1, \mathcal{L}_2 \\ L_1 > L_2}} \left[\mathcal{V}_2^{(I)}(\mathcal{L}_1, \mathcal{L}_2) + \mathcal{V}_2^{(II)}(\mathcal{L}_1, \mathcal{L}_2) \right] \tag{A.15}$$
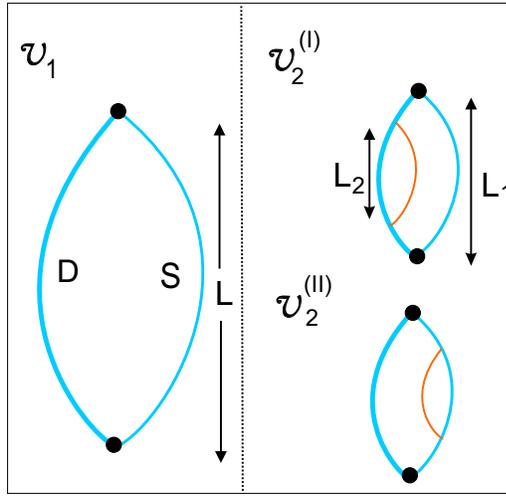
Figure A.1: Graphic representation of the first two virial terms in Eq. A.8. *Left:* $\mathcal{V}_1$ is a sum over all loops $\mathcal{L}$, composed of a dominant (thick line) and subdominant (thin line) branch. *Right:* The two contributions to $\mathcal{V}_2$ arise form spatially overlapping loops of length $L_1 > L_2$. The two cases distinguish whether the smaller loop belongs to the dominant (I) or subdominant (II) branch.

where

$$\mathcal{V}_2^{(I)}(\mathcal{L}_1, \mathcal{L}_2) = \ln \left| \frac{\frac{1+W_2(B)}{1+W_2(0)} + W_1(B)}{1 + W_1(0)} \right| \tag{A.16}$$
$$- \ln \left| \frac{1 + W_1(B)}{1 + W_1(0)} \right| - \ln \left| \frac{1 + W_2(B)}{1 + W_2(0)} \right|,$$

$$\mathcal{V}_2^{(II)}(\mathcal{L}_1, \mathcal{L}_2) = \ln \left| \frac{1 + \frac{1+W_2(B)}{1+W_2(0)} W_1(B)}{1 + W_1(0)} \right|$$
$$- \ln \left| \frac{1 + W_1(B)}{1 + W_1(0)} \right|. \tag{A.17}$$

Taking the disorder average and writing (A.15) as a sum over loop lengths we have

$$\overline{\mathcal{V}_2} = \sum_{k_1=0}^{K} \sum_{k_2 > k_1}^{K} \frac{N}{2^{k_2}} \overline{\ln \left| 1 + \frac{W_1(B)(Z_2 + Z_2^{-1} - 2)}{(1 + W_1(B))^2} \right|}^{a_{1,2}, f_{1,2}} \tag{A.18}$$

where $Z_2 = (1 + W_2(B))/(1 + W_2(0))$.

118

A.1.3.3 Higher order terms

For sufficiently large loops, $L_\mathcal{L} \gg 1$, the disorder average simplifies. Indeed only very small values of $f_{\mathcal{L}_i}$ are relevant, since the connected functions F^c fall off rapidly when one if its arguments $f_{\mathcal{L}_i}$ is larger than $L_{\mathcal{L}_i}^{-\theta}$. On the other hand, we will see that small scales contribute negligibly to magnetoconductance as long as $B \ll 1$, so we can concentrate on $L_\mathcal{L} \gtrsim \ell_B$. Thus, for each variable f in the disorder average, we can safely approximate $\int df\, da\, \rho(f, a)... \approx \int df\, da\, \rho_a(a)...$, cf. Eq. (A.6).

Introducing $F_i \equiv f_{\mathcal{L}_i} L_{\mathcal{L}_i}^\theta$, the disorder-average of the n-th virial term becomes

$$
\begin{aligned}
\overline{\mathcal{V}_n} &= \sum_{\{\mathcal{L}_1 \neq ... \neq \mathcal{L}_n\}} \left(\prod_{i=1}^n \frac{1}{L_{\mathcal{L}_i}^\theta} \right) I_n, & \text{(A.19)} \\
I_n &= \prod_{i=1}^n \left(\int_0^\infty dF_i \int_{-\infty}^\infty \rho_a(a_i) da_i \right) F^c(H_1, H_2, \cdots, H_n),
\end{aligned}
$$

using the notation $H_i \equiv (F_i, a_i)$.

A.2   Scalings in the droplet expansion

A.2.1   Weak fields: $BN^{1+\zeta} \ll 1$

For weak fields one can expand I_n in the enclosed fluxes, the result being dominated by the largest scale N. Expanding Eq. (A.14) in B, and integrating over the rescaled F variables, we find the leading contribution to the magnetoconductance

$\ln \Delta \sigma_N(B)$

$$\overline{\mathcal{V}_1} \approx -\frac{1}{4} \int \rho_a(a) a^2 da \, B^2 N \sum_{k=0}^{K} \ell_k^2$$
$$\approx -\frac{1}{3} \int \rho_a(a) a^2 da \, B^2 N^3, \qquad (A.20)$$

which is negative, as expected for bosonic magnetoconductance. Likewise, one can check from (A.18), that $\mathcal{V}_2 \sim O(B^2 N^{2(1+\zeta)-2\theta})$. More generally one finds that higher order terms are suppressed by the prefactors $\prod_{i=1}^{n} L_i^{-\theta}$ in Eq. (A.19) with $L_i \sim N$, which leads to the subdominant scaling $\mathcal{V}_k \sim O(B^2 N^{2(1+\zeta)-k\theta})$.

Note that the leading scaling (A.20) is *independent* of the wandering exponent, by virtue of the relation $\theta = 2\zeta - 1$. One therefore obtains the same scaling as in a non-disordered case, for which the exponents $\zeta = 1/2, \theta = 0$ hold. However, we stress that in the disordered case the result (A.20) arises as a result of disorder averaging, which masks some of the physics. The *distribution* of $\mathcal{V}_1$ is wide, and the average (A.20) is dominated by a few rare disorder configurations. The latter occur with probability $\sim N^{-\theta}$, but contribute a large $\mathcal{V}_1 \sim B^2 N^{2(1+\zeta)}$, while in most other realizations the wavefunctions are much less affected by quantum interference. [1]

[1]Since the response in the perturbative regime is strongly inhomogeneous, it is not clear whether the logarithmically disorder-*averaged* $\Delta \sigma_N$ with $N = R_{\text{hop}}$ is the only relevant quantity determining transport. In particular one should be cautious when using these results as inputs for transport problems on larger scales, such as variable range hopping. We are not aware of any theoretical approach which take into account the statistical distribution of the B-effects on wavefunction properties, rather than assuming a homogeneous average effect on all wavefunctions.
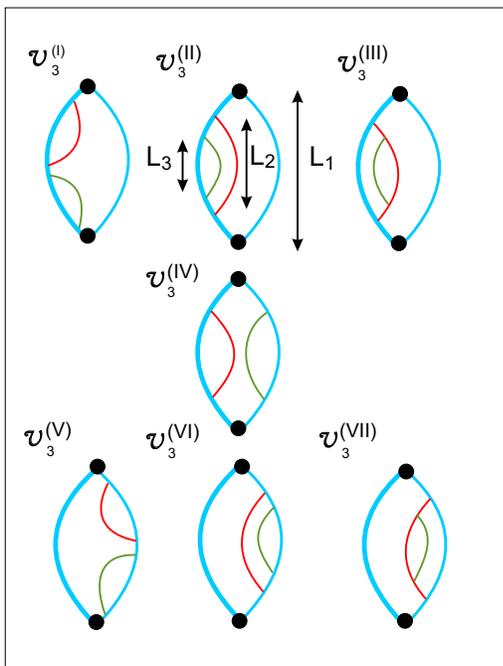
Figure A.2: Graphic representation of the third order terms $\mathcal{V}_3$ in Eq. (A.8) with L_1 (blue) $\geq L_2$ (red) $\geq L_3$(green).

A.2.2 Strong fields: $BN^{1+\zeta} \gg 1$

The perturbative expansion holds only for weak fields for which the distance between end points is smaller than the 'magnetic length', $N \ll \ell_B$. For stronger fields, the dominant contribution comes from loops at the scale ℓ_B. To see this, let us approximate the sum over discrete loop sizes in (A.14) as an integral, $\sum_k \approx 1/\ln(2) \int d\ell/\ell$,

$$\overline{\mathcal{V}_1} \approx \frac{N}{2\ln(2)} \int_1^N \frac{d\ell}{\ell^2} \overline{\ln\left[1 - \frac{\sin^2\left(\frac{a}{2}B\ell^{1+\zeta}\right)}{\cosh^2\left(\frac{f}{2}\ell^\theta\right)}\right]}^{a,f}. \tag{A.21}$$

Rescaling the free energies and changing variables to $u \equiv \ell/\ell_B$, we obtain

$$\overline{\mathcal{V}_1} = -c_1 \frac{N}{\ell_B^{1+\theta}} = -c_1 N B^{\frac{2\zeta}{1+\zeta}} = -c_1 N B^{4/5}, \tag{A.22}$$

with the numerical coefficient

$$
\begin{aligned}
c_1 \approx \quad & -\frac{1}{2\ln(2)} \int_0^\infty \frac{du}{u^{2+\theta}} \int_0^\infty dF \times \\
& \int_{-\infty}^\infty da \rho_a(a) \ln\left[1 - \frac{\sin^2(au^{1+\zeta}/2)}{\cosh^2(F/2)}\right].
\end{aligned}
\tag{A.23}
$$

For the particular choice (A.6) for $\rho_a(a)$ (with $\rho_0 = a_0 = 1$) we find

$$
c_1 \approx 0.86.
\tag{A.24}
$$

Note that the dominant contribution comes indeed from $u = O(1)$, i.e., from loops of size ℓ_B. We have extended the limits of the u-integral to 0 and ∞, as it converges rapidly on both sides. This result implies a leading correction to the localization length as

$$
\Delta(\xi^{-1}) = c_1 B^{\frac{2\zeta}{1+\zeta}}.
\tag{A.25}
$$

A.2.3 Subleading corrections

In the non-perturbative regime, subleading corrections are interesting to analyze in more detail, as they correct the leading behavior (A.25). As we shall see below, there is a direct correlation between the order of a term in the virial expansion and its scaling with B, which justifies using the virial expansion in the first place. Roughly speaking, each loop contributes a scaling factor of $B^{\frac{\theta}{1+\zeta}}$ on disorder averaging, causing the n-th virial term with n spatially overlapping loops to contain as many such factors.

A more precise formulation follows. We begin with the second order term $\mathcal{V}_2$. As before, we can rewrite $\overline{\mathcal{V}_2}$ as a sum over pairs of loop lengths, $L_j = 2^{-j}N$ and

122

$L_k = 2^{-k} N$, and take the continuum limit of the discrete sums over j and k

$$
\begin{aligned}
\overline{\mathcal{V}_2} &= \sum_{\substack{j,k \\ k>j}} \frac{N}{L_k} \left[\overline{\mathcal{V}_2^{(I)}}(L_j, L_k) + \overline{\mathcal{V}_2^{(II)}}(L_j, L_k) \right] \qquad\qquad\qquad \text{(A.26)} \\
&\approx \frac{N}{(\ln 2)^2} \int_1^N \frac{d\ell_1}{\ell_1} \int_1^{\ell_1} \frac{d\ell_2}{\ell_2^2} \left[\overline{\mathcal{V}_2^{(I)}}(\ell_1, \ell_2) + \overline{\mathcal{V}_2^{(II)}}(\ell_1, \ell_2) \right].
\end{aligned}
$$

Here, $\mathcal{V}_2^{(I)}(\ell_1, \ell_2)$ and $\mathcal{V}_2^{(II)}(\ell_1, \ell_2)$ are given by Eqs. (A.16,A.17) (loop $\mathcal{L}_i$ being referred to by its length ℓ_i). The overbar denotes the average over $f_{1,2}$ and $a_{1,2}$ with the appropriate probability distributions

$$
\overline{[\cdots]} \equiv \int_0^\infty df_1 \rho_f(f_1) \int_0^\infty df_2 \rho_f(f_2)
$$

$$
\int_{-\infty}^\infty da_1 \rho_a(a_1) \int_{-\infty}^\infty da_2 \rho_a(a_2) [\cdots],
$$

Substituting $u_1 = \frac{\ell_1}{\ell_B}$ and $u_2 = \frac{\ell_2}{\ell_B}$, we obtain the subleading correction

$$
\overline{\mathcal{V}_2} = -c_2 \frac{N}{\ell_B^{(1+2\theta)}} = -c_2 N B^{\frac{4\zeta-1}{1+\zeta}}, \qquad\qquad\qquad \text{(A.27)}
$$

with the numerical coefficient

$$
c_2 \approx -\frac{1}{(\ln 2)^2} \int_0^\infty \frac{du_1}{u_1^{1+\theta}} \int_0^{u_1} \frac{du_2}{u_2^{2+\theta}} \int_0^\infty dF_1 \int_0^\infty dF_2 \int_{-\infty}^\infty da_1 \rho_a(a_1) \int_{-\infty}^\infty da_2 \rho_a(a_2)
$$

$$
\times \ln \left| 1 + \frac{e^{-F_1 + i a_1 u_1^{1+\zeta}}}{\left(1 + e^{-F_1 + i a_1 u_1^{1+\zeta}}\right)^2} \left(\frac{1 + e^{-F_2 + i a_2 u_2^{1+\zeta}}}{1 + e^{-F_2}} + \frac{1 + e^{-F_2}}{1 + e^{-F_2 + i a_2 u_2^{1+\zeta}}} - 2 \right) \right|. \quad \text{(A.28)}
$$

Note that the integrals converge both for $u_{1,2} \to 0$ and $u_{1,2} \to \infty$.

We have computed the (F_1, F_2, a_1, a_2)-integral in Eq. (A.28) using Monte-Carlo sampling, followed by numerically carrying out the (u_1, u_2)-integration. With the density ρ_a given in (A.6), c_2 turns out to be negative.

To the first subleading order we find the correction to the inverse localization length as

$$\Delta(\xi^{-1}) = -c_1 B^{4/5} \left(1 + \frac{c_2}{c_1} B^{1/5} + O(B^{2/5}) \right). \tag{A.29}$$

Note that the subleading corrections vary slowly with B and thus are expected to affect fits of the magnetoconductance to a simple power law B^γ. Indeed defining an 'effective exponent' as

$$\gamma = \frac{d \ln |\Delta(\xi^{-1})|}{d \ln B} = \frac{4}{5} + \frac{1}{5} \frac{B^{1/5}}{c_1/c_2 + B^{1/5}} + O(B^{2/5}), \tag{A.30}$$

one expects to see apparent exponents that deviate from the asymptotically exact value $4/5$ for any small but finite $B \ll 1$. The sign of the correction depends on the relative sign of c_1 and c_2.

The numerical data obtained for the full lattice model is consistent with a positive correction to the exponent, cf. inset of Fig. 3 in main text.. However, the normalized hierarchical model predicts the opposite sign. We believe that this qualitative difference is due to the fact that the normalized recursion neglects correlations of free energy differences at different scales, as explained above.

A more realistic model, which builds in such correlations was given in Eq. (A.3), where the normalizing factors are dropped in the recursive definition of path weights. The expression for $\mathcal{V}_2$ is easy to derive in this case as well,

$$
c_2 \approx -\frac{1}{(\ln 2)^2} \int_\Lambda^\infty \frac{du_1}{u_1^{1+\theta}} \int_\Lambda^{u_1} \frac{du_2}{u_2^{2+\theta}} \int_1^\infty dF_1 \int_0^\infty dF_2 \int_{-\infty}^\infty da_1 \rho_a(a_1) \int_{-\infty}^\infty da_2 \rho_a(a_2) \left[\mathcal{V}_2^{(I)} + \mathcal{V}_2^{(II)} \right] \quad (A.31)
$$

$$
\mathcal{V}_2^{(I)} = \ln \left| \frac{1 + e^{-F_1 + ia_1 u_1^{1+\varsigma}} + e^{-F_2 + ia_2 u_2^{1+\varsigma}}}{1 + e^{-F_1} + e^{-F_2}} \right| - \ln \left| \frac{1 + e^{-F_1 + ia_1 u_1^{1+\varsigma}}}{1 + e^{-F_1}} \right| - \ln \left| \frac{1 + e^{-F_2 + ia_2 u_2^{1+\varsigma}}}{1 + e^{-F_2}} \right|
$$

$$
\mathcal{V}_2^{(II)} = \ln \left| \frac{1 + e^{-F_1 + ia_1 u_1^{1+\varsigma}} (1 + e^{-F_2 + ia_2 u_2^{1+\varsigma}})}{1 + e^{-F_1}(1 + e^{-F_2})} \right| - \ln \left| \frac{1 + e^{-F_1 + ia_1 u_1^{1+\varsigma}}}{1 + e^{-F_1}} \right|
$$

where the cutoff Λ is a fraction indicating that the recursion ends at $L_k = \Lambda \ell_B$ (we used $\Lambda = 0.125$ for the numerical computation of c_2 below). This cutoff is required since the u_2-integral in Eq. (A.31) does not converge at infinitesimally small length-scales. At such length-scales, it can be conjectured that the alternative non-normalized recursion fails to capture the nontrivial distribution of $S_\mathcal{L}$ at $B = 0$ (cf. section A.2). One can, however, reasonably assume that these smaller loops enclose negligible flux. Thus, they do not contribute significantly to magnetoconductance, making any nontrivial distribution at the smallest length scales irrelevant. This revised recipe leads to a similar virial expansion in powers of $B^{1/5}$, however with different coefficients $c_{k>1}$.

The integral (A.31) yields $c_2 \approx 4.9 \times 10^{-2}$. This has the *same* sign as c_1 and thus leads to an "effective exponent" which is bigger than 4/5, and thus comes closer to the phenomenology observed in the full lattice model, as one may expect. As mentioned before, the various definitions of the hierarchical construction only affect the coefficients of the *subleading* terms in the virial expansion.

A.2.4 Effect of small denominators and resonances

The quantitative effect of the subleading terms is of course non-universal, as are the coefficients $c_{1,2}$. A variation of such effects is actually also found in the full lattice sum of forward-directed paths. It may seem dangerous to evaluate path sums of products of denominators which can become arbitrarily small. While the logarithmic average of such sums is mathematically well-defined, it is known that backscattering and self-energy effects, or a Coulomb gap in the density of states, reduce the influence of such resonances. For this reason the toy models considered in the earlier literature [2, 138] have restricted themselves to finite denominators.

Numerically evaluating the sum over all paths as given in the maintext, without restricting the occurrence of resonant denominators, we found effective exponent of the order of $\gamma \approx 0.88$. However, the deviation from $4/5$ turned out to be much smaller for a toy model where we restricted onsite energies to the interval $[1/2, 1]$. It is thus suggestive to attribute the stronger deviations with resonances included to an enhanced value of c_2.

A.2.5 Higher terms in the droplet expansion

It is not difficult to write down the disorder-average of the higher order terms in Eq. A.8 as appropriate integrals. One can check that the generic term $\overline{\mathcal{V}_k}$ varies as

$$\overline{\mathcal{V}_k} = c_k N B^{\frac{1+k\theta}{1+\zeta}} \tag{A.32}$$

To illustrate the procedure, we give the diagrams contributing to $\mathcal{V}_3$ in Fig.

A.2. The corresponding expressions for the connected terms are given below. Subscripts 1, 2 and 3 denote three loops with lengths $L_1 \geq L_2 \geq L_3$. For brevity, we only consider for the normalized model and give the *connected* terms in $\mathcal{V}_3^{(k)}$ as $V_3^{(k)}(B) - V_3^{(k)}(B = 0)$, where

$$
\begin{aligned}
V_3^{(I)}(B) &= \ln|1 + W_1 + W_2 + W_3 + W_2 W_3|, \\[2mm]
V_3^{(II)}(B) &= \ln|1 + W_1 + W_2 + W_3|, \\[2mm]
V_3^{(III)}(B) &= \ln|1 + W_1 + W_2 + W_2 W_3|, \\[2mm]
V_3^{(IV)}(B) &= \ln|1 + W_1 + W_2 + W_1 W_3|, \\[2mm]
V_3^{(V)}(B) &= \ln|1 + W_1 + W_1 W_2 + W_1 W_3 + W_1 W_2 W_3|, \\[2mm]
V_3^{(VI)}(B) &= \ln|1 + W_1 + W_1 W_2 + W_1 W_3|, \\[2mm]
V_3^{(VII)}(B) &= \ln|1 + W_1 + W_1 W_2 + W_1 W_2 W_3|,
\end{aligned}
$$

where $W_1 \equiv W_{\mathcal{L}_1}(B)$. Continuing along these lines, $\ln \Delta \sigma_N(B)$ can be calculated to any desired order at a given field B.

A.2.6   Remarks on fermions

It might be interesting to generalize the hierarchical model to the case of fermions. Since the locator expansion yields path amplitudes with positive and negative signs, it would seem natural to include random signs $s_{\mathcal{L}}$ in a hierarchical droplet model. However, several subtleties may need further modifications to capture the details of fermionic magnetoconductance. For example, a weak field can have a significant effect on small loops whose branches have nearly opposite

amplitudes. This may reflect in a non-trivial dependence of free energy costs $f_{\mathcal{L}}$ on B, which may enhance subleading corrections and potentially even change their exponent. It is possible that the observed effective fermionic exponents $\gamma < 4/5$ in the non-perturbative regime are due to such effects. More detailed investigations are necessary to clarify these issues.

Appendix B

Calculation of the parameters e_j in exact solution of ac-driven two-level system

In this Appendix, we provide explicit expressions for the parameters e_j's, which determine the explicit form of our exact solution for the external field (6.22). As mentioned in the main text, the particular expressions for these parameters, e_j, depend on the relative values of Δ_a and $\Delta_\pm$. For the choice corresponding to

$$\Delta_a \geq \frac{\Delta_- + \Delta_+}{2}, \tag{B.1}$$

we have

$$e_1^{(1)} = \frac{1}{3}(2 - a_+ - a_-),$$

$$e_2^{(1)} = \frac{1}{3}(2a_- - a_+ - 1), \tag{B.2}$$

$$e_3^{(1)} = \frac{1}{3}(2a_+ - a_- - 1).$$

In the opposite case of

$$\frac{\Delta_+ - \Delta_-}{2} \leq \Delta_a \leq \frac{\Delta_- + \Delta_+}{2}, \tag{B.3}$$

we have

$$e_1^{(2)} = \frac{1}{3}(2a_- - a_+ - 1),$$

$$e_2^{(2)} = \frac{1}{3}(2 - a_- - a_+), \tag{B.4}$$

$$e_3^{(2)} = \frac{1}{3}(2a_+ - a_- - 1).$$

Finally when

$$\Delta_a \leq \frac{\Delta_+ - \Delta_-}{2}, \tag{B.5}$$

we have

$$e_1^{(3)} = \frac{1}{3}(2a_- - a_+ - 1),$$
$$e_2^{(3)} = \frac{1}{3}(2a_+ - a_- - 1), \tag{B.6}$$
$$e_3^{(3)} = \frac{1}{3}(2 - a_- - a_+).$$

We also remind the reader, that the coefficients $a_\pm$ in the above equations are given

by $a_\pm = 2\Delta_+/(\Delta_+ + 2\Delta_a \pm \Delta_-)$.

B.1   Exact solution for the function $f(t)$: special cases

In this Appendix, we consider a few special cases, where the exact solution

given by (6.23) (which is generally described by three independent parameters) is

reduced to a degenerate function with simpler properties, which is characterized by

two parameters only. The first case we consider corresponds to $\Delta_a \to 0$. As shown

below, the choice of $\Delta_- \simeq \Delta_+$, corresponds to an external field of the following

form, $f(t) \simeq \Delta_+[1 + q\cos(2\Delta_+ t)]$ with $q \ll 1$. Another case considered here is the

limit $\Delta_- \to 0$, but with both Δ_a and Δ_+ kept finite. In that case, $f(t)$ can be

represented as a single isolated soliton.

B.1.1 Limit of $\Delta_a \to 0$

Our goal here is to recover the limiting case for our solution corresponding to $\delta_a = 0$. It can be shown that in this limit,

$$\kappa = \frac{1 - k'}{1 + k'}, \quad k' = \delta_-, \quad k = \sqrt{1 - k'^2} \tag{B.7}$$

and the solution for the driving field reads:

$$f(t) = \Delta_+ \left\{ \frac{2}{\mathcal{P}[k\Delta_+(t - t_0)] + 1 - e_3} - 1 \right\}. \tag{B.8}$$

We demonstrate below that the expression in the brackets can be cast into single Jacobi elliptic function $\mathrm{dn}(\Delta_+ t, k)$. For this, we use the identity

$$\mathcal{P}\left(\frac{u}{\sqrt{e_1 - e_3}} \right) = e_3 + (e_1 - e_3)\frac{1}{\mathrm{sn}^2(u, \kappa)}, \tag{B.9}$$

such that it gives

$$f(t) = \Delta_+ \left[\frac{\mathrm{sn}^2(u, \kappa) - (e_1 - e_3)}{\mathrm{sn}^2(u, \kappa) + (e_1 - e_3)} \right] \tag{B.10}$$

and variable u equals $u = \frac{1}{2}(1 + \delta_-)\Delta_+ t$. This expression can be further simplified by means of the following relation between the Jacobi elliptic functions:

$$\mathrm{dn}(u_1, \kappa_1) = \frac{1 - \kappa \mathrm{sn}^2(u, \kappa)}{1 + \kappa \mathrm{sn}^2(u, \kappa)}, \tag{B.11}$$

where

$$u_1 = (1 + \kappa)u, \quad \kappa_1 = \frac{2\sqrt{\kappa}}{1 + \kappa} \tag{B.12}$$

Indeed, from expressions (B.6) for $\Delta_a = 0$ we have

$$\kappa = \sqrt{\frac{e_2 - e_3}{e_1 - e_3}} = \frac{1 - \delta_-}{1 + \delta_-} = \frac{1}{e_1 - e_3}, \tag{B.13}$$

131

so that $\kappa_1 = k$ and we find:

$$f(t) = -\Delta_+ \text{dn}[\Delta_+(t - t_0), k]. \tag{B.14}$$

Finally, when $k \to 0$ ($\Delta_- \to \Delta_+$) it follows [123] that

$$f(t) \simeq -\Delta_+ \left[1 + q\cos(2\Delta_+ t)\right], \quad q \ll 1, \tag{B.15}$$

We find that for the special values of parameters the line shape of the external field is given by the cosine.

B.1.2 Limit $\Delta_- \to 0$

To derive an explicit form of the driving field, $f(t)$, in this case, we work with the general solution (6.23). Let us first assume that

$$\Delta_a \leq \Delta_+/2.$$

T Then, the case $\Delta_- = 0$ corresponds to $k = 1$, which in turn implies

$$\text{sn}(u, 1) = \tanh(u), \quad u = \frac{1}{2}\lambda t \tag{B.16}$$

and $\lambda = \sqrt{\Delta_+^2 - 4\Delta_a^2}$. After some simple algebra, we find

$$f = -\left[\Delta_a + \frac{\lambda^2}{2\Delta_a - \Delta_+ \cosh(\lambda t)}\right], \tag{B.17}$$

which up to the minus sign, is exactly the same expression as the listed in Ref.[122].

Finally, let us consider the parameter range with

$$\Delta_a \geq \Delta_+/2. \tag{B.18}$$

132

According to the expressions above for that case $k = 0$ and

$$\text{sn}(u,0) = \sin(\sqrt{4\Delta_a^2 - \Delta_+^2} t/2)$$

. Therefore, it follows:

$$f = -\Delta_a + \frac{4\Delta_+(2\Delta_a - \Delta_+)/(2\Delta_a + \Delta_+)}{1 - \cos\left(\sqrt{4\Delta_a^2 - \Delta_+^2} t\right) + 2\frac{2\Delta_a - \Delta_+}{2\Delta_a + \Delta_+}}. \tag{B.19}$$

We see that when $\Delta_- = 0$ external field has a line shape of a single pulse. Note that

our solutions (B.17,B.19) do not contradict to our assumption of the periodicity of

$f(t)$ since both these solutions correspond to the case where the period of $f(t)$ goes

to infinity.

B.2 calculation of the common phase $\alpha(t)$

In this Appendix, we outline the main steps, which allow to compute the

integral (6.32) exactly. The calculation includes the following transform of the

special functions involved that reduces the integrand to a form amenable for exact

integration of the Weierstrass elliptic function: [123]

$$\int \frac{\alpha \mathcal{P}(u) + \beta}{\gamma \mathcal{P}(u) + \delta} du = \frac{\alpha}{\gamma} u + \frac{\alpha\delta - \beta\gamma}{\gamma\delta} \times$$
$$\times \left[\log \frac{\sigma(u+v)}{\sigma(u-v)} - 2u\zeta(v) \right], \tag{B.20}$$

where $\alpha, \beta, \gamma, \delta$ are some constants, a parameter v is determined from the derivative

of the Weierstass function, $\mathcal{P}'(v) = -\delta/\gamma$, $\sigma(u)$, and $\zeta(u)$ are the Weierstrass elliptic

sigma and zeta functions. [123]

The next step is to write down the function, $f(t)$, explicitly in terms of the

Weierstrass function. Combining expressions (6.18,6.20,6.22), we have:

$$f(t) = -\Delta_+ \left[\frac{\mathcal{P}(x + \omega') - 1 - e_j}{\mathcal{P}(x + \omega') + 1 - e_j} \right] - \Delta_a \tag{B.21}$$

where $a_\pm = 2\Delta_+/(\Delta_+ + 2\Delta_a \pm \Delta_-)$, $x = \frac{\Delta_+ t}{\sqrt{a_+ a_-}}$ and $j = 1, 2$ or 3 depending on the value of Δ_a (see Appendix A). Let us now consider the first integral in (6.32):

$$\int_0^t \frac{d_+^2}{f^2(t') - d_+^2} dt' =$$

$$\frac{\sqrt{a_+ a_-}}{2\Delta_+} \int_0^x \left\{ \frac{d_+ \left[\mathcal{P}(x' + \omega') + 1 - e_j \right]}{(\Delta_+ + \Delta_a - d_+)\mathcal{P}(x' + \omega') + (\Delta_a - d_+)(1 - e_j) - \Delta_+(1 + e_j)} \right.$$

$$\left. -(d_+ \to -d_+) \right\} dx' \quad \text{(B.22)}$$

Here the index j of the coefficient e_j is determined by the value of Δ_a (see Appendix A). The remaining terms can be written in a similar form and the corresponding integrals can be evaluated using (B.20), as we have done for the first one (B.22). Since the resulting expressions for the $\alpha(t)$ turn out to be too cumbersome, we do not list them here.

Bibliography

[1] V.L. Nguen, B.Z. Spivak, and B.I. Shklovskii. Tunnel hopping in disordered systems. *Sov. Phys. JETP*, 62(5):1021, 1985.

[2] B.I. Shklovskii and B. Spivak. *Hopping Transport in Solids*. Elsevier Science, 1991.

[3] W. A. Phillips. Tunneling states and the low-temperature thermal expansion of glasses. *Journal of Low Temperature Physics*, 11:757, 1973.

[4] C. Musgrave. *private communication*.

[5] P. W. Anderson. Absence of diffusion in certain random lattices. *Phys. Rev.*, 109:1492, 1958.

[6] J. Bardeen, L. N. Cooper, and J. R. Schrieffer. Microscopic theory of superconductivity. *Phys. Rev.*, 106:162, 1957.

[7] A. Altland and B. Simons. *Condensed Matter Field Theory*. Cambridge University Press, 2006.

[8] V. F. Gantmakher and V. T. Dolgopolov. Superconductor-insulator quantum phase transition. *Physics-Uspekhi*, 53(1):1–49, 2010.

[9] M. Randeria. *Bose-Einstein condensation*. Cambridge University Press, 1985.

[10] D. DiVincenzo and D. Loss. Quantum information is physical. *SuperLatt. & Microstruct.*, 23:419, 1998.

[11] J. M. Martinis and *et al*. Decoherence in josephson qubits from dielectric loss. *Phys. Rev. Lett.*, 95:210503, 2005.

[12] P. W. Anderson, B. Halperin, and C. M. Varma. Anomalous low-temperature properties of glasses and spin-glasses. *Philosophical Magazine*, 25:1, 1972.

[13] A. F. Hebard and M. A. Paalanen. Magnetic-field-tuned superconductor-insulator transition in two-dimensional films. *Phys. Rev. Lett.*, 65:927, 1990.

[14] M. A. Paalanen, A. F. Hebard, and R. R. Ruel. Low-temperature insulating phases of uniformly disordered two-dimensional superconductors. *Phys. Rev. Lett.*, 69:1604, 1992.

[15] D. Shahar and Z. Ovadyahu. Superconductivity near the mobility edge. *Phys. Rev. B*, 46:10917, 1992.

[16] V. F. Gantmakher, M. V. Golubkov, V. T. Dolgopolov, G. E. Tsydynzhapov, and A. A. Shashkin. Destruction of localized electron pairs above the magnetic-field-driven superconductor-insulator transition in amorphous ino films. *JETP Lett.*, 68:337, 1998.

[17] G. Sambandhamurthy, L.W. Engel, A. Johansson, and D. Shahar. Superconductivity-related insulating behavior. *Phys. Rev. Lett.*, 92:107005, 2004.

[18] G. Sambandhamurthy, L. W. Engel, A. Johansson, E. Peled, and D. Shahar. Experimental evidence for a collective insulating state in two-dimensional superconductors. *Phys. Rev. Lett.*, 94:017003, 2005.

[19] H. Q. Nguyen, S. M. Hollen, M. D. Stewart Jr., J. Shainline, Yin Aijun, J. M. Xu, and J. M. Valles Jr. Observation of giant positive magnetoresistance in a cooper-pair insulator. *Phys. Rev. Lett.*, 103:157001, 2009.

[20] T. I. Baturina, A. Yu. Mironov, V. M. Vinokur, M. R. Baklanov, and C. Strunk. Hyperactivated resistance in tin films on the insulating side of the disorder-driven superconductor-insulator transition. *Pis' ma v ZhETF*, 88(11):867–872, 2008.

[21] Benjamin Sacépé, Thomas Dubouchet, Claude Chapelier, Marc Sanquer, Maoz Ovadia, Dan Shahar, Mikhail Feigel'man, and Lev Ioffe. Localization of preformed cooper pairs in disordered superconductors. *Nature Phys.*, 7:239–244, 2011.

[22] M.P.A. Fisher. Quantum phase transitions in disordered two-dimensional superconductors. *Phys. Rev. Lett.*, 65:923, 1990.

[23] A.M. Finkelstein. Superconducting transition temperature in amorphous films. *JETP Lett.*, 45:46, 1987.

[24] M. V. Feigel'man, L. B. Ioffe, V. E. Kravtsov, and E. Cuevas. Fractal superconductivity near localization threshold. *Annals of Physics*, 325(7):1390–1478, 2010.

[25] A Ghoshal, M. Randeria, and N. Trivedi. Inhomogeneous pairing in highly disordered s-wave superconductors. *Phys. Rev. B*, 65:014501, 2001.

[26] V. M. Galitski and A. I. Larkin. Superconducting fluctuations at low temperature. *Phys. Rev. B*, 63:174506, 2001.

[27] Y. Dubi, Y. Meir, and Y. Avishai. Nature of the superconductor-insulator transition in disordered superconductors. *Nature*, 449:876, 2007.

[28] M. Müller and B. I. Shklovskii. Compensation-driven superconductor-insulator transition. *Phys. Rev. B*, 79:134504, 2009.

[29] V. L. Pokrovsky, G. M. Falco, and T. Nattermann. Phase diagram of electron systems near the superconductor-insulator transition. *Phys. Rev. Lett.*, 105:267001, 2010.

[30] P. A. Lee and T. V. Ramakrishnan. Disordered electronic systems. *Rev. Mod. Phys.*, 57:287, 1985.

[31] P. Reunchan, X. Zhou, S. Limpijumnong, A. Janotti, and C. G. Van de Walle. Vacancy defects in indium oxide: An ab-initio study. *Current Applied Physics*, 11:296–300, 2011.

[32] P. J. Baker, R. J. Ormeno, C. E. Gough, Y. Matsushita, and I. R. Fisher. Microwave surface impedance measurements of $tl_x pb_{1-x}te$: A proposed negative-u induced superconductor. *Phys. Rev. B*, 81:064506, 2010.

[33] J. Schmalian and M. Dzero. Superconductivity in charge kondo systems. *Phys. Rev. Lett.*, 94:157003, 2005.

[34] A. L. Efros and B. I. Shklovskii. Coulomb gap and low temperature conductivity of disordered systems. *J. Phys. C*, 8:49–51, 1975.

[35] M. V. Feigel'man, L. B. Ioffe, and M. Mézard. Superconductor-insulator transition and energy localization. *Phys. Rev. B*, 82:184534, 2010.

[36] Y. Dubi, Y. Meir, and Y. Avishai. Theory of the magnetoresistance of disordered superconducting films. *Phys. Rev. B*, 73:054509, 2006.

[37] Tianran Chen, B. Skinner, and B. I. Shklovskii. Coulomb gap triptych in a periodic array of metal nanocrystals. *arXiv : 1204.4935v1*, 2012.

[38] T. Chen, B. Skinner, and B. I. Shklovskii. Theory of hopping conduction in arrays of doped semiconductor nanocrystals. *arXiv:1203.3889v2*, 2012.

[39] A. L. Efros and B. I. Shklovskii. *Electronic properties of doped semiconductors.* Springer Berlin, 1984.

[40] F .G. Pikus and A. L. Efros. Critical behaviour of density of states in disordered systems with localized electrons. *Phys. Rev. Lett.*, 73:3014, 1994.

[41] M. Müller and S. Pankov. Mean field theory for the three-dimensional coulomb glass. *Phys. Rev. B*, 75:144201, 2007.

[42] A. Möbius, P Karmann, and M Schreiber. Coulomb gap revisited - a renormalization approach. *J. Phys.: Conf. Ser.*, 150:022057, 2009.

[43] E. I. Levin, V. L. Nguen, B. I. Shklovskii, and A. L. Efros. Coulomb gap and hopping electric conduction. *Sov. Phys. JETP*, 65:842, 1987.

[44] S. D. Baranovskii, A..L. Efros, B. L. Gelmont, and B. I. Shklovskii. Coulomb gap in disordered systems : computer simulation. *J. Phys. C*, 12:1023–1034, 1979.

[45] M. Goethe and M. Palassini. *to be published.*

[46] E. Bardalen, J. Bergli, and Y.M. Galperin. coulomb glasses: a comparison between mean-field and monte carlo results. *Phys. Rev. B*, 85:155206, 2012.

[47] H. Kamimura and A. Kurobe. Theoretical model on the interplay of disorder and electron correlations. *J. Phys. Soc. Japan*, 51:1904, 1982.

[48] A. Vaknin, A. Frydman, Z. Ovadyahu, and M. Pollak. High-field magneto-conductance in anderson insulators. *Phys. Rev. B*, 54:13604, 1996.

[49] Subir Sachdev. *Quantum Phase Transitions.* Cambridge University Press, 2000.

[50] M. Schechter and P.C.E. Stamp. Low-temperature universality in disordered solids. condmat: 0910.1283.

[51] Allen Miller and Elihu Abrahams. Impurity conduction at low concentrations. *Phys. Rev.*, 103:745, 1960.

[52] A. Amir, Y. Oreg, and Y. Imry. Variable range hopping in the coulomb glass. *Phys. Rev. B*, 80:245214, 2009.

[53] V. Ambegaokar, B. I. Halperin, and J.S. Langer. Hopping conductivity in disordered systems. *Phys. Rev. B*, 4:2612, 1971.

[54] Hui Lin Zhao, B. Z. Spivak, M. P. Gelfand, and Shechao Feng. Negative magnetoresistance in variable-range-hopping conduction. *Phys. Rev. B*, 44:10760, 1991.

[55] Markus Müller. Giant positive magnetoresistance and localization in bosonic insulators. *arXiv : 1109.0245v2*, 2011.

[56] P. W. Anderson. Theory of dirty superconductors. *J.Phys. Chem. Solids*, 11:26, 1959.

[57] Michael Ma and Patrick A. Lee. Localized superconductors. *Phys. Rev. B*, 32:5658, 1985.

[58] N. P. Armitage, E. Helgren, and G. Gruner. Frequency-dependent conductivity of electron glasses. *Phys. Rev. B.*, 69:014201, 2004.

[59] J. G. Massey and M. Lee. Direct observation of the coulomb correlation gap in a nonmetallic semiconductor, si: B. *Phys. Rev. Lett.*, 75:4266, 1995.

[60] A. Vaknin, Z. Ovadyahu, and M. Pollak. Nonequilibrium field effect and memory in the electron glass. *Phys. Rev. B*, 65:134208, 2002.

[61] E. Lebanon and M. Müller. Memory effect in electron glasses: Theoretical analysis via a percolation approach. *Phys. Rev. B*, 72:174202, 2005.

[62] O. Naaman, W. Tezier, and R. C. Dynes. Fluctuation dominated josephson tunneling with a scanning tunneling microscope. *Phys. Rev. Lett.*, 87:097004, 2001.

[63] E Abrahams, editor. *50 years of Anderson Localization*. World Scientific, 2010.

[64] F. Evers and A. D. Mirlin. Anderson transitions. *Rev. Mod. Phys.*, 80:1355, 2008.

[65] M. Kardar. *Statistical Physics of Fields*. Cambridge University Press, 2007.

[66] V. F. Gantmakher. Localized superconductive pairs. *Low Temp. Phys.*, 37(1):59, 2011.

[67] Yen-Hsiang Lin and A. M. Goldman. Magnetic-field-tuned quantum phase transition in the insulating regime of ultrathin amorphous bi films. *Phys. Rev. Lett.*, 106:127003, 2011.

[68] M. A. Steiner, G. Boebinger, and A. Kapitulnik. Possible field-tuned superconductor-insulator transitions in high-t_c superconductors : Implications for pairing at high magnetic fieldsg. *Phys. Rev. Lett.*, 94:107008, 2005.

[69] Joe Mitchell, Anirban Gangopadhyay, Victor Galitski, and M. Müller. Two-component coulomb glass in disordered superconducting films. *Phys. Rev. B*, 85:195141, 2011.

[70] Tianran Chen, Brian Skinner, and B. I. Shklovskii. Coulomb gap triptychs, $\sqrt{2}$ effective charge, and hopping transport in periodic arrays of superconductor grains. *Phys. Rev. B*, 86:045135, 2012.

[71] Markus Müller. Giant positive magnetoresistance and localization in bosonic insulators. *arXiv: 1109.0245v1*, 2011.

[72] E. Medina and M. Kardar. Quantum interference effects for strongly localized electrons. *Phys. Rev. B*, 46:9984, 1992.

[73] O. Entin-Wohlmann, U. Sivan, and Y. Imry. Orbital magnetoconductance in the variable-range-hopping regime. *Phys. Rev. Lett*, 60:1566, 1988.

[74] B. I. Shklovskii. Variable-range hopping conduction in a strong magnetic field. *JETP Lett*, 36:287, 1982.

[75] S.V. Syzranov, A. Moor, and K.B. Efetov. Strong quantum interference in strongly disordered bosonic insulators. *Phys. Rev. Lett.*, 108:256601, 2012.

[76] D. A. Huse and C.L. Henley. Pinning and roughening of domain walls in ising systems due to random impurities. *Phys. Rev. Lett.*, 54:2708, 1985.

[77] Tim Halpin-Healy and Y.-C. Zhang. Kinetic roughening, stochastic growth, directed polymers and all that. *Phys. Rep.*, 254:215–415, 1995.

[78] A. I. Larkin and Yu. N. Ovchinnikov. *J. Low Temp. Phys.*, 34:409, 1979.

[79] D. S. Fisher and D. A. Huse. Directed paths in a random potential. *Phys. Rev. B*, 43:10728, 1991.

[80] Terence Hwa and D.S. Fisher. Anomalous fluctuations of directed polymers in random media. *Phys. Rev. B*, 49:3136, 1994.

[81] D. A. Huse, C.L. Henley, and D. Fisher. Huse, henley, and fisher respond. *Phys. Rev. Lett.*, 55:2924, 1985.

[82] Lei-Han Tang, B. M. Forrest, and D. E. Wolf. Kinetic surface roughening. ii. hypercube-stacking models. *Phys. Rev. A*, 45:7162, 1992.

[83] E. Medina, M. Kardar, Y. Shapir, and X.R. Wang. Interference of directed paths in disordered systems. *Phys. Rev. Lett.*, 62:941, 1989.

[84] J. Prior, A. M. Somoza, and Ortuno. Conductance fluctuations and single-parameter scaling in two-dimensional systems. *Phys. Rev. B*, 72:024206, 2005.

[85] J. Prior, A. M. Somoza, and M. Ortuno. Conductance distributions in two-dimensional localized systems with and without magnetic field. *Eur. Phys. J B*, 70:513, 2009.

[86] C. Monthus and T. Garel. Random transverse field ising model in dimension $d > 1$: scaling analysis in the disordered phase from the directed polymer model. *J. Phys. A : Math. Theor.*, 45:095002, 2012.

[87] M. Kardar, Giorgio Parisi, and Yi-Cheng Zhang. Dynamic scaling of growing interfaces. *Phys. Rev. Lett.*, 56:889, 1986.

[88] D. Forster, D. R. Nelson, and M. J. Stephen. Large-distance and long-time properties of a randomly stirred fluid. *Phys. Rev. A*, 16:732, 1977.

[89] E. Frey and U. C. Täuber. Two-loop renormalization group analysis of the burgers-kardar-parisi-zhang equation. *Phys. Rev. E*, 50:1024, 1994.

[90] B. Shklovskii and A. L. Efros. Tunnel transparency of disordered systems in a magnetic field. *Sov. Phys. JETP*, 57(2):470, 1983.

[91] B. Derrida and R. B. Griffiths. Directed polymers on disordered hierarchical lattices. *Europhys. Lett.*, 8(2):111, 1989.

[92] F. Hund. On the interpretation of molecular spectra. *Z. Phys.*, 43:805, 1927.

[93] E. Merzbacher. *Quantum Mechanics.* John Wiley & Sons, 1961.

[94] L Pauling. The rotational motion of molecules in crystals. *Phys. Rev.*, 36:430, 1930.

[95] W. A. Phillips. Low temperature dielectric relaxation in polyethylene and related hydrocarbon polymers. *Proc. Roy. Soc. Lond. A*, 319:565, 1970.

[96] A. C. Anderson. Low-temperature thermal expansion of glassy solids. *Phys. Rev. B*, 34:1317, 1986.

[97] W. A. Phillips. *Amorphous Solids : low-temperature properties (topics in current physics).* Springer Berlin, 1981.

[98] W. A. Phillips. Two-level states in glasses. *Rep. Prog. Phys.*, 50:1657, 1987.

[99] A. Wallraff and *et al.* Strong coupling of a single photon to a superconducting qubit using circuit quantum electrodynamics. *Nature*, 431:162, 2004.

[100] U. Weiss. *Quantum Dissipative Systems.* World Scientific, 2008.

[101] A. J. Leggett and *et al.* Dynamics of the dissipative two-state system. *Rev. Mod. Phys.*, 59:1, 1987.

[102] P. W. Anderson and C. C. Yu. Local-phonon model of strong electron-phonon interactions in a15 compounds and other strong-coupling superconductors. *Phys. Rev. B*, 29:6165, 1984.

[103] S. Hunklinger and A. K. Raychaudhuri. *Amorphous Solids: Low-Temperature Properties.* Springer Berlin, 1981.

[104] V. Lubchenko and P. G. Wolynes. Theory of aging in structural glasses. *J. Chem. Phys.*, 119:9088, 2002.

[105] M. A. Nielsen and I. L. Chuang. *Quantum Computations and Quantum Information.* Cambridge University Press, 2002.

[106] B. D. Gerardot and P. Öhberg. A strongly driven spin. *Science*, 326:1489, 2009.

[107] J. E. Mooij, T. P. Orlando, L. Levitov, L. Tian, C. H. van der Waal, and S. Llyod. Josephson persistent-current qubit. *Science*, 285:1036, 1999.

[108] C. H. van der Waal, A. C. J. ter Haar, F. K. Wilhelm, R. N. Schouten, C. J. P. M. Harmans, T. P. Orlando, S. Llyod, and J. E. Mooij. Quantum superposition of macroscopic persistent-current states. *Science*, 290:773, 2000.

[109] I. Chiorescu, Y. Nakamura, C. J. P. M. Harmans, and J. E. Mooij. Coherent quantum dynamics of a superconducting flux qubit. *Science*, 299:1869, 2003.

[110] G. D. Fuchs, V. V. Dobrovitski, D. M. Toyli, F. J. Heremans, and D. D. Awschalom. Gigahertz dynamics of a strongly driven single quantum spin. *Science*, 326:1520, 2009.

[111] H. Wang. Improving the coherence time of superconducting coplanar resonators. *Appl. Phys. Lett.*, 95:233508, 2009.

[112] J. Hausinger and M. Grifoni. Dissipative two-level system under strong ac driving: A combination of floquet and van vleck perturbation theory. *Phys. Rev. A*, 81:022117, 2009.

[113] H. Paik and K. D. Osborn. Reducing quantum-regime dielectric loss of silicon nitride for superconducting quantum circuits. *Appl. Phys. Lett.*, 96:072505, 2010.

[114] R. A. Barankov, L. Levitov, and B.Z. Spivak. Collective rabi oscillations and solitons in a time-dependent bcs pairing problem. *Phys. Rev. Lett.*, 93:160401, 2004.

[115] E.A. Yuzbashyan, B.L. Altshuler, and V. B. Kuznetsov. Solution for the dynamics of the bcs and central spin problems. *J. Phys. A*, 38:7831, 2005.

[116] E.A. Yuzbashyan, B. Altshuler, and V. B. Kuznetsov. Integrable dynamics of coupled fermi-bose condensates. *Phys. Rev. B*, 72:144524, 2005.

[117] E. Yuzbashyan, B. Altshuler, V. B. Kuznetsov, and V.Z. Enolskii. Nonequilibrium cooper pairing in the non-adiabatic regime. *Phys. Rev. B(R)*, 72:220503, 2005.

[118] E. Yuzbashyan and M. Dzero. Dynamical vanishing of the order parameter in ultra-cold fermi gases. *Phys. Rev. Lett.*, 96:230404, 2006.

[119] E. Yuzbashyan, O. Tsyplyatyev, and B. Altshuler. Relaxation and persistent oscillations of the order parameter in fermionic condensates. *Phys. Rev. Lett.*, 96:097005, 2006.

[120] V. M. Galitski. Nonperturbative quantum dynamics of the order parameter in the bcs pairing model. *Phys. Rev. B*, 82:054511, 2010.

[121] M. Dzero, E.A. Yuzbashyan, B.L. Altshuler, and P. Coleman. Spectroscopic signatures of nonequilibrium pairing in atomic fermi gases. *Phys. Rev. Lett.*, 99:160402, 2007.

[122] E. Yuzbashyan. Normal and anomalous solitons in the theory of dynamical cooper pairing. *Phys. Rev. B*, 78:184507, 2008.

[123] I. S. Gradstein and I. M. Ryzhik. *Tables of Integrals, Series and Products.* Academic Press, 1994.

[124] R. P. Feynman. *Statistical Mechanics: A Set of Lectures.* Addison-Wesley, New York, 1972.

[125] F. Grossmann, T. Dittrich, P. Jung, and P. Hänggi. Coherent destruction of tunneling. *Phys. Rev. Lett.*, 67:516, 1991.

[126] F. Grossmann, P. Jung, T. Dittrich, and P. Hänggi. Tunneling in a periodically driven bistable system. *Z. Phys. B*, 84:315, 1991.

[127] F. Grossmann and P. Hänggi. Localization in a driven two-level dynamics. *Europhys. Lett.*, 18:571, 1992.

[128] L. Hartmann, M. Grifoni, and P. Hänggi. Dissipative tunneling control by elliptically polarized fields. *J. Chem. Phys.*, 109:2635, 1998.

[129] L. Hartmann, M. Grifoni, I. Goychuk, and P. Hänggi. Driven-tunneling dynamics : Bloch-redfield theory versus path-integral approach. *Phys. Rev. E*, 61:4687, 2000.

[130] I. Goychuk and Hänggi. Quantum dynamics in strong fluctuating fields. *Adv. Phys.*, 54:525, 2005.

[131] Y. Nakamura, Y. A. Pashkin, and J. S. Tsai. Rabi oscillations in a josephson-junction charge two-level system. *Phys. Rev. Lett.*, 87:246601, 2001.

[132] A. Miller and E. Abrahams. Impurity conduction at low concentrations. *Phys. Rev.*, 120:745, 1960.

[133] E. T. Jaynes and F. W. Cummings. Comparison of quantum and semiclassical radiation theories with application to the beam maser. *Proceedings of the IEEE*, 51:89, 1963.

[134] V. Galitski. Quantum-to-classical correspondence and hubbard-stratonovich dynamical systems: A lie-algebraic approach. *Phys. Rev. B*, 84:012118, 2011.

[135] P le Doussal. Finite-temperature functional rg, droplets and decaying burgers turbulence. *Europhys. Lett.*, 76:457, 2006.

[136] C. Monthus and P le Doussal. Low-temperature properties of some disordered systems from the statistical properties of nearly degenerate two-level excitations. *Eur. Phys. J*, 41:535, 2004.

[137] P le Doussal. Exact results and open questions in first principle functional rg. *Ann. Phys.*, 325:49, 2010.

[138] J. Prior, A. M. Somoza, and M. Ortũno. *Eur. Phys. J*, 70:513, 2009.